MONASH University

An investigation into the occurrence and migration of ^{239,240}Pu in the Australian environment
Megan Louise Cook
B. App. Sci.

A thesis submitted for the degree of Doctor of Philosophy at
Monash University in 2020
School of Earth, Atmosphere and Environment

Copyright notice

Abstract

Understanding the transport and migration of plutonium (Pu) in Australian soil is important for assessing potential impact and risk of current and future exposure situations to improve and validate radioecological models of interest, specifically for Australian exposure situations such as Maralinga and Monte Bello Islands. The qualitative and quantitative data presented here will reduce the uncertainty of radioecological modelling, impact assessments, and ensure these are realistic and not excessively conservative.

The features of environmental transport and migration of Pu in Australian soils were investigated at the from the large scale climate impacts, to the influence of soil geochemical processes and the micro-, nano- and atomic scale of Pu hot particles. This was achieved by quantitative analysis of trace amounts of Pu in soil, using Queensland as a model system, followed by robust statistical analysis using an integrated database of physical, chemical and radiochemical soil properties. The key environmental indicators of Pu presence and accumulation were determined as the chemical characteristics of soils surrounding Pu as a contaminant, as reflected by statistical correlation with lanthanide, actinide and heavier transition metals. The physical variables of the soil ecosystem, such as wet deposition, geomorphology, landform and land use, described smaller variances.

Controlled lab-based transport experiments with soils isolated from natural systems were used to investigate the influence of abiotic climatic parameters (rainfall, soil type, weathering) and transformation kinetics (time-dependent Kds) affecting the transport of Pu. The Kd trends showed arid-type samples were affected by the rainfall intensity and extended rainless periods and a tropical sandy soil system has the potential to produce a Pu Kd of moderate mobility in a short timeframe. This confirms that Pu Kd will continue to change over time, and the thermodynamic constant concept should be replaced with rate functions.

Pu hot particles resulting from a nuclear accident or weapon detonation persist in the soil environment resulting in an undetermined, yet foreseeable risk. Assessing the environmental impact of Pu particle contamination was completed using advanced multi-method characterisation of six particles from Maralinga nuclear test site. The particles showed remarkably complex physical/chemical makeups predicting increased reactivity, and resulting from cooling of polymetallic melts within the detonation plume. Pu exists predominantly in nano-scale form within the fragile particles, indicating that physical breakdown or ingestion by higher animals will likely result in the release of Pu nanoparticles from the hot particles to pose significant environmental and anthropogenic risks.

If it is determined that there is a significant potential for radiological exposure within an existing exposure situation, a protection strategy should be developed and justified that considers remedial actions and/or protective actions. This thesis presents site-specific data for the Australian

environment to develop an appropriate strategy and create accurate risk characterisation, reduce uncertainties in radioecological models and create true impact assessments of current and future environmental Pu contamination.

Declaration

This thesis contains no material which has been accepted for the award of any other degree or diploma at any university or equivalent institution and that, to the best of my knowledge and belief, this thesis contains no material previously published or written by another person, except where due reference is made in the text of the thesis.

Signature:

Print Name: Megan Cook

Date: 21/03/2020

Publications during enrolment

Cook, M. 2020. Agile fusion method for the determination of Pu isotopes in diverse sediments. Applied Radiation and Isotopes. Submitted - Under review.

Cook, M., de Caritat, P., Kleinschmidt, R., Brugger, J., Wong, V.N.L. 2020. Future migration: key environmental indicators of Pu accumulation in terrestrial sediments of Queensland, Journal of Environmental Radioactivity, Volumes 223-224, 106398 https://doi.org/10.1016/j.jenvrad.2020.106398.

Cook, M., Kleinschmidt, R., Brugger, J., Wong, V.N.L. 2020. Transport and migration of Pu in different soil types and rainfall regimes. Journal of Environmental Radioactivity. Submitted – Under review

Cook, M., Estchmann, B., Cumberland, S., Ram, R., Ignatyev, K., Brugger, J., Gervinskas, G., Wong, V.N.L. 2020. The Nature of Pu-bearing particles from the Maralinga Nuclear Testing Site (Australia): significance for predicting their environmental fate. Environmental Science and Technology. Submitted – Under review.

Thesis including published works declaration

This thesis includes no original papers published in peer-reviewed journals and four submitted publications. The core theme of the thesis is the transport and migration of Pu in the Australian soil environment. The ideas, development and writing up of all the papers in the thesis were the principal responsibility of myself, the student, working within the School of Earth, Atmosphere and Environment under the supervision of Dr Vanessa Wong, Professor Joël Brugger and Dr Ross Kleinschmidt.

(The inclusion of co-authors reflects the fact that the work came from active collaboration between researchers and acknowledges input into team-based research.)

In the case of Chapters 2 to 5, my contribution to the work involved the following:

Thesis Chapter	Publication Title	Status *(published, in press, accepted or returned for revision, submitted)*	Nature and % of student contribution	Co-author name(s) Nature and % of Co-author's contribution*	Co-author(s), Monash student Y/N*
2	Agile fusion method for the determination of Pu isotopes in diverse sediments	Submitted	100% concept, data collection, data analysis, writing first draft, and finalising manuscript.		
3	Future migration: key environmental indicators of Pu accumulation in terrestrial sediments of Queensland, Australia	Published	70% Concept, sample analysis, data collection, data analysis, writing first draft, and finalising manuscript.	**Patrice de Caritat**: data analysis, finalising manuscript (13%) **Ross Kleinschmidt**: finalising manuscript (2%) **Joël Brugger:** input into manuscript, finalising manuscript (10)% **Vanessa NL Wong:** finalising manuscript (5%)	N N N N
4	Transport and migration of Pu in different soil types and rainfall regimes	Submitted	80% Concept, sample analysis, data collection, data analysis, writing first draft and	**Ross Kleinschmidt:** finalising manuscript (2%) **Joël Brugger:** finalising manuscript (5%)	N N N

				Barbara Etschmann: concept, data analysis, input into manuscript, finalising manuscript (10%)	N
			finalising manuscript.	Vanessa NL Wong: concept, input into manuscript, finalising manuscript (13%)	
				Rahul Ram: data analysis, finalising manuscript (2%)	N
				Joël Brugger: data analysis, input into manuscript, finalising manuscript (7%)	N
5	The Nature of Pu Hot Particles	Submitted	68% Concept, sample preparation, sample analysis, data collection, data analysis, writing first draft and finalising manuscript.	Konstantin Ignatyev: sample analysis, data collection, data analysis (2%)	N
				Gediminas Gervinskas: sample analysis (2%)	N
				Susan Cumberland: sample analysis, data collection, finalising manuscript (2%)	N
				Steven Conradson: finalising manuscript (2%)	N
				Vanessa NL Wong: sample analysis, finalising manuscript (5%)	N

*If no co-authors, leave fields blank

Laboratory Analysis and Collaborations

Geoscience Australia

Through Geoscience Australia, the Commonwealth Government created a nationwide geochemical database through the National Geochemistry Survey of Australia (NGSA). The NGSA program sampled sediments from 1186 major river catchments across the Australian continent, covering 80% of Australia across all states and territories. In Queensland, 311 catchments were sampled. Catchments were sampled near, or as close as possible to, their outlet, or their lowest point. The sampling took advantage of the natural mixing of materials derived from various source rocks within catchments and the subsequent deposition in low-energy environments near their outlets. Ideally, the chemistry of the outlet sediments can represent the average background Pu activity

concentration present in the Australian environment. In total, 73 NGSA soil samples were utilised for this study.

Queensland Health

Australian Radiation Protection and Nuclear Safety Agency (ARPANSA)

Australian Synchrotron

Diamond Light Source

I have not renumbered sections of submitted or published papers in order to generate a consistent presentation within the thesis.

Student signature: **Date:**   **21/03/2020**

The undersigned hereby certify that the above declaration correctly reflects the nature and extent of the student's and co-authors' contributions to this work. In instances where I am not the responsible author I have consulted with the responsible author to agree on the respective contributions of the authors.

Main Supervisor signature: **Date:**

Acknowledgements

First and foremost I would like to express my gratitude to my main supervisor, Dr Vanessa Wong, for taking a chance on me, guiding me through the PhD process and always being so encouraging. Our experience at the synchrotron was just awesome, I am lucky to have had you as a support, and I look forward to working together in the future.

To my mentor and friend Dr Ross Kleinschmidt, thank you for encouraging me to start on this journey, being there for all the problem-solving discussions and teaching me how to be a researcher.

Rounding out my supervisors and support team, I would like to thank Professor Joël Brugger and Dr Barbara Etschmann for leading us through the brand new world of synchrotron analysis, teaching me so much and getting as excited about Pu as I am.

I wish to acknowledge all of my co-authors for providing their expertise and support in sample analysis, the review of data, and supporting this work as much as you all have. I highly value all your work and your time and effort is greatly appreciated.

To my employer ARPANSA, thank you for supporting my PhD and allowing me the flexibility with working hours to complete this work. It has provided me so many opportunities for growth as a radiochemist and I look forward to continuing to pursue these opportunities into the future.

I could not have gotten through the all-nighters and stressful weeks without the support of my partner and best friend Callum. Thank you for all you have done for me, for dealing with the cancelled plans and having a missing girlfriend. I can't wait for the future to unfold after this PhD.

Finally, to my family and friends, thank you for always asking how my thesis was going, supporting me at times of change and being so proud every step of the way.

Table of Contents

Introduction

1.1. Background

Pu (Pu) isotopes [239]Pu and [240]Pu are present in the global environment as contaminants, largely because of atmospheric nuclear weapons testing from the 1950s to the 1980s. [1] Australia was designated as the location for the British nuclear weapons testing program from October 1952 to September 1958. This involved the detonation of twelve atmospheric nuclear tests and hundreds of subcritical tests, dubbed the minor trials, in Maralinga, South Australia releasing radioactive Pu into the regional environment and settling in the surface sediments of mainland Australia. [2] The high energy release of Pu from a nuclear weapon results in Pu being dispersed in various forms (e.g. Pu aerosols of various sizes, Pu oxide particulates, Pu-coated particles, and sizeable lumps of Pu-contaminated structural material destroyed by the explosion) creating what is currently an undetermined yet foreseeable environmental risk. [3]

The first contamination of Maralinga, an Australian nuclear test site with plutonium hot particles resulting from nuclear detonations occurred in September 1956. [4] Twelve nuclear weapons tests and numerous minor trials investigating the performance of various components of a nuclear device took place as part of the British Nuclear Testing Program between 1952 and 1963. The secrecy surrounding the program at the time of the detonations and poor record keeping resulted in an incomplete account of the tests performed during the minor trials. [4] The incomplete account of these minor trials creates difficulty in linking particle characteristics to specific sources and in turn the prediction of interactions in the environment and a full understanding of environmental impacts and risks.

The trial site at the focus of this study, Taranaki, is 30 km north of Maralinga village, approximately 800 km NW of Adelaide in southern Australia (Figure 1). Taranaki, was utilized for both major and minor trials resulting in extensive Pu contamination; the largest contamination plume showing easily detectable contamination 18 km from ground zero. Trials consisted of one balloon-supported nuclear detonation and five series totalling 12 safety trials. The nature of these trials was subcritical hydronuclear tests combining nuclear material, 4 TBq of plutonium in each series (approximately 22 kg in total), and high explosives that purposely resulted in negligible yield in order to study nuclear materials under conditions of explosive shock compression. The explosions dispersed plutonium along particular directions and carried finely divided plutonium in the direction of prevailing winds. [2]
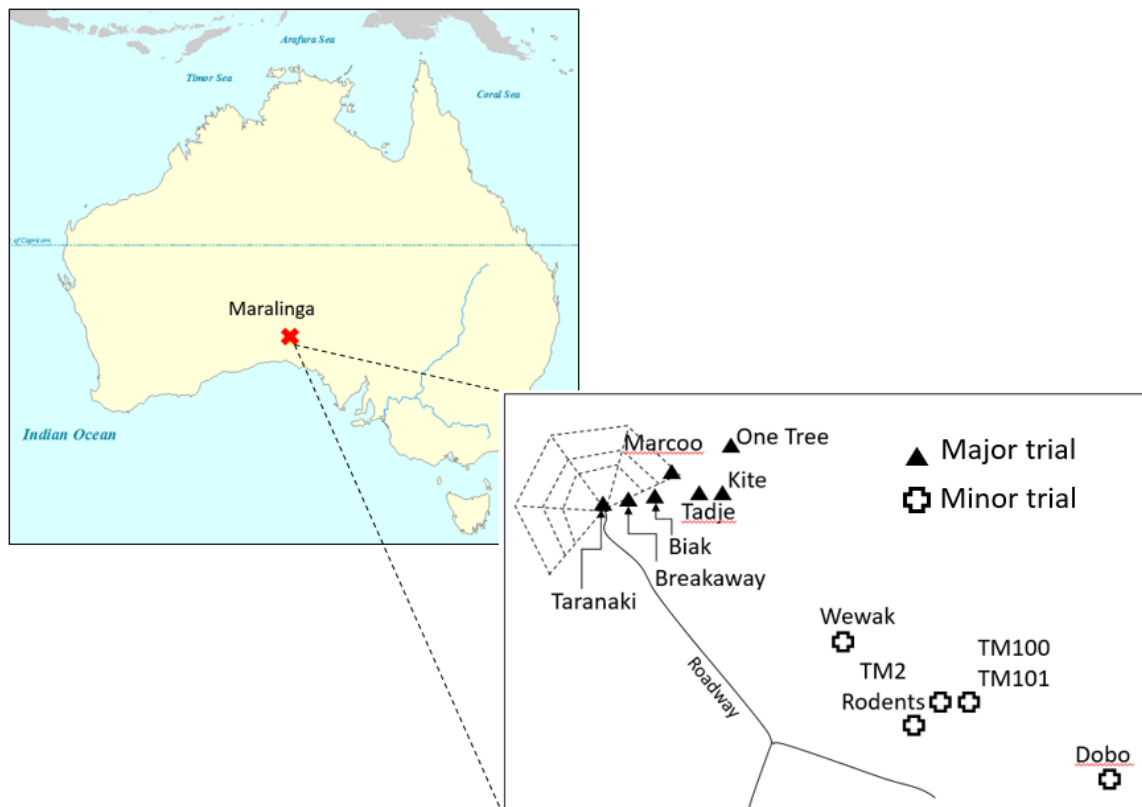
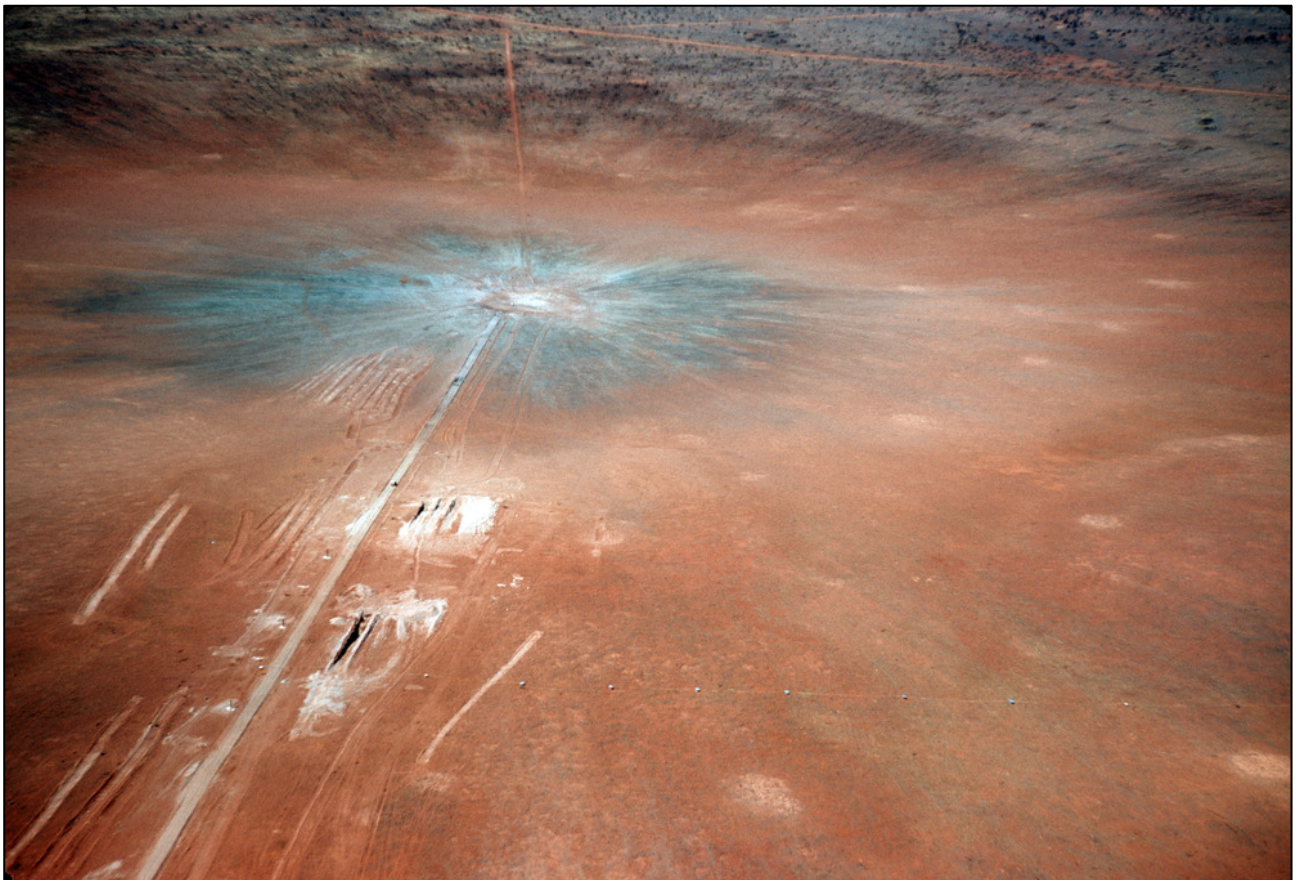*Figure 1 Location of Maralinga nuclear test site*

Figure 2 Ground zero of Taranaki detonation

The twelve major trials of the British Nuclear Testing Programme were carried out with publicity; the minor trials were more secretive. The minor trials were developmental experiments which were

designed to investigate the performance of various component parts of a nuclear device separately and together, to study new ideas, and to investigate how to obtain maximum explosive yield from a given amount of fissile material. [4] Full disclosure of the hazards and potential costs to Australia entailed in the testing program were not shared. Information passed to Australian officials was kept to the minimum necessary to facilitate their assistance in the conduct of the testing program. The use of Pu in the minor trials was not disclosed. [4] A declassification of documents has revealed a minimum of six different weapons were tested with varying design, construction and nuclear components. [5] Pu contaminant characteristics such as composition, atom and element ratios depend on the emitting source (bomb design, ground zero environment), while particle presence, size, structure and oxidation states are closely linked to the release (detonation) scenarios. [6] The withholding of the weapon identification details has affected our ability to assign these characteristics to a source or release scenario, which has limited future predictive capabilities until now. In the case of Pu, two of the most important environmental consequences of this radionuclide's transfer in the terrestrial environment are soil deposition and bioavailability, which were conditioned during nuclear testing from one global region to another by climatic factors, and soil physicochemical properties. [7] Bioavailability and transfer to the human or ecosystem food chain is the main threat to any local population's health. [1,8]

Once Pu has entered the environment, its mobility is affected by its oxidation state, complexing agents, colloid-mediation, erosion/surface water transport and biotic interactions. [9] Local environmental conditions will dictate its behaviour. Pu interactions in the environment are complex and may evolve through time. Site-specific conditions determine which Pu species predominate as well as each species' overall transport and migration characteristics. The interplay between redox transformations [10], complex formation [11], colloidal transport [12], surface erosion [13] and sediment transport [14] makes determinations of Pu migration a difficult and highly site-specific challenge. [3] Field studies suggest that Pu has the potential to migrate, and that variations in the local geology, geochemical conditions, colloidal composition and differences in initial source characteristics are important in controlling its transport. [3,14,15] The variables that may influence overall radionuclide behaviour are numerous, and the related (bio)geochemical responses complex, resulting in difficulties in estimations of radiological trends prior to observation. The ability to observe the migration and accumulation of Pu isotopes in the unique Australian environment also allows some elucidation of the radioecological effects (i.e. complex risk characterisation) these isotopes can have. With this information in hand, we can potentially assess the impact of future events.

Key factors contributing to the overall uncertainties in environmental impact assessments are the source term including radionuclide speciation, mobility, biological uptake and accumulation. For areas contaminated with hot particles, impact assessments will suffer from unacceptably large

uncertainties unless the impact of particles is taken into account. [16] It is important to acknowledge the chemical and physical form of Pu in hot particles entering the environment, which can range from refractory oxides produced at high temperatures to soluble nitrates, carbonates or hydroxides produced by neutron capture in volatilized uranium. [3] Following deposition, particle weathering and subsequent mobilisation of radionuclides depend on particle characteristics (e.g. size distribution, porosity, crystallographic structure and oxidation state of the carrying matrices) and environmental conditions (e.g. soil water pH and concentration of interacting agents, redox conditions and microbial activity). [17] Remediation activities at the Maralinga nuclear test site were based on the presence of particles and the associated overall activity concentration. [2] With an Improved understanding of the possible Pu particle transport, weathering, and bioavailability will lead to more accurate assessments of the long-term impact (greater than 100 years) on the environment and non-human biota inhabiting this site.

1.2. Rationale

Radioecology is a multidisciplinary science, which focuses on understanding and quantifying the behaviour of radionuclides in the environment, and the transportation processes through natural ecosystems to various receptors such as plants, animals and humans. These data are used for assessments of the radiological dose and its effects on humans and their environment from nuclear activities. This thesis seeks to understand and quantify the behaviour of Pu in the soil environment and the environmental variables affecting its transport and migration to identify areas of radioecological sensitivity. The results can improve and validate radioecological models of interest for Australian exposure situations such as Maralinga and Montebello Islands.

1.3. Research Objectives and Scope

This thesis aims to develop new knowledge on the dispersion and migration of Pu isotopes in soils and sediments, using Queensland sediments as a model system; establish model inputs (Kd) describing the transport of Pu in different soil and climate regimes; and characterise the microstructure of Pu particles and their effects on Pu dispersion and availability over time.

The following technical objectives are identified:
1. Quantify the trace amounts of Pu in Australian sediments;
2. Determine the major factors affecting the migration of Pu in the unique Australian environment;
3. Determine site-specific transport and migration phenomena of Pu through column experiments including a comparison of classical batch Kd (solid/liquid partition coefficients) determinations;

4. Characterise the range of chemical and physical attributes of Pu hot particles that can affect transport and weathering processes, and the availability of Pu

1.4. Methods

These objectives are achieved through interagency collaborations, radioanalytical method development, synchrotron analysis techniques and focused-ion beam (FIB) imaging.

1.4.1   Radioanalytical method development

The development of an agile fusion technique is required for the analysis of Pu in sediments of varied and complex chemistry. The procedure aims to improve the previously used acid leaching processes whilst addressing the capacity to employ an increased sample size and the removal of interfering elements for ease of analysis. This would enable research into the radioecological impacts of Pu isotopes in the environment with trace level detection limit and can be utilised in emergency response scenarios producing highly repeatable, succinct and high quality analysis.

1.4.2   Synchrotron analysis techniques

Synchrotron-based imaging is the only technique that achieves the scientific aims of this study, to obtain a quantitative view of the speciation and particle surface chemistry of Pu in soils in an accurate, integrated, and efficient manner. The techniques utilised include SXRF (synchrotron X-ray fluorescence), XANES (X-ray absorption near edge structure), EXAFS (extended X-ray absorption fine structure), XRD (X-ray diffraction) and µXRF-tomography.

1.4.3   FIB imaging

Focused-ion beam (FIB) energy-dispersive X-ray spectroscopy (EDX) provides elemental distribution and texture analysis of Pu hot particles. FIB imaging should be utilized for its reduced resolution at approximately 0.05µm providing definition of the crystal formations, interstitial non-fissile formations, porosity, thermal cracks, and amorphised lines along with areas of structural weakness.

1.5. Thesis structure

Chapter 1 is an overview of the dissertation work. The history of the presence of Pu in the Australian environment, specifically, the Maralinga nuclear test site, is provided underlining the need for site-specific measurements of Pu in the soil environment. The complexity of Pu, referred to as the 'ornery element' by its discoverer Glenn Seaborg, is discussed including the complexities presented by the presence of Pu hot particles. To avoid large uncertainties, radioecological models require site-specific values to appropriately describe the transport and migration of Pu in the

Australian environment. Following this, the rationale, research objectives and methods used for this dissertation are presented.

Chapter 2 addresses objective 1, and describes the development of a trace-level radioanalytical procedure for the analysis of ^{238}Pu and ^{239,240}Pu in a large range of soil/sediment types using fusion for complete destruction of refractive Pu particles. Overall the method maintains a greater than 70% tracer recovery and a trace-level detection limit of 0.04 mBq.g^{-1}. This procedure is utilised throughout all laboratory-based analysis of the dissertation.

Chapter 3 addresses objectives 1 and 2, and determines key environmental indicators of Pu migration and accumulation using the analysis of 73 soil samples from Queensland as a model system. The isotopic ratios of ^{238}Pu:^{239,240}Pu are defined to determine the source term of the measured distal Pu as both Maralinga and Monte Bello Island nuclear detonations. Several samples are used to provide an initial brief examination of the vertical transport of Pu. These data are combined with the National Geochemical Survey of Australia by Geoscience Australia to build an integrated database of physical, chemical and radiochemical soil properties. The key environmental indicators of Pu presence are revealed using this database and a modified Principal Component Analysis (PCA) using distance correlation factors to analyse non-linear relationships. More than 80% of the variance of the system is explained by the chemical characteristics of Pu as an actinide plus the physical variables of the soil environment (wet deposition caused by rainfall with the passing of the detonation plume, geomorphology, landform, and land use).

Chapter 4 addresses objective 3, with the design of a column transport experiment using two soil types (sandy and clay) and two rainfall regimes (high and low) to determine the variability and effect on Pu transport in the soil environment. It is identified that abiotic climatic parameters (rainfall, soil type, weathering) and transformation kinetics (time-dependent Kds) affecting the transport of Pu in similar environmental systems will aid in reducing uncertainties in environmental impact assessments.

Chapter 5 addresses objective 4, and utilises information from particle characterisation experiments to distinguish the composition and texture of hot particles from the Maralinga nuclear test site at the micro-, nano- and atomic scales. The remarkable complexity of the particles validates the requirement for their distinctiveness to be included in environmental impact assessments. Pu is shown to exist predominantly in nano-scale form within the fragile particles; this is significant for the physical breakdown or ingestion of the particles as this will likely result in the release of bioavailable Pu.

Chapter 6 summarises all the findings presented in this thesis, and discusses the applications to current radiation protection practices. Additionally, future research opportunities are proposed.

1.6. References

1. UNSCEAR (1993) Report to the general assembly (Annex B—Exposures from man-made sources of radiation). http://www.unscear.org/docs/reports/1993/1993c_pages%2091-120.pdf. Accessed 7 March 2020

2. MARTAC (2003) Rehabilitation of former nuclear test sites at Emu and Maralinga (Australia) 2003. The Maralinga Rehabilitation Technical Advisory Committee: Canberra, Australia

3. Kersting AB (2013) Plutonium transport in the environment. Inorg Chem 52 (7):3533-3546. doi:10.1021/ic3018908

4. Symonds J (1985) A history of British atomic tests in Australia.

5. Williams G (2020) Antler - Weapon Identification

6. Eriksson M (2002) On weapons plutonium in the Arctic environment (Thule, Greenland).

7. Zhu YG, Shaw G (2000) Soil contamination with radionuclides and potential remediation. Chemosphere 41 (1-2):121-128

8. UNSCEAR (2000) Report to the general assembly (Annex A—Dose assessment methodologies). http://www.unscear.org/docs/reports/annexa.pdf. Accessed 7 March 2020

9. Smith B, Amonette A (2006) The Environmental Transport of Radium and Plutonium: A Review. Institute for Energy and Environmental Research,

10. Zhao P, Begg JD, Zavarin M, Tumey SJ, Williams R, Dai ZR, Kips R, Kersting AB (2016) Plutonium (IV) and (V) sorption to goethite at sub-femtomolar to micromolar concentrations: redox transformations and surface precipitation. Environmental science & technology 50 (13):6948-6956

11. Bagawde S, Ramakrishna V, Patil S (1976) Complexing of tetravalent plutonium in aqueous solutions. Journal of Inorganic and Nuclear Chemistry 38 (7):1339-1345

12. Kersting A, Efurd D, Finnegan D, Rokop D, Smith D, Thompson J (1999) Migration of plutonium in ground water at the Nevada Test Site. Nature 397 (6714):56

13. Xu Y, Qiao J, Hou X, Pan S (2013) Plutonium in soils from northeast China and its potential application for evaluation of soil erosion. Scientific reports 3:3506

14. Everett SE, Tims SG, Hancock GJ, Bartley R, Fifield LK (2008) Comparison of Pu and (137)Cs as tracers of soil and sediment transport in a terrestrial environment. J Environ Radioact 99 (2):383-393. doi:10.1016/j.jenvrad.2007.10.019

15. Hakonson TE (2007) The distribution and transport of radionuclides in dryland ecosystems. Radioactivity in the Environment 10:177-191. doi:10.1016/s1569-4860(06)10008-x

16. Salbu B (2001) Actinides associated with particles. Radioactivity in the Environment 1 (C):121-138. doi:10.1016/S1569-4860(01)80011-5

17. Salbu B, Lind O, Skipperud L (2004) Radionuclide speciation and its relevance in environmental impact assessments. Journal of Environmental Radioactivity 74 (1-3):233-242

1　# Agile fusion method for the determination of Pu

2　# isotopes in diverse sediments

3　Megan Cook[1]

4　*[1]School of Earth, Atmosphere & Environment, Monash University, Wellington Road,*

5　*3800 Clayton, Australia*

6　## Abstract

7　Atmospheric nuclear testing has occurred worldwide resulting in trace amounts of

8　plutonium (Pu) isotopes in soils and sediments across the globe. Soil and sediments can

9　vary greatly in both physical and chemical properties within close geographic regions

10　presenting a major challenge for sample preparation in the analysis of fallout

11　radionuclides. An agile method for the analysis of Pu isotopes in soils/sediments has been

12　developed utilizing borate and peroxide fusion, TEVA extractive chromatographic resin,

13　and alpha spectrometry. The integration of borate and peroxide flux materials creates a

14　sample dissolution procedure that is greater than the sum of its parts. This method is

15　applicable to the analysis of $^{239/240}$Pu in soil/sediment samples ranging from 0.05-5000

16　mBq/g achieving ^{242}Pu tracer recoveries between 50-94%, with a trace-level detection

17　limit of 0.04 mBq/g and measurement uncertainties down to 19%, adjustable to

18　measurement priorities with variation in count time. Achieving these parameters provides

19　a highly adaptable standard method for $^{239/240}$Pu in soil/sediment analysis applicable to

20　samples from radioecological research at trace environmental levels to emergency

21　response scenarios with 48-hour turn-around producing highly repeatable, succinct and

22　high-quality analysis.

23　## Keywords

24   Plutonium, soil, sediment, fusion, alpha spectrometry

Introduction

26   Plutonium (Pu) isotopes, ^{240}Pu ($T_{1/2}$ = 6561 years), and ^{239}Pu ($T_{1/2}$ = 24,110 years) are

27   artificially produced and have long half-lives with alpha emissions and high radiological

28   toxicities. They appear in the environment as a result of global and local fallout from

29   atmospheric nuclear weapons tests (1945–1980) (Waters, Syvitski et al. 2015), and

30   fateful nuclear accidents like Chernobyl (1986) and Fukushima (2011) (IAEA 2015).

31   They are also produced in the normal operation of nuclear installations as waste in re-

32   processing of nuclear fuels. Experiences with significant radiological incidents have

33   shown that extensive measurement of environmental samples is required in response to

34   the incident. During the initial response, the measurement of environmental samples must

35   be conducted as rapidly as possible in order for timely decision-making. Later, during the

36   recovery phase, the measurement time-frames may increase, but so too does the number

37   of samples requiring measurement. This high workload can easily overwhelm the

38   capacity of a radioanalytical laboratory. The development of rapid radiochemical

39   methods with appropriate measurement quality objectives and a compromise between

40   precise analytical determinations and the timeliness necessary for emergency response

41   activities is required. To better assess Pu mobility in non-emergency exposure scenarios,

42   detailed long-term monitoring of Pu activity, involving adequate bulk sample collection

43   and radioanalytical measurements, is required. For example, the benefit of detailed

44   monitoring before (background), during, and after an accidental release would enable a

45   more complete assessment of the extent of plutonium activity in the affected

46   environment. In the context of an accidental release long-term Pu monitoring utilising the

47   methodology described herein would enable assessment of proximal high levels of

48   contamination, distal trace-levels of contamination and everything intermediary. The

49   affected soil/sediment samples of unspecified mineral content and chemistry require a

50   robust and comprehensive dissolution technique to achieve accurate and precise analysis

51   of the contaminant Pu. Although a large number of methods have been established for

52   analysis of actinides in soil or sediment samples (Croudace, Warwick et al. 1998,

53   Guogang, Testa et al. 1998, Kim, Lee et al. 1998, Galindo, Mougin et al. 2007, Maxwell

54   2008, Harrison, Zawadzki et al. 2011, Tims, Fifield et al. 2013, Reading, Croudace et al.

55   2015, Sahli, Röllin et al. 2017, Luo, Xing et al. 2018, Sáez-Muñoz, Ortiz et al. 2020)

56   many of them are tedious, time-consuming and may not achieve complete dissolution or

57   be sufficiently sensitive to meet the measurement objectives. Pu presents

58   physicochemical behaviors that are among the most complexof any element in the

59   periodic table. (Clarke, Dunster et al. 1996) The pure element exhibits seven distinct

60   crystal phases, is highly reactive, and is known to form compounds, complexes, or alloys

61   with virtuallyevery other element. When elemental plutonium reacts to give up its

62   valence electrons, it can form a wide variety of positively charged ions with the ability

63   toform up to twelve chemical bonds to other ions or molecules in solution. The element

64   can exhibit five oxidation states, and under certain chemical conditions, four different

65   oxidation states can be present in appreciable amounts simultaneously. (Clarke, Dunster

66   et al. 1996) Pu resuting from nuclear detonations is likely to be refractory, having been

67   exposed to the intense heat of a nuclear or radiological explosion and, as evidenced by

68   Maxwell, Hutchison (Maxwell 2008), may result in up to 40% deficiency in analyte

69   recovery if complete dissolution is not achieved. Historically, acid leaching (incomplete

70   dissolution) has been the preferred sample preparation technique for soils or sediments

71   (Guogang, Testa et al. 1998, Kim, Lee et al. 1998, Lu, Kung et al. 1998, M. Toribio, J.F.

72   Garc´ıa et al. 2001, Taylor, Warneke et al. 2003, Child, Hotchkis et al. 2008, Maxwell

73   2008, Harrison, Zawadzki et al. 2011, Tims, Fifield et al. 2013) with the possibility of

74   larger sample sizes to achieve lower detection limits and ease of analysis with fewer

75   matrix interferences in subsequent separations. Heat, pressure, or chemical attack is

76   affective for most matrices but leaves mineral refractory particles unaffected (Maxwell

77   2008). Pu associated with these refractory particles is resilient to acid leaching

78   techniques, which renders these sample preparation methods inappropriate for the

79   analysis of Pu isotopes in soils or sediments.

80   Fusion overcomes the obstacle of refractory particles providing a complete dissolution of

81   all minerals and silicates within minutes resulting in a hot, lava-like melt that becomes

82   crystalline and dissolvable in a weak acid. Borate fusion is well established as a sample

83   digestion or dissolution method in analytical chemistry and geochemistry and is known to

84   be effective in dissolving minerals and rocks comprising oxides, carbonates, chlorides,
85   sulfates, and phosphates. It can also be applied to organic, sulphidic and even metallic
86   materials if preceded by an oxidation step (Reading, Croudace et al. 2015, Sahli, Röllin et
87   al. 2017, Luo, Xing et al. 2018, Sáez-Muñoz, Ortiz et al. 2020). A robust oxidation-
88   reduction process leaves the constituent elements in a more soluble form achieving
89   complete dissolution. Borate fusion salts have been previously selected as fusion flux
90   materials due to their ability to rapidly and effectively dissolve higher amounts of sample.
91   (Braysher, Russell et al. 2019) Customisation of fusion salts for sample-specific
92   chemistry can be performed, however, lithium meta/tetraborate is agile and has the
93   capability to dissolve difficult material (silicates, oxides, sulfates) as well as dissolving
94   carbonates and halides. This makes it very attractive where rapid digestions of varied
95   soil types of unspecified chemistry are required. Fusion with sodium peroxide offers
96   similar benefits in terms of destruction of refractory particles, and complete dissolution
97   whilst avoiding the use of hydrofluoric acid. Sodium peroxide fusion destroys the lattice
98   structure of soils and sediments to greatly improve the accuracy of refractory particle
99   species, in addition to reducing analysis time and volume of reagents in comparison with
100   leaching procedures. The use of lithium meta/tetraborate or sodium peroxide as a molten
101   flux can overcome the problem associated with the partial dissolution of minerals. The
102   method presented herein utilises the highly oxidative properties of sodium peroxide and
103   the efficacious properties of both borate and peroxide as fusion flux products to expedite
104   sample preparation by removing the need for the destruction of organic material prior to
105   fusion creating a sample dissolution procedure that is greater than the sum of its parts.

106   Following this, a trace level detection limit for Pu isotopes is achievable analysing
107   samples larger than one gram using alpha spectrometry or mass counting techniques
108   (ICP-MS). Alpha spectrometry can provide complete isotopic information about alpha-
109   emitting Pu isotopes, ^{238}Pu, $^{239+240}$Pu, and radioactive Pu tracers e.g. ^{242}Pu, are also
110   detected straightforward in the same spectra. Alpha spectrometry is the most frequently
111   used technique for the routine determination of Pu isotopes due to the relatively high
112   sensitivity, selectivity, and the relatively low-cost instrumentation that is well adapted for
113   high through-put routine analyses using multi-chamber spectrometers. (Vajda and Kim
114   2010) In general, the sensitivity of quadrupole ICP-MS for ^{239}Pu and ^{240}Pu is typically

115   not higher than that of alpha spectrometry, the basic advantage is that the ^{239}Pu/^{240}Pu ratio

116   can be measured. On the other hand the short-lived ^{238}Pu can be determined only by alpha

117   spectrometry, which means that the two techniques are complementary and do not

118   replace each other. Greatly improved automated fusion systems are commonly available

119   in radioanalytical laboratories for highly repeatable processes and greatly decreased

120   preparation and separation times. The accessibility and cost of alpha spectrometry or

121   ICP-MS techniques combined with succinct, high-quality sample preparation mean the

122   rapid determination of trace levels of Pu in sediments in large numbers is realised.

123   To obtain the best results for analysing ultra-trace levels of actinides in environmental

124   samples, the specificity of the sample matrix, the requirements for measurement

125   techniques, and the costs of labour and reagents should be considered to develop optimal

126   preconcentration and radiochemical separation procedures. The procedure presented here

127   improves on the historically used acid leaching processes whilst addressing the capacity

128   to employ an increased sample size with commonly available equipment, and the removal

129   of interfering elements for ease of analysis using accessible, low-cost analysis techniques.

130   A major benefit is the completion of sample preparation and analysis within 48 hours.

131   This development can be utilised within emergency response scenarios producing highly

132   repeatable, succinct analysis with a rapid turn-around-time as well as enabling research

133   into the radioecological impacts of Pu isotopes in the environment with its high

134   throughput, trace level detection limit and high-quality analysis.

135   Improvements in the application of lithium borate and peroxide fusions are presented for

136   the determination of Pu isotopes in a diverse range of sediments, at an increased sample

137   mass, with varying physical and chemical properties. Fusion with lithium borates plus a

138   sodium peroxide oxidative catalyst provides a robust sample dissolution technique.

139   Complete dissolution is followed by an oxalate co-precipitation for separation from

140   interfering soil matrix ions and utilisation of TEVA® extraction chromatographic resin to

141   separate Pu from interfering isotopes. Samples are analysed using alpha spectrometry

142   with the possibility of ICP-MS analysis using the same preparation procedure.

143   **Experimental**

144   All reagents used were of analytical grade and used without further purification. TEVA

145   resin (100-150µm) was supplied from Eichrom Technologies, Inc. The [242]Pu tracer was

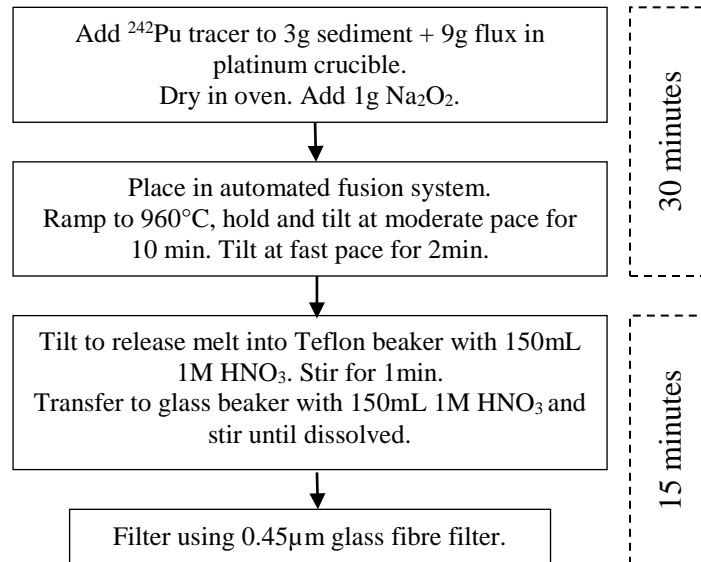146   obtained from and is traceable to NIST.

147   *Sediment samples*

148   All sediment samples used for the development of this method were supplied by

149   Geoscience Australia as part of the National Geochemical Survey of Australia (Caritat,

150   Cooper et al. 2009, Caritat and Cooper 2011). Bulk samples were <100 g, dried in an

151   oven at 80 degrees Celsius, homogenized via mechanical mixing, and sieved using

152   calibrated drum sieves to separate out the <75µm fraction and stored in double sealed

153   Ziploc bags. Aliquots of samples for analysis were accurately weighed into separately

154   labelled weighing boats for immediate analysis. Certified reference material IAEA-385,

155   Irish Sea Sediment, and Maralinga nuclear detonation site soils were used for method

156   validation.

157   *Sample Preparation*

158   Fusion was performed using the Katanax automated fusion system with a standard 30 mL

159   platinum crucible and $Li_2B_4O_7$ (66.67%): $LiBO_2$ (32.83%) flux, LiI (0.50%) wetting

160   agent plus sodium peroxide as an oxidative catalyst. Figure 1 provides a flow chart of the

161   initial sample preparation method for Pu isotopes in sediments. A sediment sample (3g)

162   was placed in a platinum crucible with lithium borate flux (9g, 3:1 ratio), spiked with 0.1

163   Bq [242]Pu, and placed in an oven to dry. Once dry, the sample mixture was combined until

164   homogenous. Immediately prior to fusion, sodium peroxide (1g) was added to the

165   mixture, well combined and the crucible was placed in the fusion system. The fusion

166   program was set to ramp up to 960°C, hold temperature and tilt at a moderate pace for 10

167   minutes, at a slow pace for 2 minutes then tilt fully to release the melt into a Teflon

168   beaker stirring 150mL 1M HNO_3.

169

170 Figure 1. Fusion preparation method for diverse sediments
171

```
┌─────────────────────────────────────────────┐        ┌ ─ ─ ┐
│  Add ²⁴²Pu tracer to 3g sediment + 9g flux in │
│               platinum crucible.              │          30 minutes
│          Dry in oven. Add 1g Na₂O₂.           │        
└─────────────────────────────────────────────┘        
                      │                                 
                      ▼                                 
┌─────────────────────────────────────────────┐        
│       Place in automated fusion system.       │        
│  Ramp to 960°C, hold and tilt at moderate pace │
│    for 10 min. Tilt at fast pace for 2min.    │        └ ─ ─ ┘
└─────────────────────────────────────────────┘        
                      │                                 ┌ ─ ─ ┐
                      ▼                                 
┌─────────────────────────────────────────────┐        
│  Tilt to release melt into Teflon beaker with │          15 minutes
│           150mL 1M HNO₃. Stir for 1min.       │
│  Transfer to glass beaker with 150mL 1M HNO₃  │        
│            and stir until dissolved.          │        
└─────────────────────────────────────────────┘        
                      │                                 
                      ▼                                 
┌─────────────────────────────────────────────┐        
│     Filter using 0.45µm glass fibre filter.   │        └ ─ ─ ┘
└─────────────────────────────────────────────┘        
```

187

188 The melt began to dissolve immediately and was transferred to a glass beaker containing
189 150mL 1M HNO_3 (300mL total sample solution) to complete the dissolution. Once
190 dissolved, the solution was filtered using 0.45µm glass-fiber filters to remove any excess
191 borate flux.

192 A calcium oxalate precipitation was utilised to concentrate and separate the Pu from its
193 matrix. Calcium chloride (1mL, 250mg/mL) and oxalic acid (4g) were added to the
194 sample and the pH was adjusted to 2-2.5 using ammonium hydroxide. $Ca(Pu)C_2O_4$ was
195 precipitated and centrifuged to collect. 3M HNO3 (20mL) was added to dissolve the
196 sample then stirred at 50°C for 15 minutes to ensure complete dissolution. If a large
197 volume centrifuge is not available, the precipitate can be left to settle for approximately 4
198 hours or overnight. Once settled, the supernatant can be decanted and the precipitate
199 rinsed and centrifuged for collection.

200 Valence adjustment was required prior to the use of TEVA resin to ensure that Pu is in
201 the 4+ oxidation state. Sodium nitrite (0.14g) was added to the solution, heated and
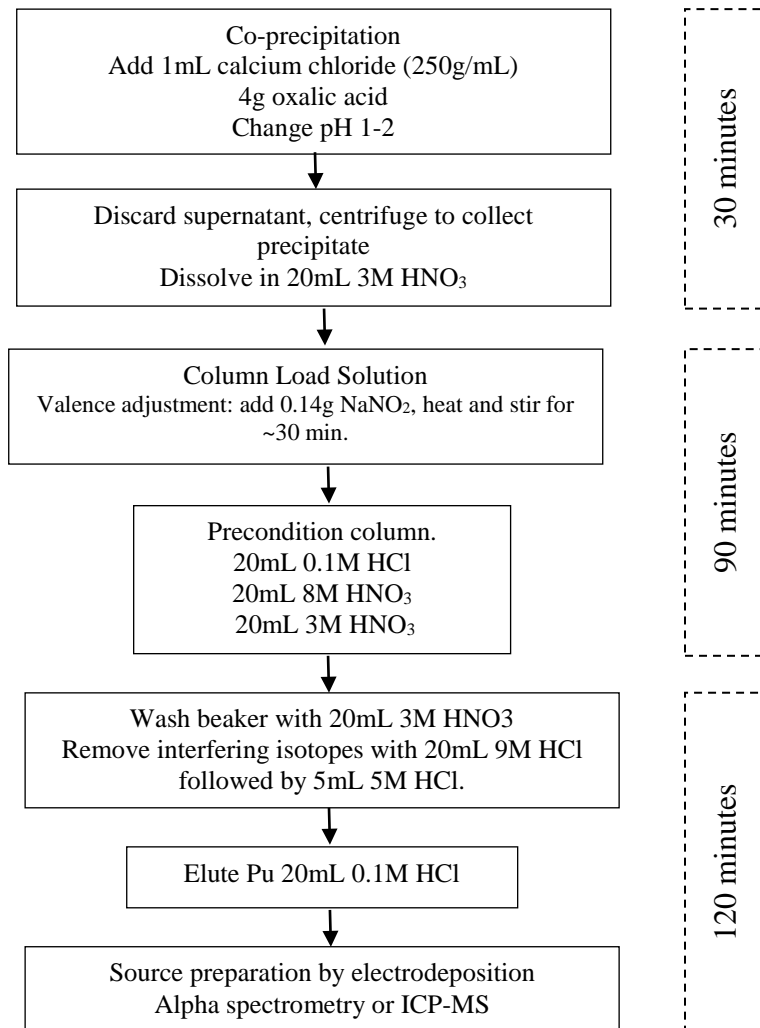202 stirred for approximately 15 minutes.

203

Column separation

205 Figure 2 provides a flow chart of the column separation method using TEVA resin for the
206 extraction of Pu. The TEVA resin (2mL) was loaded into empty columns and
207 preconditioned using 0.1M HCl (20mL), 8M HNO$_3$ (20mL) followed by 3M HNO$_3$
208 (20mL). After the dissolution of the oxalate precipitation, the sample was loaded onto the
209 column at an approximate flow rate of 1 mL/min. Wash/rinse aliquots can be loaded at a
210 flow rate of 3mL/min. The sample beaker was then washed with 3M HNO$_3$ (20mL) to
211 ensure a complete transfer and stable column load. To remove interfering isotopes, the
212 column was rinsed with 9M HCl (20mL) and 5M HCl (5mL) before eluting Pu with 0.1M
213 HCl (20mL). Figure 3 shows the resulting Pu spectra clean of interfering isotopes. The
214 elution was then transferred to a beaker and several drops of NaHSO$_4$ added to change Pu
215 to the sulfate salt for ease of final dissolution prior to evaporating to dryness.

216 *Source Preparation*

217 Electrodeposition was used to prepare the source for alpha spectrometry using a sulfate
218 system at pH 2 with stainless steel disks. The dried sample was dissolved with 10mL
219 NaSO$_4$ at pH 2 and transferred to an electrodeposition cell with a stainless steel disk and
220 platinum anode. The sample was deposited at 0.45 Amps for 1.5 hours with NH$_4$OH
221 added for the last minute to cease the deposition. Once complete, the stainless steel disk
222 was removed, rinsed with ethanol, and air-dried. Finally, the source was counted on a
223 Canberra Alpha Analyst on the first shelf for 1440 minutes.

224

225 Figure 2. The chromatographic extraction method for Pu isotopes in sediments
226
227
228
229
230
231

| Co-precipitation |
| Add 1mL calcium chloride (250g/mL) |
| 4g oxalic acid |
| Change pH 1-2 |

30 minutes

232 Discard supernatant, centrifuge to collect
233 precipitate
234 Dissolve in 20mL 3M HNO$_3$

235
236 Column Load Solution
237 Valence adjustment: add 0.14g NaNO$_2$, heat and stir for
238 ~30 min.
239

240 Precondition column.
241 20mL 0.1M HCl
242 20mL 8M HNO$_3$
243 20mL 3M HNO$_3$
244

90 minutes

245
246 Wash beaker with 20mL 3M HNO3
247 Remove interfering isotopes with 20mL 9M HCl
248 followed by 5mL 5M HCl.
249

250 Elute Pu 20mL 0.1M HCl
251
252
253 Source preparation by electrodeposition
254 Alpha spectrometry or ICP-MS

120 minutes

Results and discussion

255

256 *Sample Preparation*

257 Sample decomposition through fusion is employed most often for samples that are
258 difficult to dissolve in acids such as soils, sludges, silicates, and some mineral oxides.
259 Fusion involving Li$_2$B$_4$O$_7$ (66.67%): LiBO$_2$ (32.83%) flux and LiI (0.50%) wetting agent
260 was sufficient for the complete dissolution of the certified reference material. For fusion
261 to be successful, the sample must contain chemically bound oxygen as in oxides,
262 carbonates and silicates. To increase the capacity of these varying samples to be fused

263 sodium peroxide, a strong oxidising agent and common fusion flux material, was added

264 as a catalyst. This addition resulted in faster, complete fusions with a smaller melt that

265 was easier to dissolve.

266 Figure 3. ^{242}Pu, $^{239/240}$Pu, and ^{238}Pu isotopes after removal of interfering isotopes

267
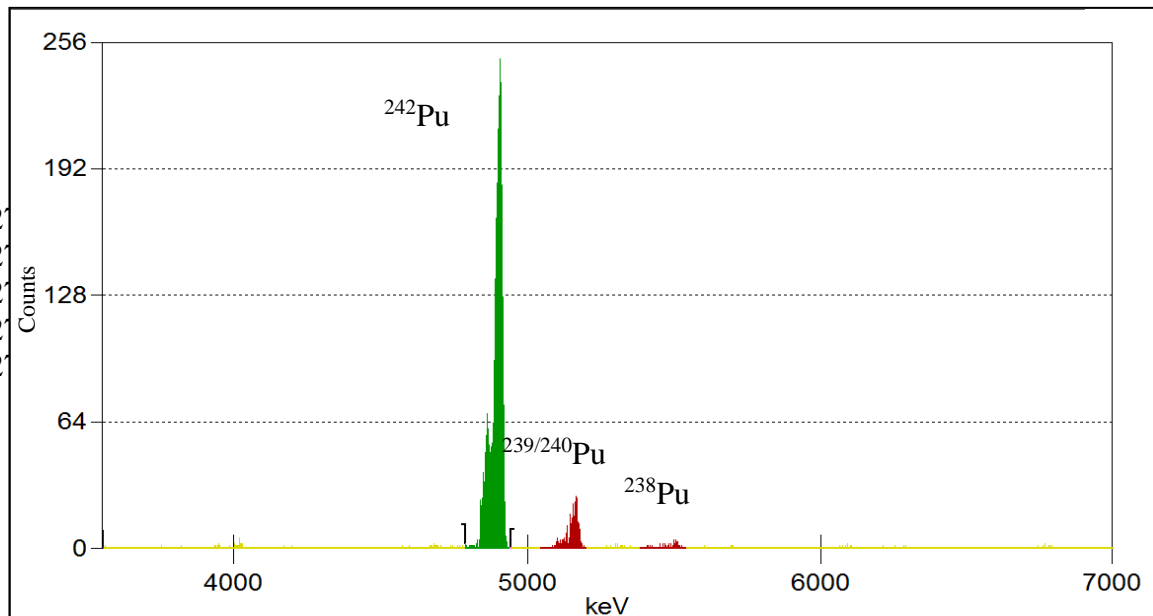
286 The addition of sodium peroxide expedites the complete destruction of soil/sediment

287 samples as it removes the need for a pre-ashed sample, the destruction of organic material

288 in a furnace prior to fusion. This can drastically reduce the sample preparation time (up to

289 16 hours! (Sahli, Röllin et al. 2017)). The use of a standard 30mL platinum crucible for

290 automated fusion means no special equipment is required ensuring that radioanalytical

291 laboratories within emergency response networks can apply the method presented as a

292 standard method for sample preparation. The sample mass (3g) ensures that there is less

293 impact on bulk sampling requirements whilst also reaching trace-level detection limits.

294 The consideration of these factors for sample preparation enhances an already rapid

295 procedure and reduces the burden of resources on radioanalytical laboratories.

296 For large research or environmental monitoring programs with a high throughput of

297 varied sample analysis, combining the strengths of borate and peroxide fluxes makes it

298 possible to achieve complete dissolution of soil/sediment samples without needing prior

299 knowledge of mineralogical makeup. The integration of borate and peroxide fluxes
300 provides increased consistency of results over the diverse sediment chemistries (Table 5).

301 *Plutonium separation*

302 Co-precipitation is a technique utilized often in radiochemical separations due to the
303 ability to exploit the similarities of radioactive and non-radioactive elements. Calcium
304 oxalate was chosen to separate Pu from its fusion matrix for the reason that abundant
305 inorganic sediment species (e.g Fe, K, Na) dissolved in the melt along with Pu, remain in
306 solution and no longer present a matrix interference for further chemical separations.
307 Using oxalate co-precipitation, controlling the pH and keeping it below pH 3, ensures
308 silicates that can clog up a column remain in solution and are removed via centrifugation.
309 This removes the need for PEG-silicate precipitation prior to plutonium separation
310 resulting in a streamlined, faster purification process. In addition, the only interfering
311 isotopes that may be co-precipitated along with Pu are thorium isotopes, which are
312 readily separated using TEVA resin.

313 TEVA resin has an active component of an aliphatic quaternary amine and is specific for
314 tetravalent actinides. Valence adjustment is required to ensure all available Pu is in the 4+
315 state prior to loading onto the column. Exposure of Pu to oxygen and water in the natural
316 environment results in the formation of PuO_{2+x} with the presence of four oxidation states
317 (3, 4, 5 and 6) possible. Sample preparation using fusion as described here creates a high
318 temperature system which oxidises Pu^{3+} to Pu^{4+}, removes water to form PuO_2 eliminating
319 the higher oxides and therefore leaving Pu^{4+} in the fusion melt. (Haschke, Allen et al.
320 2000) Increased valence adjustment of the column load solution to include the reduction
321 of Pu^{6+} to Pu^{4+} was investigated with no appreciable change in Pu recovery. Horwitz,
322 Dietz et al. (1995) show that Pu^{4+} is strongly held at 3M HNO_3 while thorium isotopes
323 are easily separated at 9M HCl. This results in the clean spectra seen in Figure 3.

324 Electrodeposition was chosen as the source preparation for alpha spectrometry analysis
325 due to the reliability and resolution afforded by the technique. An electrodeposition
326 procedure should produce good quality sources that lead to high deposition yields

327 (>90%), save time, and be sufficiently straightforward. A sulfate system achieves each of
328 these requirements for Pu analysis.

329 *Method Validation*

330 The following parameters have been determined with the use of certified reference
331 materials, replicate analysis, testing of blank samples, and a comparison of results:
332 accuracy, precision, uncertainty, and minimum detectable limit. Measurement quality
333 objectives to be achieved for application to emergency response scenarios and
334 environmental research or monitoring are defined in Table 1. All uncertainties and
335 detection limits were determined using the Kragten method. (Kragten 1994) In the
336 development of this procedure, the certified reference material IAEA-385 Irish sea
337 sediment was chosen as a representative analog for the sediment samples to be analysed
338 in a future study. Applied to IAEA-385 with a 24-hour count time, this method gave an
339 average ^{242}Pu tracer recovery of 77.9% (RSD: 11%) and $^{239/240}$Pu recovery of 95.4%
340 (RSD: 1.38%) (Table 2). This shows good agreement with the certified reference
341 activities and exhibits the reliability of the method. The minimum detection limit was
342 determined with replicate analysis of reagent blank samples, flux materials with ^{242}Pu
343 tracer only. With a detector efficiency of 31%, a 7-day cumulative background count, 24-
344 hour sample count, and average tracer recovery of 95.3% (RSD: 2.9%), the average
345 reagent blank net count rates were 0.0007 counts per minute (CPM). This results in a
346 trace-level detection limit of 0.04 mBq/g (0.0056 net CPM) (RSD: 15.1%) (Table 3).

347 **Table 1 Measurement Quality Objectives**

Variable	Emergency response scenario	Environmental research or monitoring
Measurement uncertainty	<50%	<20%
Detection/reporting limit	<100mBq/g	<0.1mBq/g
Timeframe	<48 hours	>10 samples/week

348

349

350 **Table 2 Certified Reference Material IAEA385**

Sample ID	$^{239+240}$Pu measured mBq/g	Uncert. k=2	Uncert. %	$^{239+240}$Pu reference mBq/g	$^{239+240}$Pu recovery %	^{242}Pu tracer recovery %	detection limit mBq/g
1	2.78	0.30	11		94	91	0.04
2	2.84	0.47	16		96	84	0.04
3	2.80	0.49	17		95	75	0.04
4	2.84	0.47	17	2.98 (2.81-3.13)	95	82	0.04
5	2.80	0.49	18		94	77	0.04
6	2.90	0.62	21		97	68	0.04
7	2.88	0.62	18		97	68	0.04
Average	2.83	1.33	16.91		95.36	77.94	0.04
Std Dev	0.04	0.11	3.20		1.31	8.57	0.00
% RSD	1.56				1.38	11.00	0.00

351

352 **Table 3 Reagent blank replicate analysis**

Sample ID	^{242}Pu tracer recovery %	Detection Limit mBq/g
B1	93.6	0.04
B2	92.4	0.05
B3	96.5	0.06
B4	97.2	0.04
B5	91.9	0.04
B6	99.6	0.04
B7	95.7	0.04
Average	95.3	0.04
Std Dev	2.8	0.01
%RSD	2.9	15.09
Reagent blank net counts *		0.0007
Detection limit net counts*		0.0056

*counts per minute over 24-hour count

353

354 High activity samples from a former nuclear test site at Maralinga, Australia showed
355 good linearity and high-quality results with an average activity concentration of 6125
356 mBq/g (RSD: 7%), overall uncertainty of 6.6% and ^{242}Pu tracer recovery of 86% (RSD:
357 7.5%) over a 24-hour count (Table 4). The range of applicability of the method, including

interferences, was tested using sediments supplied by Geoscience Australia from the
National Geochemical Survey of Australia (NGSA) (Caritat and Cooper 2011). Table 6
displays the descriptive statistics of the complex sample chemistries and physical
attributes. The activity concentration of these samples ranged from 0.04-0.22 mBq/g with
an average uncertainty of 60% and an average tracer recovery of 69% (RSD: 25%) over a
24-hour count (Table 5). Extending to a 3-day count reduced the uncertainty of these
measurements to an average of 19%. The extended count time for these low activity
samples achieves the measurement quality objectives for application with environmental
measurements. This shows good applicability to such a large range of samples with 50-
94% tracer recovery. The detection limit varied slightly by 4.9% based on background
and reagent blank.

Table 4 High activity Maralinga sample analysis

Sample ID	Major mineralogy	$^{239/240}$Pu mBq/g	Uncert. k=2	Uncert. %	^{242}Pu tracer recovery %	Detection Limit mBq/g
M1		6700	200	3.0	92.6	0.04
M2	SiO_2,	6200	400	6.5	90.4	0.04
M3	Fe_2O_3, OM[*], Ca	6000	700	11.7	78.2	0.04
M4		5600	300	5.4	84.3	0.04
Average		6125	221	6.6	86.4	0.04
Std Dev	-	457	216	3.7	6.5	0.00
%RSD		7			7.5	0.00

*organic matter by loss on ignition

Table 5 Environmental sample analysis

Sample ID	Major mineralogy	$^{239/240}$Pu measured value mBq/g	Uncert. k=2	Uncert. %	^{242}Pu tracer recovery %	Detection Limit mBq/g
S0542	SiO_2, Al_2O_3	0.09	0.07	80.23	50.04	0.04
S0841	SiO_2, Al_2O_3, Fe_2O_3	0.04	0.04	93.02	93.57	0.04
S1364	SiO_2, Al_2O_3, Fe_2O_3, Cu, Zn	0.17	0.09	55.62	51.97	0.04
S1274	SiO_2, Al_2O_3	0.15	0.08	52.35	79.54	0.05
S0144	SiO_2, Al_2O_3, Fe_2O_3, Ni, Mn, Co	0.15	0.08	54.42	62.35	0.04
S0585	SiO_2, Al_2O_3, Fe_2O_3	0.15	0.09	59.86	51.76	0.04
S0568	Al_2O_3, SiO_2, OM	0.19	0.09	46.77	64.62	0.04

S0044	SiO$_2$		0.09	0.06	59.57	90.67	0.04
S0654	SiO$_2$		0.08	0.06	70.37	73.79	0.04
S1190	SiO$_2$, Al$_2$O$_3$		0.22	0.08	36.74	92.09	0.04
S0830	SiO$_2$, Al$_2$O$_3$, Fe$_2$O$_3$, Pb		0.22	0.11	47.32	50.99	0.04
Average			0.14	0.08	59.66	69.22	0.04
Std Dev	-		0.06	0.02	16.10	17.53	0.00
%RSD			41.46	25.11	26.98	25.33	4.86

372

373 **Table 6 Descriptive statistics of diverse sediment samples**

Category	Variable	Unit	Maximum	Minimum	Mean	Std Dev
Chemical Variables	SiO$_2$	XRF %	97.1	27.7	70.5	10.8
	TiO$_2$	XRF %	7.1	0.4	1.2	0.9
	Al$_2$O$_3$	XRF %	26.0	0.5	11.3	3.9
	Fe$_2$O$_3$	XRF %	14.7	0.1	4.3	2.2
	MgO	XRF %	3.1	0.0	0.7	0.5
	MnO	XRF %	0.2	0.0	0.1	0.0
	CaO	XRF %	5.5	0.0	0.8	0.8
	Na$_2$O	XRF %	2.8	0.0	0.8	0.7
	K$_2$O	XRF %	3.2	0.0	1.3	0.7
	P$_2$O$_5$	XRF %	0.4	0.0	0.1	0.1
	LOI	%	42.5	1.6	8.9	5.8
	pH	-	8.8	3.8	6.1	1.0
	E:C	-	6310.0	4.0	183.5	796.7
Physical Variables	Sand	%	97.3	19.3	46.0	21.6
	Silt	%	61.5	2.1	40.4	15.4
	Clay	%	35.4	0.5	12.3	7.7

374

Using an oxalate co-precipitation can form complexes with a range of metal-bearing minerals (Ca, Cd, Co, Cu, Mn, Sr, Zn, Ni, and Pb) which can impact Pu recoveries. Any sample with a significant component of these elements will form a larger amount of precipitate which may cause some column blocking on the TEVA resin resulting in a reduced Pu recovery. This can be seen in samples S0830 (SiO$_2$, Al$_2$O$_3$, and Fe$_2$O$_3$ with increased Pb content), S0144 (SiO$_2$, Al$_2$O$_3$, and Fe$_2$O$_3$ with increased Mn content), and IAEA385 (increased TiO$_2$). In the case of IAEA385, this has resulted in a slight but consistent negative skewing of $^{239/240}$Pu recoveries (Table 2). This is one factor but it is

383   not clear that this is the controlling factor of reduced tracer recovery. Though there is
384   some small evidence of column blocking, there are no clear trends within the sample
385   chemistry to predict an increased or decreased tracer recovery. Therefore, we can confirm
386   that this method is optimised and fit for application to a diverse range of soils/sediments.

387   The method presented achieves the measurement quality objectives for emergency
388   response scenarios using a 24 hour count time, a reporting limit of 1 mBq/g with 35%
389   overall uncertainty at the reporting limit, and a total turn-around-time, including reporting
390   of results, of less than 48 hours. One analyst can easily complete 40 samples within one
391   week without over-burdening and using standard radioanalytical laboratory equipment.
392   Extending to a 3 day count time enables a reduced 19% overall uncertainty and achieves
393   both prompt throughputs of a large number of samples, with high quality, sufficient
394   sensitivity, and a trace-level detection limit for radioecological research or environmental
395   monitoring practices.

396   **Conclusions**

397   Pu isotopes present in soil/sediments may result from nuclear detonations and fallout
398   increasing the likelihood of a refractory form. Fusion as a sample preparation technique
399   provides an efficient, complete dissolution of solid samples for radiochemical analysis.
400   The integration of borate and peroxide fluxes has enabled the preparation of a diverse
401   range of complex sediment chemistries with a tracer recovery of 50-94% applicable to
402   both emergency response scenarios and environmental research or monitoring as a
403   standard, routine procedure. The measurement quality objectives have been achieved for
404   emergency response scenarios with a reporting limit of 1 mBq/g, measurement
405   uncertainty of 35%, and results available within 48 hours. Extending the alpha
406   spectrometry counting time from 24 hours to 3 days achieves the measurement quality
407   objectives for environmental research or monitoring with a trace-level detection limit of
408   0.04 mBq/g, measurement uncertainty of 19% and the ability to analyze up to 40 samples
409   per week for prompt analysis of large sample datasets.

Acknowledgments

References

Braysher, E., B. Russell, S. Woods, M. García-Miranda, P. Ivanov, B. Bouchard and D. Read (2019). "Complete dissolution of solid matrices using automated borate fusion in support of nuclear decommissioning and production of reference materials." Journal of Radioanalytical and Nuclear Chemistry **321**(1): 183-196.

Caritat, P. d. and M. Cooper (2011). National Geochemical Survey of Australia: The Geochemical Atlas of Australia., Department of Resources, Energy and Tourism.

Caritat, P. d., M. Cooper, M. E. Lech, A. A. McPherson and C. Thun (2009). "National Geochemical Survey of Australia: Sample Preparation Manual." Geoscience Australia Record **2009/08**: 28.

Child, D. P., M. A. C. Hotchkis and M. L. Williams (2008). "High sensitivity analysis of plutonium isotopes in environmental samples using accelerator mass spectrometry (AMS)." Journal of Analytical Atomic Spectrometry **23**(5): 765.

Clarke, R. H., J. Dunster, J. Nenot, H. Smith and G. Voeltz (1996). "The environmental safety and health implications of plutonium." J. Radiol. Prot. **16**(2): 91-105.

Croudace, I., P. Warwick, R. Taylor and S. Dee (1998). "Rapid procedure for plutonium and uranium determination in soils using a borate fusion followed by ion-exchange and extraction chromatography." Analytica Chimica Acta **371**(2–3): 217-225.

Galindo, C., L. Mougin and A. Nourreddine (2007). "An improved radiochemical separation of uranium and thorium in environmental samples involving peroxide fusion." Applied Radiation and isotopes **65**(1): 9-16.

Guogang, J., C. Testa, D. Desideri, F. Guerra and C. Roselli (1998). "Sequential separation and determination of plutonium, americium-241 and strontium-90 in soils and sediments." Journal of Radioanalytical and Nuclear Chemistry **230**(1-2): 21-28.

Harrison, J. J., A. Zawadzki, R. Chisari and H. K. Wong (2011). "Separation and measurement of thorium, plutonium, americium, uranium and strontium in environmental matrices." J Environ Radioact **102**(10): 896-900.

Haschke, J., T. H. Allen and L. A. Morales (2000). "Surface and corrosion chemistry of plutonium." Los Alamos Science **26**(2): 252-273.

Horwitz, E. P., M. L. Dietz, R. Chiarizia, H. Diamond, S. L. Maxwell and M. R. Nelson (1995). "Separation and preconcentration of actinides by extraction chromatography using a supported liquid anion exchanger: application to the characterization of high-level nuclear waste solutions." Analytica Chimica Acta **310**(1): 63-78.

IAEA (2015). The Fukushima Daiichi Accident. Vienna, INTERNATIONAL ATOMIC ENERGY AGENCY.

Kim, C., M. Lee, C. Kim and K. Kim (1998). "90Sr, 137Cs, 239+ 240Pu and 238Pu concentrations in surface soils of Korea." Journal of Environmental Radioactivity **40**(1): 75-88.

451 Kragten, J. (1994). "Tutorial review. Calculating standard deviations and confidence
452 intervals with a universally applicable spreadsheet technique." Analyst **119**(10): 2161-
453 2165.
454 Lu, N., K. S. Kung, C. F. V. Mason, I. R. Triay, C. R. Cotter, A. J. Pappas and M. E. G.
455 Pappas (1998). "Removal of Plutonium-239 and Americium-241 from Rocky Flats Soil
456 by Leaching." Environmental Science & Technology **32**(3): 370-374.
457 Luo, M., S. Xing, Y. Yang, L. Song, Y. Ma, Y. Wang, X. Dai and S. Happel (2018).
458 "Sequential analyses of actinides in large-size soil and sediment samples with total
459 sample dissolution." Journal of environmental radioactivity **187**: 73-80.
460 M. Toribio, J.F. Garcʹıa, G. Rauret, R. Pilviö and M. Bickel (2001). "Plutonium
461 determination in mineral soils and sediments by a procedure involving microwave
462 digestion and extraction chromatography." Analytica Chimica Acta **447**: 179-189.
463 Maxwell, S. L., III (2008). "Rapid method for determination of plutonium, americium
464 and curium in large soil samples." Journal of Radioanalytical and Nuclear Chemistry
465 **275**(2): 395-402.
466 Reading, D. G., I. W. Croudace, P. E. Warwick and R. Britton (2015). "A rapid
467 dissolution procedure to aid initial nuclear forensics investigations of chemically
468 refractory compounds and particles prior to gamma spectrometry." Analytica chimica
469 acta **900**: 1-9.
470 Sáez-Muñoz, M., J. Ortiz, S. Martorell, J. Gómez-Arozamena and A. Cearreta (2020).
471 "Sequential determination of uranium and plutonium in soil and sediment samples by
472 borate salts fusion." Journal of Radioanalytical and Nuclear Chemistry **323**(3): 1167-
473 1177.
474 Sahli, H., S. Röllin, V. Putyrskaya, E. Klemt, B. Balsiger, M. Burger and J. A. C.
475 Alvarado (2017). "A procedure for the sequential determination of radionuclides in soil
476 and sediment samples." Journal of Radioanalytical and Nuclear Chemistry **314**(3): 2209-
477 2218.
478 Taylor, R. N., T. Warneke, J. A. Milton, I. W. Croudace, P. E. Warwick and R. W.
479 Nesbitt (2003). "Multiple ion counting determination of plutonium isotope ratios using
480 multi-collector ICP-MS." Journal of Analytical Atomic Spectrometry **18**(5): 480-484.
481 Tims, S. G., L. K. Fifield, G. J. Hancock, R. R. Lal and W. T. Hoo (2013). "Plutonium
482 isotope measurements from across continental Australia." Nuclear Instruments and
483 Methods in Physics Research Section B: Beam Interactions with Materials and Atoms
484 **294**: 636-641.
485 Vajda, N. and C.-K. Kim (2010). "Determination of Pu isotopes by alpha spectrometry: a
486 review of analytical methodology." Journal of Radioanalytical and Nuclear Chemistry
487 **283**(1): 203-223.
488 Waters, C. N., J. P. M. Syvitski, A. Gałuszka, G. J. Hancock, J. Zalasiewicz, A. Cearreta,
489 J. Grinevald, C. Jeandel, J. R. McNeill, C. Summerhayes and A. Barnosky (2015). "Can
490 nuclear weapons fallout mark the beginning of the Anthropocene Epoch?" Bulletin of the
491 Atomic Scientists **71**(3): 46-57.
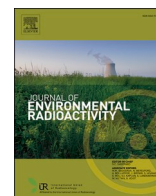
492

Future migration: Key environmental indicators of Pu accumulation in terrestrial sediments of Queensland, Australia

Megan Cook [a,*], Patrice de Caritat [b], Ross Kleinschmidt [c], Joël Brugger [a], Vanessa NL. Wong [a]

[a] School of Earth, Atmosphere & Environment, Monash University, Clayton, VIC, 3800, Australia
[b] Geoscience Australia, GPO Box 378, Canberra, ACT, 2601, Australia
[c] Epic Environmental, PO Box 13058, Brisbane, Queensland, 4003, Australia

ARTICLE INFO

ABSTRACT

Plutonium (Pu) interactions in the environment are highly complex. Site-specific variables play an integral role in determining the chemical and physical form of Pu, and its migration, bioavailability, and immobility. This paper aims to identify the key variables that can be used to highlight regions of radioecological sensitivity and guide remediation strategies in Australia. Plutonium is present in the Australian environment as a result of global fallout and the British nuclear testing program of 1952–1958 in central and west Australia (Maralinga and Montebello islands). We report the first systematic measurements of $^{239+240}$Pu and ^{238}Pu activity concentrations in distal ($\geq$1000 km from test sites) catchment outlet sediments from Queensland, Australia. The average $^{239+240}$Pu activity concentration was 0.29 mBq.g $^{-1}$ (n = 73 samples) with a maximum of 4.88 mBq.g $^{-1}$. ^{238}Pu/$^{239+240}$Pu isotope ratios identified a large range (0.02–0.29 (RSD: 74%)) which is congruent with the heterogeneous nuclear material used for the British nuclear testing programme at Maralinga and Montebello Islands. The use of a modified PCA relying on non-linear distance correlation (dCorr) provided broader insight into the impact of environmental variables on the transport and migration of Pu in this soil system. Primary key environmental indicators of Pu presence were determined to be actinide/lanthanide/heavier transition metals, elevation, electrical conductivity (EC), CaO, SiO$_2$, SO$_3$, landform, geomorphology, land use, and climate explaining 81.7% of the variance of the system. Overall this highlighted that trace level Pu accumulations are associated with the coarse, refractive components of Australian soils, and are more likely regulated by the climate of the region and overall soil type.

1. Introduction

The plutonium (Pu) isotopes ^{238}Pu, ^{239}Pu and ^{240}Pu are present globally as environmental contaminants, largely as a result of atmospheric nuclear weapons testing from the 1950s to the 1980s. Australia was designated as the location for the British nuclear weapons testing program from October 1952 to September 1958. This involved the detonation of twelve atmospheric nuclear tests and hundreds of subcritical (non-nuclear or low yield) tests at the Montebello Islands (Western Australia) and at Maralinga (South Australia), releasing radioactive Pu into the regional environment, some of which settled onto surface soils and sediments of mainland Australia (Symonds, 1985). The high energy release of Pu from a nuclear weapon results in the dispersion of Pu in various forms (e.g. Pu aerosols of various sizes,

Pu-oxide particulates, Pu-coated particles, and sizeable lumps of Pu-contaminated structural material destroyed by the explosion), creating what is currently an undetermined yet foreseeable environmental risk (Kersting, 2013). To our knowledge, the fate of Pu in locations distal ($\geq$1000 km) to the nuclear test sites potentially impacted by the contaminant plumes has not yet been studied in the Australian environment. In particular, site-specific data for $^{239+240}$Pu (unresolved ^{239}Pu and ^{240}Pu) activity concentrations in different soil types across a large geographical area and under varying climatic conditions are not currently available. These data will improve the environmental assessment methodologies for Australian tropical and subtropical ecosystems in the event of an accidental release in the Asia-Pacific region, taking into account the transboundary nature of atmospheric currents that can disperse any future nuclear discharges across Australia and throughout

---

* Corresponding author.
  E-mail address: megan.cook@monash.edu.au (M. Cook).

the region. Moreover, the site-specific data can be applied to an environmental assessment of proposed nuclear activities.

Plutonium interactions in the environment are complex and their nature may evolve through time. Site-specific conditions determine the dominant Pu species and overall transport and migration characteristics of each species. The interplay between redox transformations (Zhao et al., 2016), aqueous solubility controlled by complex formation (Bagawde et al., 1976; Brugger et al., 2016), colloidal transport (Kersting et al., 1999), surface erosion (Xu et al., 2013) and sediment transport (Everett et al., 2008) makes determinations of Pu migration a difficult and site-specific challenge (Kersting, 2013). Field studies suggest that Pu has the potential to migrate, and that variation in the local geology, geochemical conditions, colloidal composition, and differences in initial source characteristics are important in controlling its transport (Everett et al., 2008; Hakonson, 2007; Kersting, 2013).

In the last 20 years, the methodologies for environmental impact assessments (i.e. complex radioecological modelling) have improved considerably for ecosystems affected by tropical, subtropical, and arid climates (IAEA, 2009). These radioecological models are used to assess the radiological risk to people and other terrestrial, freshwater, and marine biota. The aim is to model the mechanisms influencing the transport and migration of radionuclides by considering results from a wide range of field and laboratory experiments. There are data available for Australian locations, but the number of radionuclides considered is limited, the geographical coverage is variable, and only a limited number of soil types have been studied (IAEA, 2010). Although the direct influence of climatic conditions on radionuclide transport and migration appears to be minimal, the indirect effects through changes in soil properties can be significant (Uchida, 2007). Comparative studies of temperate and subtropical climates have shown that the behaviour of radionuclides is modified by many environmental features in these ecosystems (IAEA, 2009, 2010; Payne and Edis, 2012; Uchida, 2007). These factors include climate and rainfall characteristics; soil mineralogy and other physical properties; and organic matter content and cycling. Models developed based on data from the northern hemisphere are generally not directly applicable to Australian environments due to differences in recent land use, and the age of the land surface and degree of weathering; these factors influence the soil physical, chemical, and biological properties.

This study aims to identify the most prominent site-specific variables that need to be incorporated in conceptual models used to predict how Pu migrates in the surface and subsurface of Australian soils. It is hypothesized that site-specific variables (e.g. climate, landform, soil mineralogy and texture) play an integral role in determining the formation of environmental Pu complexes, their migration, bioavailability, and mobility. As a result, several key environmental variables are expected to determine the radioecological sensitivity of a particular region. Conceptual models can define important processes involved in contaminant migration and transport in an environmental system. This can lead to highly valuable, predictive capabilities that are used to guide policy decisions and remediation strategies. Specifically, the purpose of this study is to identify the primary mechanisms driving biogeochemical processes that can result in the accumulation of Pu in distal Australian soil ecosystems, based on a regional study in Queensland. This is achieved by integrating ultra-low detection limit radioanalytical measurements with a large soil geochemical dataset for a range of near-surface soils. Soils are the primary Pu sink, and this work focusses on a wide range of processes that can influence the behaviour and movement of Pu in the environment. These include climatic (humidity, temperature, rainfall, etc.), edaphic (soil properties and geomorphology), and land-use characteristics. This approach will aid in overcoming the challenge of spatial and temporal heterogeneity and provide baseline Pu levels and isotope ratios to determine the source of contamination and the impact of future events.

2. Materials and methods

2.1. Atmospheric transport

The dispersion of Pu as a contaminant was quantified using an atmospheric transport and dispersion model. The National Oceanic and Atmospheric Administration (NOAA) Air Resources Laboratory's (ARL) Hybrid Single-Particle Lagrangian Integrated Trajectory Model (HYSPLIT) is a complete system for computing air parcel trajectories as well as complex transport, dispersion, chemical transformation, and deposition simulations (Stein et al., 2015). Here, a simple trajectory model was constructed from the recorded date and time of detonation (Symonds, 1985) with the height of trajectory based on the reported kiloton range (Table 1; Fig. 1).

The model utilizes a vertical velocity calculation method with a forward trajectory of 48 hours from detonation. NOAA meteorology is utilised to plot the rainfall (mm.h^{-1}) at each hourly measurement point of the model, to account for both wet and dry deposition, the two main transport pathways for Pu aerosols as fallout from nuclear testing. Herein, this variable is referred to as 'rainfall'. Fig. 1 shows the modelled trajectories from each nuclear detonation at Maralinga and the Montebello Islands, and the locations of reference sample points.

2.2. Sampling methodology and characterisation

This study utilised selected samples from Geoscience Australia's National Geochemical Survey of Australia (NGSA) (Caritat and Cooper, 2011a, 2016; Caritat et al., 2009), with a focus on Queensland catchments. The soil sample selection strategy was based on the modelled plume pathways (Fig. 1), assuming that these pathways define the primary areas where Pu would enter the soil system. The model identified a large area across the north-east of the continent, including Queensland, that would be affected by slow, dry deposition, i.e. gravitational settling that leads to plume depletion with increasing distance and a modified vertical atmospheric aerosol distribution of concentration (Stein et al., 2015). Small areas of rapid wet deposition, due to scavenging by rainfall, were also identified along the coast (Fig. 2). 73 NGSA catchments under these plume pathways were identified as possible sinks for Pu as well as representing different climate zones with different soil types, geomorphology and land uses (Fig. S1).

The target landform for sampling in the NGSA was floodplains at or near the outlet of large catchments. This approach ensured that the collection of representative samples due to the natural mixing of

Table 1
British nuclear testing detonations (Symonds, 1985) used in the HYSPLIT atmospheric transport model.

| Detonation	Date (DD/MM/YYYY) Time (hh:mm UTC)	Trajectory	Approx. Height (m)
Buffalo Round 1	27/09/1956 7:00	ENE from Maralinga	8000
Buffalo Round 2	4/10/1956 7:00	E from Maralinga	4500
Buffalo Round 3	11/10/1956 6:00	ENE from Maralinga	5500
Buffalo Round 4	22/10/1956 14:00	NE from Maralinga	6000
Mosaic G1	16/05/1956 4:00	W from Montebello Islands	500
Mosaic G2	19/06/1956 2:00	E from Montebello Islands	10,000
Antler Round 1	14/09/1957 5:00	N, NE from Maralinga	7500
Antler Round 2	25/09/1957 0:30	NE from Maralinga	4000
Antler Round 3	9/10/1957 6:45	E from Maralinga	5000
Hurricane	3/10/1952 0:00	Montebello Islands	6500
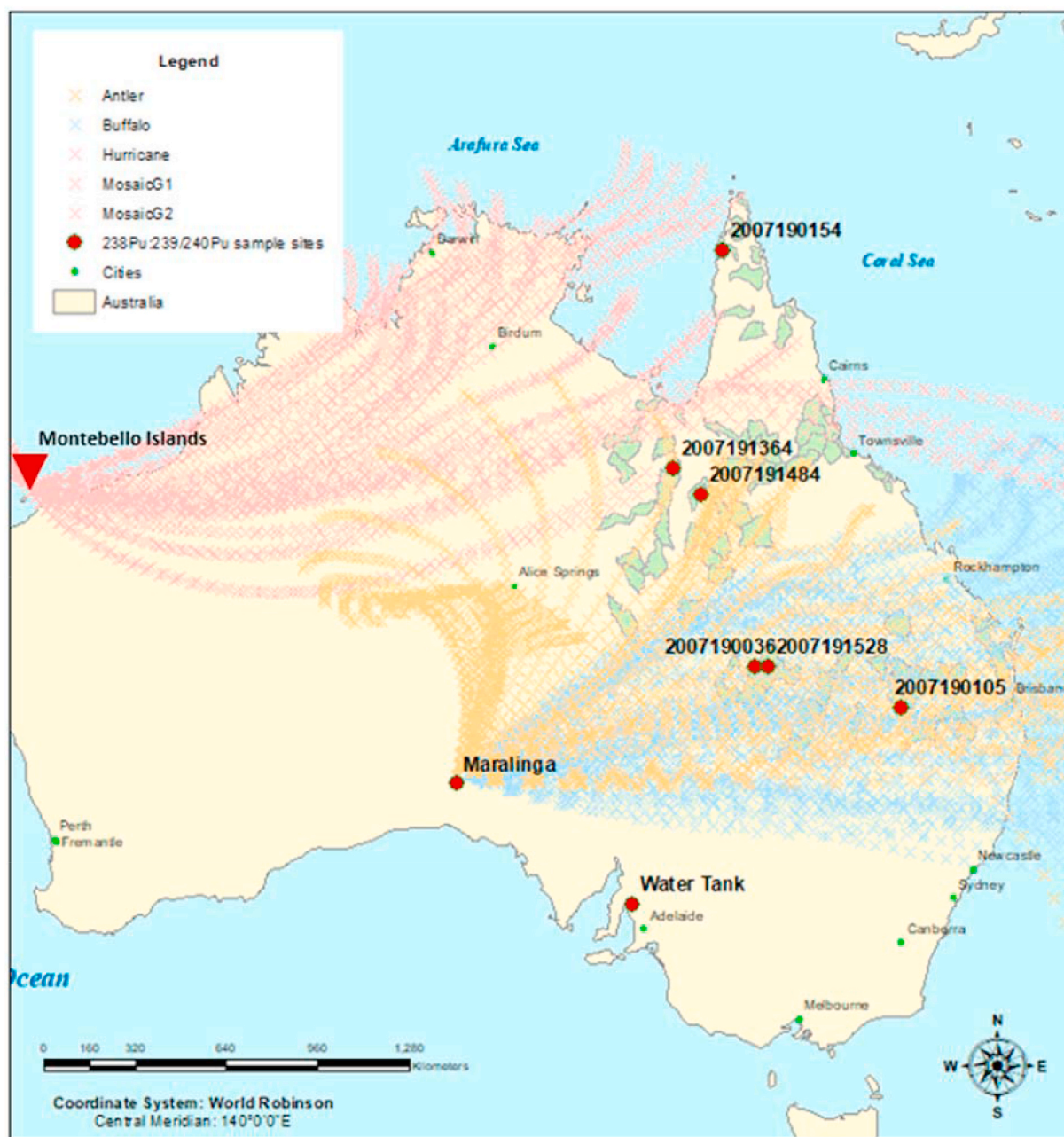
Fig. 1. Sampled NGSA catchments (green polygons, n = 73) and sample locations for Pu activity ratio determination (red circles, labelled with sample ID, n = 6), overlaid with NOAA plume predictions (orange crosses = Operation Antler detonations, red crosses = Montebello Island Operation Hurricane and Mosaic detonations, and blue crosses = Operation Buffalo detonations). (For interpretation of the references to colour in this figure legend, the reader is referred to the Web version of this article.)

materials derived from various source rocks and soil types within catchments, their subsequent mixing during colluvial or fluvial transport, and final deposition in low-energy environments near their outlets. It is assumed that the chemistry of the outlet sediments (including Pu activity concentration) represents the average background composition present in the catchment area at the time of sampling (2007–2009). The NGSA sampling regime consisted of a Top Outlet Sediment (TOS) sample collected from 0 cm to 10 cm depth (below the grass root zone, if applicable), and a Bottom Outlet Sediment (BOS) collected on average from 60 cm to 80 cm depth at each site. Each sample was air-dried then sieved to a <2 mm fraction and a <75 μm fraction. Only the <75 μm fraction TOS samples are reported in this work. To ensure that a representative sample was taken at each site, every TOS sample was

collected from a shallow (10 cm) soil pit and thoroughly mixed *in situ* before sampling.

Every NGSA sample in the publicly available database (Caritat and Cooper, 2011b) has been analysed for major oxides by XRF (x-ray fluorescence) and trace elements by total digestion followed by ICP-MS (inductively coupled plasma-mass spectrometry) (Caritat et al., 2009). The NGSA chemical dataset can be found here: https://ecat.ga.gov.au/geonetwork/srv/eng/catalog.search#/metadata/71973; and the sampling site characterisation can be found here: https://ecat.ga.gov.au/geonetwork/srv/eng/catalog.search#/metadata/70478. Radiochemical analyses for Pu were performed as part of this study; see next section for details. Overall statistics for the characteristics of the Australian surface sediments used in this study are presented in Table 2.
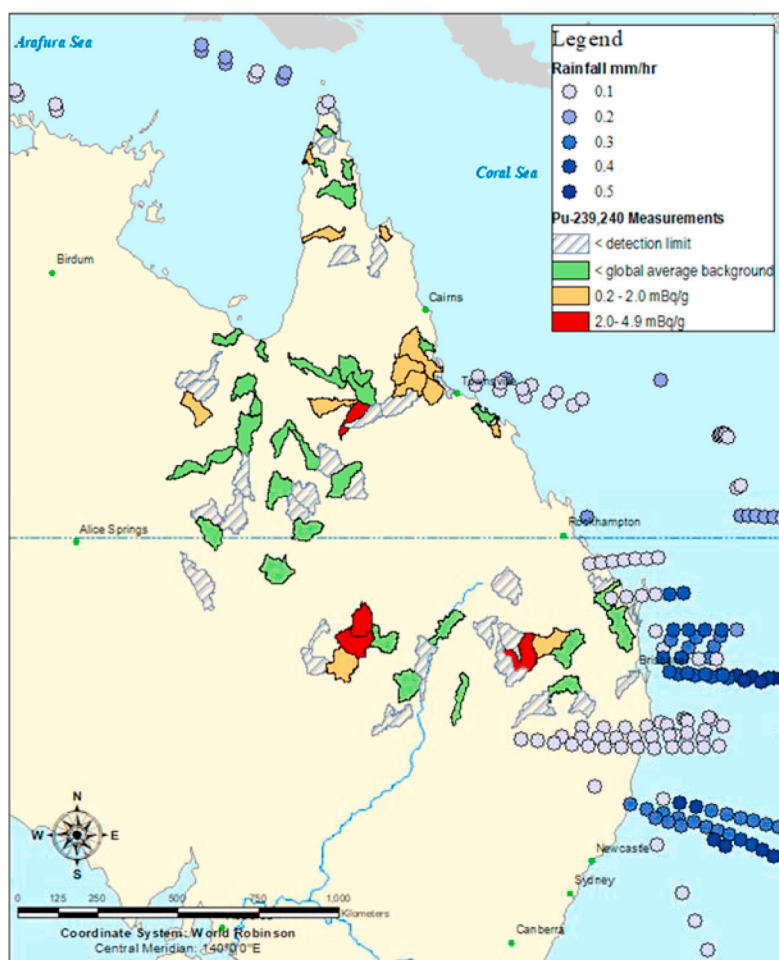
Fig. 2. $^{239+240}$Pu activity concentrations in selected NGSA catchment outlet sediments with HYSPLIT model plume contours of rainfall events. < detection limit = <0.04 mBq/g; < global average background = approx. 0.2 mBq/g (Kelley et al., 1999).

The sediment samples collected by the NGSA aim to be internally consistent, applicable at scales ranging from hundreds of km to the whole continent, and useful to evaluate the concentration levels and distributions of chemical elements in surface and near-surface soils and sediments. During NGSA fieldwork, sample duplicates were collected every 10 sites to determine the repeatability of sampling, sample preparation, and analysis methods. Based on the dataset's analytical precision, overall precision (sampling, sample preparation, and analytical errors), bias, method comparison, and censored proportions, Caritat and Cooper (2011c) deemed the NGSA data to be fit-for-purpose for continental-scale geochemical mapping. We here extend this to trace-level $^{239+240}$Pu analysis and mapping. There are clear limitations to this dataset, however, including its ultra-low sampling density, and the sampling strategy of avoiding areas of *in-situ* soil, fresh rock outcrop, and active erosion, which we acknowledge.

In addition to the NGSA samples, two higher activity samples associated with the Maralinga test site were also analysed (see Fig. 1 for mapped locations) to provide a source comparison for the distal samples analysed in this study. These include one high activity (>20,000 mBq. g^{-1}) proximal soil sample, labelled 'Maralinga' and collected 2 km north of the Maralinga ground zero, and one intermediate activity (>5000 mBq.g^{-1}) meso-distal sediment sample dubbed 'Water Tank' and collected from the accumulated material of a water tank located approximately 2000 km south-east of the test site in Balaklava, South Australia. This water tank was identified as being impacted by secondary detonation plumes. A secondary detonation plume is a high cloud composed of fine particles that are the source of 'long-range' or 'delayed'

fallout.

2.3. Quantitative radiochemical analysis

Radiochemical analyses for Pu were performed at the radioanalytical laboratories of Radiation and Nuclear Sciences, Department of Health, Queensland, and Australian Radiation Protection and Nuclear Safety Agency (ARPANSA), Victoria over two years. Plutonium isotopes present in sediments resulting from nuclear detonations and fallout are likely to occur in a refractory, non-reactive form (Prăvălie, 2014). Therefore, complete dissolution of samples is required for $^{239+240}$Pu analysis to avoid under-reporting the Pu activity concentration (Maxwell, 2007). Briefly, samples (3 g) were fused using a Li$_2$B$_4$O$_7$: LiBO$_2$ flux with a LiI wetting agent (66.67%:32.83%:0.50%) with *in situ* sodium peroxide oxidative catalyst at 960 °C for the complete dissolution of refractory elements. Once fused, the samples were treated using extraction chromatographic resins and analysed via alpha spectrometry. Alpha spectrometry provides complete isotopic information about the alpha-emitting Pu isotopes, since ^{238}Pu, $^{239+240}$Pu (unresolved ^{239}Pu and ^{240}Pu), and a Pu tracer (^{242}Pu in our case) are all detected concurrently. In this work, only $^{239+240}$Pu activity concentration is reported for all samples, with ^{238}Pu activity concentration reported for samples meeting data quality objectives of <20% $^{239+240}$Pu uncertainty and <90% ^{238}Pu uncertainty. This is due to the low activity concentrations and high uncertainties of ^{238}Pu associated with environmental analyses. Alpha spectrometry is the most frequently used technique for the routine determination of Pu isotopes due to the relatively high sensitivity,

Table 2

Descriptive statistics of 73 NGSA sediment samples from Queensland (TOS <75 μm fractions). Analytical methods are XRF (x-ray fluorescence) for major oxides, ICP-MS (inductively coupled plasma-mass spectrometry) for trace elements, and alpha spectrometry for Pu isotopes; LOI (loss on ignition) and SumOx (sum of oxides) determined by calculation. Unit ppm is parts per million (or mg.kg^{-1}), dd is decimal degrees, and m (asl) is meters above sea level; EC is electrical conductivity and MAD is median absolute deviation. Physical variables are defined in Caritat and Cooper (2011a) with an overview provided in Table S1 and Table S2.

Category	Variable	Unit	Range	Median	95th Percentile	MAD
Major Oxides	Al_2O_3	%	0.55–26.0	11.2	15.2	1.92
	CaO	%	0.03–5.53	0.62	2.04	0.37
	Fe_2O_3	%	0.09–14.8	4.24	6.65	0.97
	K_2O	%	0.007–3.25	1.17	2.48	0.37
	MgO	%	0.024–3.1	0.60	1.34	0.27
	MnO	%	0.007–0.20	0.08	0.15	0.03
	Na_2O	%	0.015–2.78	0.58	1.98	0.33
	P_2O_5	%	0.023–0.38	0.09	0.20	0.03
	SiO_2	%	27.7–97.0	71.1	82.1	5.1
	SO_3	%	0.014–0.47	0.04	0.13	0.01
	TiO_2	%	0.36–7.08	1.00	1.81	0.11
	LOI	%	1.6–42.3	7.7	15.0	2.5
	SumOx	%	57.7–98.2	92.2	95.7	2.5
Trace Elements	As	ppm	0.6–12.9	3.5	7.9	1.2
	Au	ppm	<0.001–0.032	0.001	0.003	NA
	Ba	ppm	13.8–601.3	357	495	65.7
	Be	ppm	0.34–3.90	1.60	3.18	0.37
	Bi	ppm	0.03–0.96	0.23	0.64	0.07
	Ce	ppm	7.93–179.3	59.0	151.6	9.34
	Co	ppm	2.19–33.3	13.3	23.6	3.2
	Cr	ppm	17.0–183.8	62.9	104.9	13.4
	Cs	ppm	0.49–11.8	2.85	8.37	0.67
	Cu	ppm	1.86–42.0	17.5	35.4	4.2
	Dy	ppm	2.95–11.9	5.36	10.6	0.84
	Er	ppm	2.09–8.56	3.38	6.63	0.48
	Eu	ppm	0.07–3.45	1.22	1.99	0.19
	F	ppm	100–540	220	448	80
	Ga	ppm	0.70–26.9	13.1	23.3	2.40
	Gd	ppm	1.60–12.99	5.30	10.51	0.91
	Ge	ppm	0.30–0.91	0.60	0.74	0.10
	Hf	ppm	7.11–72.6	20.3	44.9	6.54
	Ho	ppm	0.70–2.85	1.10	2.21	0.15
	La	ppm	4.42–92.7	29.0	71.9	4.88
	Lu	ppm	0.35–1.46	0.55	1.14	0.11
	Nb	ppm	8.0–94.4	13.6	24.0	3.0
	Nd	ppm	3.4–75.1	27.6	61.5	4.9
	Ni	ppm	3.1–61.2	17.1	34.0	4.2
	Pb	ppm	1.99–41.1	15.1	31.3	3.03
	Pr	ppm	0.83–20.8	7.0	16.8	1.2
	Rb	ppm	0.30–160.6	51.8	130.1	15.6
	Sc	ppm	8.2–24.3	12.3	16.7	1.2
	Se	ppm	0.01–0.66	0.07	0.26	0.03
	Sm	ppm	0.87–17.5	6.1	12.8	1.04
	Sn	ppm	0.70–23.9	1.8	4.3	0.5
	Sr	ppm	2.50–409.2	114.1	270.2	47.1
	Tb	ppm	0.35–2.23	0.92	1.91	0.17
	Th	ppm	4.52–42.5	10.9	37.8	2.73
	U	ppm	1.44–47.8	2.95	9.21	0.79
	V	ppm	6.10–216.3	80.3	135.1	17.4
	Y	ppm	20.8–96.2	34.4	70.9	4.8
	Yb	ppm	2.37–9.67	3.80	7.46	0.68
	Zn	ppm	1.20–135.2	49.2	88.8	12.5
	Zr	ppm	301.4–3079	791.8	1827	250.8
	$^{239+240}Pu$	mBq/g	<0.04–4.88	0.09	1.53	0.07
	pH $_{1:5}$	–	3.8–8.8	6.3	7.6	0.7
	EC $_{1:5}$	μS.cm^{-1}	3.99–6310	39.6	403	22.4
Physical Variables	Rainfall	mm.hr^{-1}	0.0–0.1	0.0	0.1	0.0
	Elevation	m (asl)	0–415	122	314	79
	Landform	–	13 classes	alluvial plain	anastomatic plain	–
	Geomorphology	–	9 classes	overbank stream flow	water	–
	Land Use	–	18 classes	grazing natural vegetation	irrigated sugar	–
	Latitude	dd	−28.98–−11.03	−21.62	−12.53	3.50
	Longitude	dd	138.04–152.82	143.11	152.19	2.58
	Sand	%	12.1–98.3	45.6	88.7	17.2
	Silt	%	1.7–63.3	36.2	56.2	10.9
	Clay	%	0.0–36.8	13.5	29.8	6.5

selectivity, and the relatively low-cost instrumentation that is well adapted for high throughput routine analyses using multi-chamber spectrometers (Vajda and Kim, 2010). This method achieves a detection limit approximately 10 times lower than the expected global background (Kelley et al., 1999). With a detector efficiency of 31%, a 7-day cumulative background count, a 3-day sample count, and average tracer recovery of 95.3% (relative standard deviation, RSD: 2.9%), the average reagent blank net count rates were 0.0007 counts per minute (CPM). This results in a trace-level detection limit of 0.04 mBq/g (10.4×10^{-12} ppm or mg/kg; 0.0056 net CPM) (RSD: 15.1%). Field and analytical duplicates, internal standards (^{242}Pu) and certified reference materials (CRM, IAEA-385) were introduced at regular intervals (approximately one in every 10 samples), using a quality control sample (CRM with internal ^{242}Pu spike) and blank (fusion flux with internal ^{242}Pu spike) with every batch of samples in the radiochemical analysis (Cook, 2016). Field duplicates were sediments sampled at the same time and location but given unique identifiers, processed as individual samples, and reported as the average of the duplicates and propagation of errors. Field duplicate repeatability for $^{239+240}$Pu activity concentration ranged from 18% to 45%, which in part at least reflects the inherent heterogeneity of soil/sediments containing refractory particles exhibiting variation in Pu activity concentrations (Jernström, 2006). Analytical duplicates were sediment samples split during sample preparation and measured as direct replicates. Analytical duplicate repeatability for $^{239+240}$Pu activity concentration ranged from 10% to 23%, with the mean activity concentration and error of the replicates reported with propagation of errors. Care was taken throughout the project to minimise contamination, cross-contamination, and mislabelling risks. All uncertainties and detection limits were determined using the Kragten method (Kragten, 1994). Factors included in the uncertainty budget and detection limit were background count rate, reagent blank count rate, tracer recovery, sample mass, and count time with propagation of errors.

2.4. Statistical data treatment

Principal component analysis (PCA) can effectively reduce the dimension of a complex multivariate dataset by using only the first few principal components (PCs) (Magyar et al., 2013), while still preserving its structure (Pozo et al., 2012). Therefore, PCA is commonly employed in environmental studies to identify key environmental indicators (KEIs) of environmental processes. The PCA was modified to incorporate distance correlation (dCorr) to replace Pearson's linear correlation and measure the non-linear interrelationship between the environmental variables, which are inherently non-linear in nature (Chu et al., 2018). Distance correlation coefficients are always positive (absolute values) and are zero only if the variables are independent (Székely et al., 2007). The ability to visualise these non-linear interrelationships is the reason a modified PCA using distance correlation was used to analyse this dataset.

The modified PCA was performed using MATLAB R2019b with imputed and normalised data; creating a matrix of data divergence and ensuring that all input variables (Table 2) were directly comparable. Censored (below detection limits) or missing geochemical data were imputed by the nearest neighbour methodology using the 'impRZilr' function, which employs an isometric log-ratio (ilr) transformation of the data, of the 'robCompositions' package (Hron et al., 2010) in the R statistical package (Hornik, 2012). 39% of reported Pu activity concentration data was imputed for this analysis. All imputed values were reported in the same units as the original data. For inclusion into the PCA, categorical variables (landform, geomorphology, and land use) were assigned an identifying integer and transformed into independent continuous variables by dummy coding (Alkharusi, 2012). The data were then centred and scaled by subtracting the sample mean from each observation, then dividing by the sample standard deviation. The dataset was reversed to focus on the sample variables rather than the samples themselves. The dCorr was then measured between these

variables establishing the comprehensive matrix (Chu et al., 2018). This matrix was used to solve for eigenvalues and determine the PCs (scores) of the matrix. Factor loadings for the variables were also determined. Graphical representation of these PCs (scatterplot) allowed for the determination of clustering and outliers to determine the KEIs of Pu accumulation in Australian soils. Analysis of factor loadings was then completed in order to compare distance correlation coefficients and support any findings within the PC matrix.

Outliers were identified by graphically reviewing a scatterplot of each PC and identifying variables that were consistently non-normally distributed (Fig. S1). Further outliers were identified by the high amount of imputed data (>50%) or multi-tiered secondary variables. Ten variables were identified as outliers and were excluded from the final PCA analysis (geomorphology subtype, land-use site and catchment subtypes, field pH, P_2O_5, Na_2O, Co, Sn, Sr, Pb) leaving 61 variables for determination of KEIs of Pu accumulation (Fig. S1). The Kaiser Meyer Olkin (KMO) test (Chu et al., 2018) was used to estimate the sampling adequacy for the appropriateness to proceed with PCA. The KMO result was 0.56, confirming the sampling to be adequate. A KMO result >0.7 is preferred for direct utilisation of the results in modelling, this means our results should not be used for regression analysis or predictive modelling purposes. To confirm the results of the modified PCA and provide a comparison of linear relations and strength of association, Pearson and Spearman's rank correlations was also undertaken (see Figs. S3 and S4).

3. Results and discussion

3.1. $^{239+240}$Pu activity concentration in distal soils

The results of activity concentrations of $^{239+240}$Pu and their distribution in all soil samples are summarized in Fig. 2. The full dataset is available here: https://doi.org/10.26186/144101 This includes the mapping of selected NGSA catchments, range of Pu activity concentration (mBq/g), and the rainfall (mm/hr) as defined in HYSPLIT model plume contours.

Analysis of NGSA sediment samples revealed a heterogeneous spread of detectable $^{239+240}$Pu with no discernible geographical or rainfall-related pattern (Fig. 2). The activity concentration of these samples ranged <0.04–4.88 mBq/g with an average tracer recovery of 69% (RSD: 25%) over a 3-day count. Total analytical uncertainty ranged from 19% to 90% at close to detection limits. Analytical results for 39% of samples were below detection limits.

3.2. Pu activity ratios

Pu isotope ratios alongside those of its transmutation products, namely ^{241}Am, are widely applied to trace the Pu source in environmental samples because Pu isotopic ratios vary with reactor type, nuclear fuel burn-up time, neutron flux and energy, and for the fallout from nuclear detonations, weapon type and yield. Among the Pu isotopes, ^{239}Pu is a principal isotope of weapons-grade plutonium, whereas long-lived ^{238}Pu, ^{240}Pu, and ^{241}Am are products of thermal neutron capture and decay. Grade of Pu is determined by the amount of incorporated contaminant (^{240}Pu, ^{241}Pu, ^{241}Am) present in the device, with the highest weapons grade Pu containing only minimal amounts (e.g. <7%) of contaminant. There are multiple decay and mass measurement techniques available for determining combinations of these isotopes, each able to provide valuable information on the Pu source. (Gascó et al., 1997; Lee and Clark, 2005). For this work, alpha spectrometry allowed measurements of ^{238}Pu, as a product of ^{241}Am thermal neutron capture and decay, and $^{239+240}$Pu to define an activity ratio and isotopic 'fingerprint' (^{238}Pu/$^{239+240}$Pu) as a baseline for this area. A large range of ^{239}Pu/^{241}Am isotopic ratios at both Maralinga (^{239}Pu/^{241}Am 5.0–22.4) (Burns et al., 1986) and the Montebello Islands ($^{239+240}$Pu/^{241}Am 5.8–24.1) (Cooper and Hartley, 1979) has been previously established. This large range makes it difficult to attribute the

source of any distal sample to a singular detonation or test campaign.

Six NGSA samples of higher Pu activity were chosen to determine ^{238}Pu/$^{239+240}$Pu isotopic ratios. These samples fulfilled the following data quality objectives: less than 20% $^{239+240}$Pu uncertainty and less than 90% ^{238}Pu uncertainty at close to the detection limit. In general, higher ratios (>0.2) indicate increased ^{238}Pu presence and identify the contribution from less-refined fuel, such as that used in the 'safety trials' at Maralinga (Symonds, 1985). Global fallout is defined as having a ^{238}Pu/$^{239+240}$Pu isotopic ratios of 0.025 (UNSCEAR, 1982). The NGSA sediment ^{238}Pu/$^{239+240}$Pu ratios ranged 0.02–0.29 (RSD: 74%) with an average uncertainty of 68% (RSD: 28%) (Table 3).

The proximal 'Maralinga' and meso-distal 'Water Tank' samples characterise the ^{238}Pu/$^{239+240}$Pu isotopic signature of the Maralinga test site (Table 3, Fig. 1). The distinct difference between the isotopic ratios of the meso-distal 'Water Tank' and the proximal 'Maralinga' soil sample is representative of the range of nuclear materials used during the Maralinga nuclear detonations and safety trials (Burns et al., 1986).

The northernmost NGSA samples, i.e., 2007190154 (Weipa), 2007191484 (Julia Creek) and 2007191364 (Dobbyn) (Fig. 1), have the highest ^{238}Pu/$^{239+240}$Pu isotopic ratios in the dataset. These isotopic compositions are consistent with the G2 Mosaic detonation on Montebello Islands having impacted these sites (Cooper and Hartley, 1979), as suggested by the plume modelling (Fig. 1), since these ratios signify a comparatively greater ^{238}Pu presence in line with the largest yield of any detonation in Australia.

3.3. Modified principal component analysis

An overview of the results of $^{239+240}$Pu analysis together with the chemical and physical parameters from the NGSA is shown in Table 2. The modified PCA was conducted to select the representative quality indicators and determine the KEIs from our pool of PEIs (Possible Environmental Indicators). The results from the PCA are used qualitatively, and not for predictive modelling. The results presented in Fig. 3 show that the first five PCs accounted for greater than 80% of the total variance of the system.

The PC scores were investigated to identify trends, patterns, or clustering describing the variance of the system. To achieve this, scatter plots of one PC score were plotted against another PC score (Fig. 4a–d). There were no clear trends; however, clustering of the PEIs with the variable of $^{239+240}$Pu activity concentration revealed important relationships at the studied sites. PC1 explains 50.8% of the variance, showed absolute dCorr correlation coefficients from 0.004 to 0.26 (Table S3a) and revealed clustering between $^{239+240}$Pu and elevation, electrical conductivity (EC), CaO, SiO$_2$, SO$_3$, Eu, Nb, Sc, Se, Zn, As, and Ge (Fig. 4a).

PCs 2 to 5, explaining 30.9% of the variance, showed absolute dCorr correlation coefficients from 0.0003 to 0.32 (Table S3a), and highlighted additional variables as potential factors in Pu presence; landform, land use, latitude, Lu, Yb, Th, U, Ce, Cr, Dy, Er, Gd, Ho, Nd, Pr, Sm, Tb, and V (Fig. 4b–d).

Investigating the factor loadings to aid in the construction of KEIs, we employed a criterion focussed on $^{239+240}$Pu to determine the most appropriate indicators (Andrews et al., 2002). Only variables with a correlation coefficient within 50% of the $^{239+240}$Pu correlation coefficient (using absolute values) are reported from each PC (Table S3b). PC1 (50.8% variance) with a Pu correlation coefficient of 0.019 (0.0097–0.029) revealed correlation with Se, Sc, Eu, SumOx, SiO$_2$. PC2 (15.6% variance) with a Pu correlation coefficient of 0.002 (0.001–0.003) showed correlation with geomorphology. PC3 (6.9% variance) with a Pu correlation coefficient of 0.029 (0.015–0.044) showed correlation with Zr, Yb, V, Th, Pr, Nd, Lu, Ho, Hf, Er, Dy, landform, and geomorphology. PC4 (4.9% variance) with a Pu correlation coefficient of 0.045 (0.023–0.068) showed additional correlation with EC$_{1:5}$, LOI, pH$_{1:5}$, rainfall, MnO$_2$, Y, U, Ga, and Cu. PC5 (3.5% variance) with a Pu correlation coefficient of 0.059 (0.030–0.089) showed additional correlation with La, As, Zn, Nb, Lu, Cs, Ba, SO$_3$, TiO$_2$, MgO. These factor loadings support the overall findings of the modified PC scores biplots (Fig. 4a–d) and show some non-linear dependence between these environmental variables. Correlation coefficients reveal the correlation of trace level $^{239+240}$Pu with a range of lanthanides (rare earth elements), actinides, and heavy metals; physical variables of landform, geomorphology and rainfall; major oxides CaO, SO$_3$, SiO$_2$, TiO$_2$, MgO; and chemical variables of SumOx, LOI, EC$_{1:5}$ and pH$_{1:5}$.

The Pearson correlation coefficients of $^{239+240}$Pu and the chemical and physical (non-categorical) variables (Fig. S3) ranged from −0.26 to +0.19 (p = 0.05 at |r| = 0.23), indicating a moderate negative linear correlation and weak positive linear correlation with any environmental variable, showing no conclusive trends. The Spearman's correlation coefficients of Pu (Fig. S4) ranged from −0.31 to +0.34 (p = 0.05 at |r| = 0.23), showing improved strength of association for environmental variables when rank rather than raw values are used. This is due to the presence of numerical and ordinal variables within the dataset and the monotonic relationship of environmental variables that Spearman's correlation coefficients define. In comparison with Pearson correlation for bivariate normal data, distance correlation is always less than the absolute value of the population parameter: dCorr ≤ |r|. Distance correlation is close to, but in many cases less than, the absolute value of the Pearson estimate. Nevertheless, the distance correlation is closely
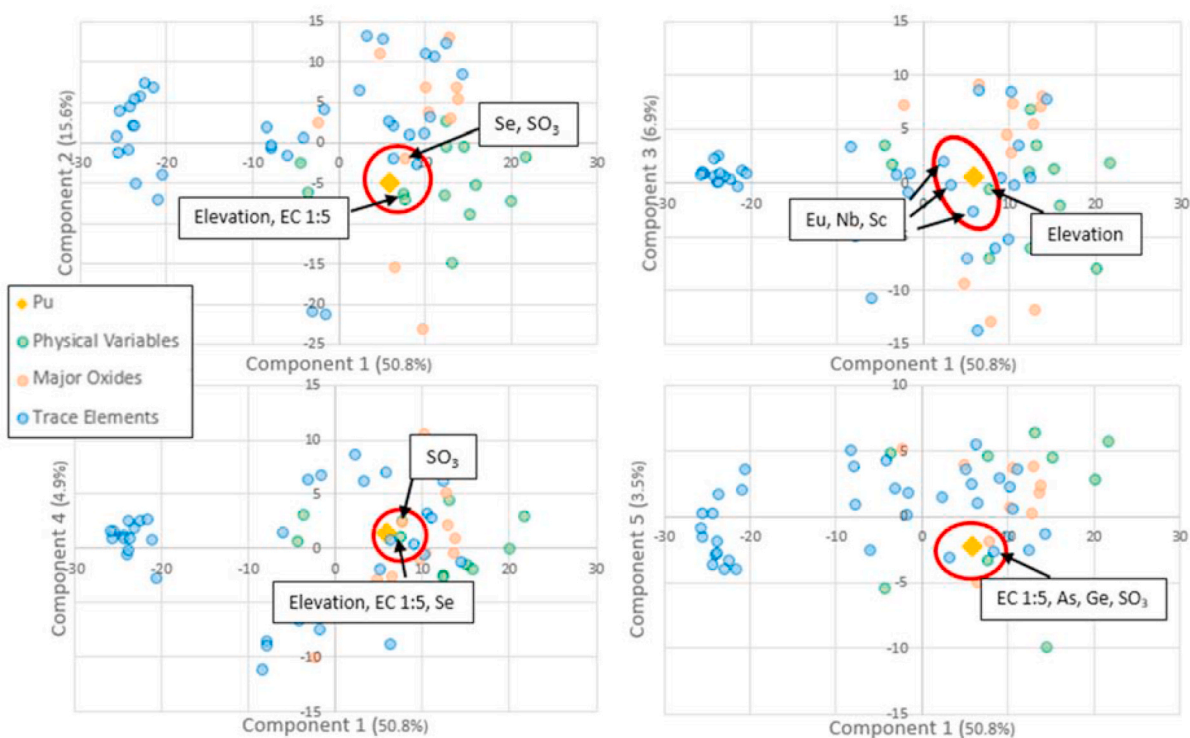

Fig. 3. Variance explained (%) by each principal component (bars) with cumulative variance explained (%) above (line).

Table 3
$^{239+240}$Pu, ^{238}Pu, and ^{238}Pu/$^{239+240}$Pu activity ratios of six selected NGSA Queensland samples, two more proximal samples, and the global average. Bracketed values are overall analytical uncertainty at 95% confidence.

Sample Site	$^{239+240}$Pu mBq. g^{-1}	^{238}Pu mBq. g^{-1}	^{238}Pu/$^{239+240}$Pu Ratio
2007190105	0.58 (0.08)	0.05 (0.04)	0.09 (0.07)
2007190036	4.88 (0.67)	0.07 (0.06)	0.02 (0.01)
2007190154	0.30 (0.04)	0.07 (0.06)	0.23 (0.19)
2007191528	2.00 (0.27)	0.10 (0.04)	0.05 (0.02)
2007191484	0.24 (0.03)	0.07 (0.06)	0.29 (0.25)
2007191364	0.18 (0.02)	0.04 (0.03)	0.23 (0.17)
Meso-distal 'Water Tank'	6.38 (0.87)	1.15 (0.54)	0.18 (0.09)
Proximal 'Maralinga'	5400 (900)	90 (40)	0.02 (0.009)
Global average (UNSCEAR, 1982**)**	–	–	0.025

Fig. 4a. PCA biplots of PC1 vs PC2, 3, 4 and 5. Circled points (red) show variables of interest (Table 1) clustered with Pu. (For interpretation of the references to colour in this figure legend, the reader is referred to the Web version of this article.)
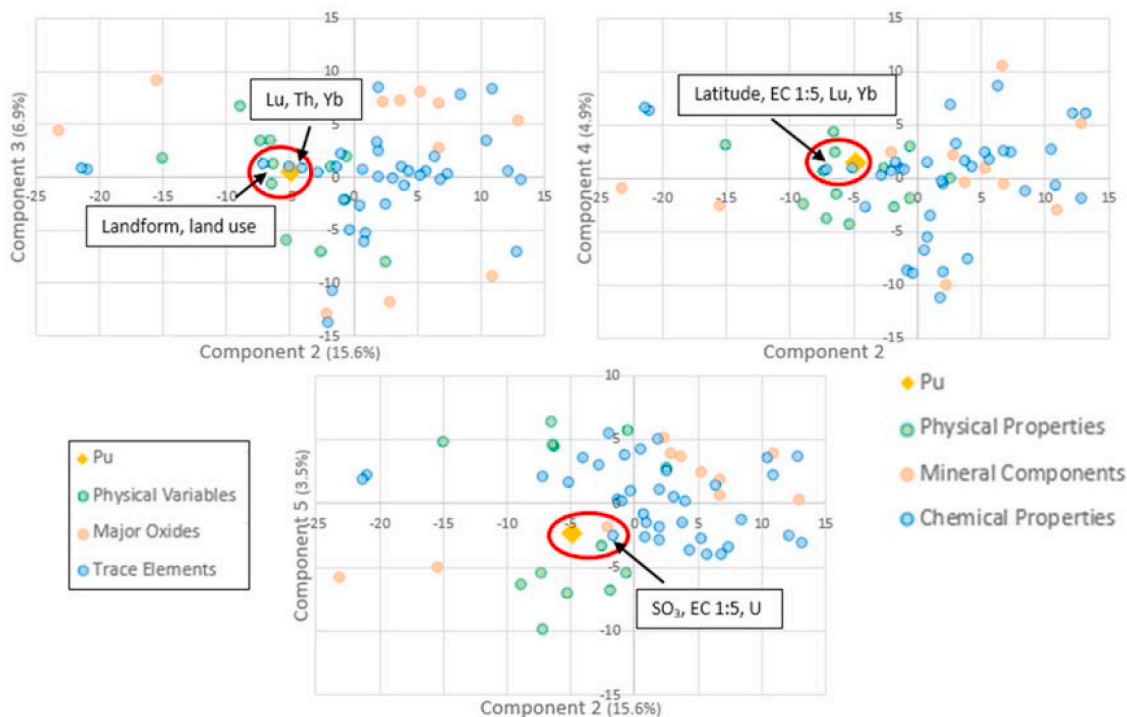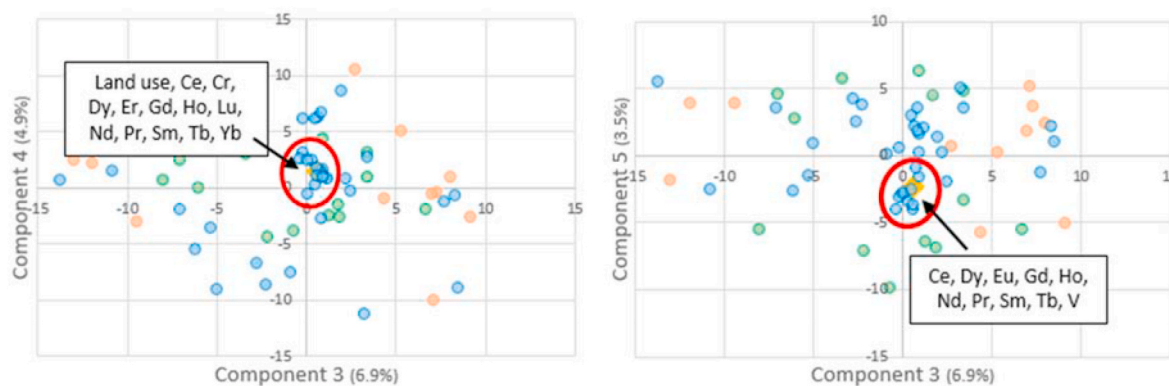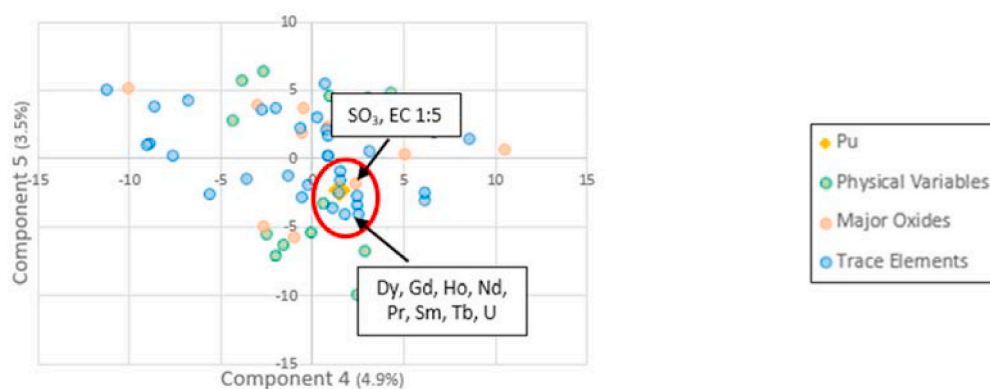

Fig. 4b. PCA biplots of PC2 vs PC3, 4 and 5. Circled points (red) show variables of interest clustered with Pu. (For interpretation of the references to colour in this figure legend, the reader is referred to the Web version of this article.)

related to the Pearson correlation for correlated normal data. The linear correlation analysis supported the importance of lanthanides, actinides and some transition metals in reflecting the concentration, and, using these as a proxy, the mobility of Pu in the studied systems. Combined with a strong positive correlation with the sand fraction (Fig. S3) and

negative correlations with rainfall and the fine soil fractions (clay and silt), this suggests an association of Pu with coarse material. The elemental associations are characteristic of resistant minerals than survived mid-to long-distance sedimentary transport in high energy river systems, such as zircon (Zr, Hf, U, rare earth elements), monazite and

Fig. 4c. PCA biplots of PC3 vs PC4 and 5. Circled points (red) show variables of interest clustered with Pu. (For interpretation of the references to colour in this figure legend, the reader is referred to the Web version of this article.)

Fig. 4d. PCA biplots of PC4 vs PC5. Circled points (red) show variables of interest clustered with Pu. (For interpretation of the references to colour in this figure legend, the reader is referred to the Web version of this article.)

xenotime (rare earth elements + Y + Sc, Th, P), magnetite/chromite (Fe, Mn, Ti, Cr, V, Co), or rutile (Ti, Nb).

The differences in correlations shown by each statistical method reveal the many different types of relationships that may be present in environmental systems. The Pearson's Correlation analysis identified Cu, Ge and elevation whereas Spearman's Correlation analysis did not. Pearson's Correlation analysis also identified latitude as negatively correlated to Pu and Spearman's Correlation analysis showed the opposite (Figs. S3 and S4). Spearman's Correlation analysis revealed many more correlations with Ga, MnO_2, Bi, Hf, Nb, Zr, U, TiO_2, EC 1:5, and SiO_2. These were also shown by dCorr correlation, however, Sn, Fe_2O_3, Co, Cr, Ce, sand, clay and silt as identified by Spearman's Correlation analysis were not shown by dCorr. The non-linear relationships that dCorr revealed that were not identified (factors close to zero) by Pearson's or Spearman's Correlations were As, Cs, Ba, SO_3, MgO, LOI, SumOx, and the categorical variables geomorphology, landform and land use. dCorr has successfully demonstrated a broader insight into non-linear dependencies in complex environmental systems.

Analysis of modified PC scores plots and factor loadings, alongside Pearson's and Spearman's coefficients suggests that trace levels of Pu are transported or migrated more effectively by physical processes affecting the surrounding soils rather than via a mobile phase (chemical interactions). The modified PCA revealed clustering with a combination of lanthanides, actinides, and transition metals. All five PC scores identified Eu, Nb, Sc, Au, Se, Zn, As, Ge, Lu, Yb, Th, U, Ce, Cr, Dy, Er, Gd, Ho, Nd, Pr, Sm, Tb, and V, again highlighting association with the coarse, refractive components of the soils (heavy minerals).

Earlier studies have clearly demonstrated the potential significance of weather and water movement when describing contaminant movement in the soil matrix (Grifoll and Cohen, 1996). Wet deposition, caused by rainfall at the crossing of the primary detonation plume (Fig. 2), or secondary detonation plume, in combination with physical transport processes, such as advection, can affect Pu mobility. PCs 1 and 2 scores plots, describing 66.4% of the variance of the system show the effect of depositional rainfall at the crossing of a plume in correlation with elevation, landform, and geomorphology of the sample sites. These variables also control the energy of the depositional environment, and the coarseness of the sediments, and/or deposition of heavy minerals. The NOAA plume model (Fig. 2) utilizes historic meteorological data to determine rainfall events at the times and locations of the predicted plume pathways. Rainfall on 29 September 1956 following a nuclear detonation from Operation Buffalo during the British Nuclear Testing Programme at Maralinga, resulted in detectable fallout of Pu up to 200 km along the east coast of Australia (Arnold and Smith, 2006). This and other small rain events occurred but were not recorded as they did not meet the meteorological criteria for a rain event (Arnold and Smith, 2006). Knowledge of the relative contributions of dry and wet deposition is an important element of post-accident analysis because it determines the duration of high abundance fallout, initial interception, and retention of airborne radioactive particles by vegetation, their subsequent transfer pathways in soil-plant systems and their dose impact to humans.

Considering elevation, landform, and geomorphology of the sample sites within the depositional environment, it is important to note that the main landforms of the studied area are alluvial plains, formed from alluvium deposited by riverine processes. The highly mobile nature of this type of sediment on alluvial plains is enhanced by steeper gradients of change in sub/tropical climates and increased climatic rainfall (as

opposed to rainfall at the crossing of a plume). Sediments can form aggregates in wet conditions which can then be transported as bedload and persist during transport over longer distances (Maroulis and Nanson, 1996). The deposited sediments and aggregates with associated Pu then accumulate in low energy depositional areas. It is evident from PCs 1, 2 and 4, describing 71.3% of the variance of the system, that rainfall and water movement affect the accumulation of Pu. The variables of elevation, latitude (indicative of climate), and EC (indicative of evaporation) affect changes in these processes at the sample sites. Regional rainfall is important in describing the impact of these variables. There are clear gradients with increasing rainfall at lower latitudes, and rainfall decreasing with increasing distance from the coast. EC is linked with increasing evaporation, and with increasing distance from the coast. This suggests that Pu mobility should increase at lower latitudes and with proximity to the coast.

The physical landscape and larger-scale ecosystem processes are identified by the PCA. Specifically, climate, as indicated by latitude as a proxy (Fig. S2) and driven by climatic rainfall and temperature variation. Climate can induce advective transport with increased rainfall in the sub/tropical climates of this region. Chemical weathering processes, in comparison to physical weathering, dominate in warm and wet climates, which can enhance the physical soil transport processes (Ruxton, 2002). Use of the physical landscape and land use patterns (PC4 4.9% variance) have an increasingly greater effect on the distribution of Pu in surface soils with increasing distance from the detonation sites. Almost two-thirds of the land in Australia has been modified for human uses, primarily grazing of natural vegetation (Beeton et al., 2006). These physicochemical changes affect the availability of organic matter, soil pH, and the formation of colloids, which have the ability to directly impact the mobility of Pu. Higher intensity grazing can decrease organic matter, contribute to aggregate breakdown and increases the formation of colloids, and can also result in decreases in soil pH. Conversely, the low intensity of natural vegetation can be correlated with higher amounts of organic matter.

Finally, the inclusion of CaO, SO_3 (as a proxy for soil sulfate) and SiO_2 (PC 1, 2 and 5 69.9% variance) shows that calcareous, gypsiferous, and/or arenaceous soils are not independent of $^{239+240}Pu$ accumulation, most likely due to the larger pore size, higher water infiltration rates and decreased potential for sorption. Therefore, it is possible to propose that there is a level of dependency of $^{239+240}Pu$ activity in these soils. Low concentrations of CaO and SO_3 in soils are likely to occur in high rainfall areas. These soils are also likely to have low water-holding capacity contributing to high water movement and increasing advective transport (flushing). Soils that occur in high rainfall areas with low concentrations of CaO and SO_3 are more likely to exhibit acidic pH values leading to reduced Pu adsorption and increased Pu mobility. These primary KEIs, actinide/lanthanide/heavier transition metals, elevation, electrical conductivity (EC), CaO, SiO_2, SO_3, landform, geomorphology, land use, and climate explain 81.7% of the variance of the system.

The use of a modified PCA relying on non-linear distance correlation (dCorr) provided broader insight into the impact of environmental variables on the transport and migration of Pu in this soil system. Pearson correlation coefficients only measure linear relationships while Spearman correlation coefficients only measure monotonic relationships. Therefore, using dCorr can identify a meaningful relationship even if the specific Pearson and Spearman correlation coefficients are close to zero. Overall, these results confirm that the modified PCA analysis provided an improved representation of the non-linear interrelationship between the environmental variables, which are inherently non-linear in nature.

Major challenges in understanding the processes controlling Pu behaviour in the environment include the complexity of the soil and sediment matrix and the range of spatial and temporal scales over which these processes occur. It is not yet understood how Pu in particular interacts with the full range of soil and sediment matrices. This study shows that a single process cannot explain the range of field observations of Pu transport in terms of environmental reactivity. This study contributes to the understanding of how macro-environmental variables interact at distal sample sites with trace levels of Pu showing that trace level Pu accumulations are more likely regulated by the climate of the region and overall soil type. Mediating environmental variables that can control longer-range transport for trace levels of Pu may include landform, elevation, and rainfall. It is also possible to postulate that Pu at higher concentrations will be controlled by variables such as increased soil organic matter, overall mineralogy, and pH as variables that are fundamental to Pu environmental interactions (Beauchamp, 1997; Kersting, 2013).

4. Conclusions

Analysis of plutonium (Pu) in distal Australian soils has revealed an average Pu activity concentration of 0.29 mBq.g^{-1} with a maximum of 4.88 mBq.g^{-1}. The higher concentrations were found at sites of lower anthropogenic land-use intensity, where physical disruption of the soil surface was absent. The isotopic fingerprint ($^{238}Pu/^{239+240}Pu$ ratio) found at sites of higher Pu activity concentration ranged 0.02–0.29, compared to the world average of 0.025. The high isotopic values reflect significant contributions of the British nuclear tests at the Maralinga and Montebello Islands nuclear test sites. Note that it is not possible to identify a specific source, because of the heterogeneity of the nuclear materials used during the British nuclear testing programme. Utilising the National Geochemical Survey of Australia database of 61 chemical and physical variables, the key environmental indicators of Pu presence were investigated using modified non-linear PCA. This process revealed that trace level Pu accumulations are more likely regulated by the climate of the region and overall soil type. These physical processes were consistent with chemical characteristics. Specifically, advective transport, evaporation, soil mineralogy (calcareous, gypsiferous and/or arenaceous soils), land use, and climate explained 81.7% of the variance of the system. This work has improved our understanding of the behaviour of Pu in the Australian environment, however, prediction of the behaviour of Pu in soil remains challenging. Without a better mechanistic understanding of the biogeochemical processes that both facilitate and limit Pu transport, advancements needed for the development of reliable transport models will remain limited. Further research should focus on the susceptibility of Pu behaviour and environmental interactions to change in these non-temperate environments.

Declaration of competing interest

The authors declare that they have no known competing financial interests or personal relationships that could have appeared to influence the work reported in this paper.

Appendix A. Supplementary data

Supplementary data to this article can be found online at https://doi.org/10.1016/j.jenvrad.2020.106398.

Author contributions

Megan Cook: Concept, sample analysis, data collection, data analysis, writing first draft, and finalising manuscript; Patrice de Caritat: sample provision, data analysis, finalising manuscript; Ross Kleinschmidt: finalising manuscript; Joël Brugger: input into manuscript, finalising manuscript; Vanessa NL Wong: finalising manuscript.

References

Alkharusi, H., 2012. Categorical variables in regression analysis: a comparison of dummy and effect coding. Int. J. Educ. 4 (2), 202.

Andrews, S.S., Mitchell, J.P., Mancinelli, R., Karlen, D.L., Hartz, T.K., Horwath, W.R., Munk, D.S., 2002. On-farm assessment of soil quality in California's central valley. Agron. J. 94 (1), 12–23. https://doi.org/10.2134/agronj2002.1200.

Arnold, L., Smith, M., 2006. Britain, Australia and the Bomb : the Nuclear Tests and Their Aftermath. Palgrave Macmillan, Basingstoke [England]; New York.

Bagawde, S., Ramakrishna, V., Patil, S., 1976. Complexing of tetravalent plutonium in aqueous solutions. J. Inorg. Nucl. Chem. 38 (7), 1339–1345.

Beauchamp, E., 1997. Nitrous oxide emission from agricultural soils. Can. J. Soil Sci. 77 (2), 113–123.

Beeton, R., Buckley, K., Jones, G.J., Morgan, M., Reichelt, R.E., Trewin, D., Committee, A.S.o. t.E., 2006. Australia State of the Environment 2006 (Independent report to the Australian Government Minister for the Environment and Heritage).

Brugger, J., Liu, W., Etschmann, B., Mei, Y., Sherman, D.M., Testemale, D., 2016. A review of the coordination chemistry of hydrothermal systems: do coordination changes make ore deposits ? Chem. Geol. 447, 219–253.

Burns, P.A., Cooper, M.B., Duggleby, J.C., Mika, J.F., Williams, G.A., 1986. Plutonium-contaminated Fragments at the Taranaki Site at Maralinga. Retrieved from. http://www.arpansa.gov.au/pubs/technicalreports/arl075.pdf.

Caritat, P. de, Cooper, M., 2011a. National Geochemical Survey of Australia: the Geochemical Atlas of Australia. In: Geoscience Australia Record, 2011/20. Geoscience Australia, Canberra.

Caritat, P. de, Cooper, M., 2011b. National Geochemical Survey of Australia: the Geochemical Atlas of Australia: Dataset. Geoscience Australia, Canberra. https://doi.org/10.11636/Record.2011.020.

Caritat, P. de, Cooper, M., 2011c. National Geochemical Survey of Australia: Data Quality Assessment. In: Geoscience Australia Record, 2011/21. Geoscience Australia, Canberra.

Caritat, P. de, Cooper, M., 2016. A continental-scale geochemical atlas for resource exploration and environmental management: the National Geochemical Survey of Australia. Geochem. Explor. Environ. Anal. 16 (1), 3–13. https://doi.org/10.1144/geochem2014-322.

Caritat, P. de, Cooper, M., Lech, M.E., McPherson, A.A., Thun, C., 2009. National Geochemical Survey of Australia: Sample Preparation Manual. Geoscience Australia Record, 2009/08.

Chu, K., Liu, W., She, Y., Hua, Z., Tan, M., Liu, X., Jia, Y., 2018. Modified principal component analysis for identifying key environmental indicators and application to a large-scale tidal flat reclamation. Water 10 (1), 69. https://doi.org/10.3390/w10010069.

Cook, M., 2016. Agile Fusion Method for the Determination of Pu Isotopes in Diverse Sediments. First International Conference on Radioanalytical and Nuclear Chemistry, Budapest, Hungary. Paper presented at the.

Cooper, M.B., Hartley, B.M., 1979. Residual Radioactive Contamination of the Monte Bello Islands from Nuclear Weapons Tests Conducted in 1952 and 1956. Retrieved from. http://www.arpansa.gov.au/pubs/technicalreports/arl010.pdf.

Everett, S.E., Tims, S.G., Hancock, G.J., Bartley, R., Fifield, L.K., 2008. Comparison of Pu and (137)Cs as tracers of soil and sediment transport in a terrestrial environment. J. Environ. Radioact. 99 (2), 383–393. https://doi.org/10.1016/j.jenvrad.2007.10.019.

Gascó, C., Antón, M.P., Espinosa, A., Aragón, A., Alvárez, A., Navarro, N., García-Toraño, E., 1997. Procedures to define Pu isotopic ratios characterizing a contaminated area in Palomares (Spain). J. Radioanal. Nucl. Chem. 222 (1), 81–86. https://doi.org/10.1007/BF02034251.

Grifoll, J., Cohen, Y., 1996. Contaminant migration in the unsaturated soil zone: the effect of rainfall and evapotranspiration. J. Contam. Hydrol. 23 (3), 185–211. https://doi.org/10.1016/0169-7722(95)00086-0.

Hakonson, T.E., 2007. The distribution and transport of radionuclides in dryland ecosystems. Radioact. Environ. 10, 177–191. https://doi.org/10.1016/s1569-4860(06)10008-x.

Hornik, K., 2012. The comprehensive R archive network. Wiley Interdiscip. Rev.: Comput. Stat. 4 (4), 394–398.

Hron, K., Templ, M., Filzmoser, P., 2010. Imputation of missing values for compositional data using classical and robust methods. Comput. Stat. Data Anal. 54 (12), 3095–3107.

IAEA, 2009. Quantification of Radionuclide Transfer in Terrestrial and Freshwater Environments for Radiological Assessments (978–92–0–104509–6). Retrieved from. https://www-pub.iaea.org/MTCD/Publications/PDF/te_1616_web.pdf.

IAEA, 2010. Handbook of Parameter Values for the Prediction of Radionuclide Transfer in Terrestrial and Freshwater Environments. Retrieved from. https://www-pub.iaea.org/MTCD/publications/PDF/trs472_web.pdf.

Jernström, J., 2006. Development of Analytical Techniques for Studies on Dispersion of Actinides in the Environment and Characterization of Environmental Radioactive particles. (PhD). University of Helsinki. Retrieved from. http://ethesis.helsinki.fi.

Kelley, J., Bond, L., Beasley, T., 1999. Global distribution of Pu isotopes and 237Np. Sci. Total Environ. 237, 483–500.

Kersting, A., Efurd, D., Finnegan, D., Rokop, D., Smith, D., Thompson, J., 1999. Migration of plutonium in ground water at the Nevada Test Site. Nature 397 (6714), 56.

Kersting, A., 2013. Plutonium transport in the environment. Inorg. Chem. 52 (7), 3533–3546. https://doi.org/10.1021/ic3018908.

Kragten, J., 1994. Tutorial review. Calculating standard deviations and confidence intervals with a universally applicable spreadsheet technique. Analyst 119 (10), 2161–2165.

Lee, M.H., Clark, S.B., 2005. Activities of Pu and Am isotopes and isotopic ratios in a soil contaminated by weapons-grade plutonium. Environ. Sci. Technol. 39 (15), 5512–5516. https://doi.org/10.1021/es0486115.

Magyar, N., Hatvani, I.G., Székely, I.K., Herzig, A., Dinka, M., Kovács, J., 2013. Application of multivariate statistical methods in determining spatial changes in water quality in the Austrian part of Neusiedler See. Ecol. Eng. 55, 82–92.

Maroulis, J., Nanson, G., 1996. Bedload transport of aggregated muddy alluvium from Cooper Creek, central Australia: a flume study. Sedimentology 43 (5), 771–790.

Maxwell, S., 2007. Rapid method for determination of plutonium, americium and curium in large soil samples. J. Radioanal. Nucl. Chem. 275 (2), 395–402.

Payne, T.E., Edis, R., 2012. Mobility of radionuclides in tropical soils and groundwater. Radioact. Environ. 18, 93–120. https://doi.org/10.1016/b978-0-08-045016-2.00003-5.

Pozo, C., Ruiz-Femenia, R., Caballero, J., Guillén-Gosálbez, G., Jiménez, L., 2012. On the use of Principal Component Analysis for reducing the number of environmental objectives in multi-objective optimization: application to the design of chemical supply chains. Chem. Eng. Sci. 69 (1), 146–158.

Prävälie, R., 2014. Nuclear weapons tests and environmental consequences: a global perspective. Ambio 43 (6), 729–744. https://doi.org/10.1007/s13280-014-0491-1.

Ruxton, B.P., 2002. Chemical weathering in australasia with emphasis on the humid tropics especially in Papua New Guinea. Paper presented at the 17th World Congress of Soil Science Symposium 25 (Paper 306). Thailand. http://citeseerx.ist.psu.edu/viewdoc/download?doi=10.1.1.5.8010&rep=rep1&type=pdf.

Stein, A.F., Draxler, R.R., Rolph, G.D., Stunder, B.J.B., Cohen, M.D., Ngan, F., 2015. NOAA's HYSPLIT atmospheric transport and dispersion modeling system. Bull. Am. Meteorol. Soc. 96 (12), 2059–2077. https://doi.org/10.1175/bams-d-14-00110.1.

Symonds, J.L., 1985. A History of British Atomic Tests in Australia. Australian Govt. Pub. Service, Canberra: Canberra.

Székely, Gabor J., Rizzo, Maria L., Bakirov, Nail K., 2007. Measuring and testing dependence by correlation of distances. Ann. Stat. 35 (6), 2769–2794. https://doi.org/10.1214/009053607000000505.

Uchida, S., 2007. Radionuclides in Tropical and Subtropical Ecosystems Radioactivity in the Environment, 10, pp. 193–209.

UNSCEAR, 1982. Ionizing Radiation: Sources and Biological Effects 1982 Report to the General Assembly. In: With Annexes, 1. United Nations, New York.

Vajda, N., Kim, C.-K., 2010. Determination of Pu isotopes by alpha spectrometry: a review of analytical methodology. J. Radioanal. Nucl. Chem. 283 (1), 203–223. https://doi.org/10.1007/s10967-009-0342-x.

Xu, Y., Qiao, J., Hou, X., Pan, S., 2013. Plutonium in soils from northeast China and its potential application for evaluation of soil erosion. Sci. Rep. 3, 3506.

Zhao, P., Begg, J.D., Zavarin, M., Tumey, S.J., Williams, R., Dai, Z.R., Kersting, A.B., 2016. Plutonium (IV) and (V) sorption to goethite at sub-femtomolar to micromolar concentrations: redox transformations and surface precipitation. Environ. Sci. Technol. 50 (13), 6948–6956.

Transport and migration of plutonium in different soil types and rainfall regimes

Megan Cook[a], Ross Kleinschmidt[b], Joël Brugger[a], Vanessa NL Wong[a]

[a]School of Earth, Atmosphere & Environment, Monash University, Australia

[b]Epic Environmental, PO Box 13058, Brisbane Queensland 4003, Australia

Highlights

· Sandy and clay soils were analysed for Pu transport characteristics under simulated high tropical and low arid rainfall events. A maximum of 0.1% Pu was eluted per rainfall event.

· Arid samples showed a stepwise response in increasing Pu mobility controlled by rainfall intensity and the extended rainless periods.

· Tropical sandy soil systems have the potential to produce a Pu Kd of moderate mobility (6,000 mL.g^{-1}) change within weeks, not years.

· This study confirms that Pu Kd will continue to change over time and accordingly will vary with rainfall events. Current radiological models cannot accurately represent the Kd distribution. The thermodynamic constant concept should be replaced with a time- or event-dependent Kd

Abstract

Leaching and transport of contaminants is a highly complex interacting system affected by a suite of environmental factors. This study demonstrates the potential significance of weather sequences and moisture movement when describing plutonium (Pu) transport in the soil matrix. Column transport experiments identified that variations in simulated rainfall events have a significant impact on Pu transport in soils. Two soil types, a sandy soil and clay-rich soil, were spiked with ^{238}Pu to observe the effect of high and low frequency rainfall events on Pu transport. Samples subjected to the low frequency rainfall events with extended rainless periods (up to 231 hours) resulted in some drying within the soils prior to the next rain event, which showed a step-wise trend of increasing Pu mobility. The determination of temporal distribution coefficients (Kd) for differing water infiltration rates into surface soil showed the

necessity for non-static Kds to accurately describe Pu transport in these systems. The Kds, determined by simulated column transport experiments fall within the bounds of anticipated values (approximately 10,000 - 300,000 mL g^{-1}) from immobile to moderately mobile. It is possible that higher rainfall intensity and less frequent events (arid-type) play a more significant role in Pu transport compared to lower intensity more frequent rainfall events (tropical-type). The overall transport rate is increased in environments where rainfall is more episodic, such as in arid regions, as opposed to the consistently abundant rainfall in tropical regions. Results also show that the low intensity, high frequency events in tropical sandy soil systems have the potential to produce a Pu Kd with increased mobility (6,000 mL.g^{-1}) over shorter periods of weeks, and not years as previously imagined. The variability of Pu mobility in these simulated environments confirms that, for site-specific models, Kd values measured at site-specific conditions should represent the transformation kinetics occurring with time- or event-dependent Kds and are important to manage uncertainties when assessing environmental impacts.

1. Introduction

Understanding plutonium (Pu) transport and migration in soils has undergone a fundamental change in the last 20 years. [1, 2] Pu was previously assumed to be immobile in a range of soil types, with very low solubility under most environmental conditions in combination with the refractory nature of fallout particles. [3] Contemporary Pu transport and migration studies have shown that changes in biogeochemical interactions (changes in pH, presence of chelating agents, microbial interactions etc.) produce an unexpected mobility [1, 4-7]. For example, colloid-mediated transport in semi-arid, well-drained sandy soils [2] show increased Pu transport attributable to increased colloid mobility with increasing water movement through the soil profile. Pu transport in more tropical environments has also been associated with the coarse, refractive components of soils (heavy minerals) and is likely regulated by the climate of the region and overall soil type. [8] The effect of water movement on contaminant transport has been closely coupled with climatic variations (e.g. rainfall) in the vadose zone. [9] Studies of non-radioactive contaminants have clearly demonstrated the potential significance of weather sequences and moisture movement when describing movement in the soil matrix. [10] However, studies on the interaction between climate variations and soils, with a focus on Pu transport remain limited.

When Pu enters the soil system as newly deposited PuO_2 at the surface, its environmental mobility is driven by complex biogeochemical relationships that have significant impacts on transport pathways. [11] Pu as a strongly sorbing contaminant attaches itself to colloidal particles (1-1000 nm) and can be transported with these particles through the soil system. [1, 12] Understanding radionuclide mobility is essential in assessing the impact of the contaminant on the environment and potential uptake by biota. The partition coefficient, Kd, is an empirical parameter that quantifies the interaction of element migration with the surrounding soil/rock, partitioning the solute between the solid and aqueous phases and is used in many environmental models to assess soil-specific behaviour of a contaminant. The Kd presents a simplified kinetic sorption model and is used to characterise the soil-solution exchange to predict the relative amounts of Pu that may be transported to natural waters compared to those which remain in the upper layers of the soil profile. Pu that is then susceptible to physical transport through sedimentation processes. Kd values are conditional parameters limited to the range of experimental data used in their determination, which limits the potential value of collections of Kd measurements. For example, radioecological model inputs have historically focused on temperate environments, which cannot be directly applied to tropical or arid climatic sites. The differences become apparent where temperature and rainfall of a target site differ significantly from that of temperate regions [13, 14]. The estimation of rainfall rates or intensities is imprecise when time-aggregated data are used. The use of an average or a single weather sequence can yield contaminant transport results that are far from the mean. [9] The general characteristics of arid and tropical rainfall climates are defined by less than 20 days in a year as rain days for an arid site and greater than 100 days for a tropical site [15]. In addition, the need to account for rainfall variability is accentuated in arid regions because rainfall is often of a convective nature and characterised by extremely variable, high-intensity, short-duration events. Therefore, this study identifies the rainfall rate, time between rainfall events, and duration of rainfall events to simulate each climate.

Kds are a key parameter used in deriving dose rates from measured or modelled activity concentrations of radionuclides in soil. The Kd model is an integral part of current radioecological modelling practices for contaminant/radionuclide transport and risk analysis, however, there is a large amount of variability in its use. [12] The ERICA tool [16] is radioecological modelling software that is a practical implementation of the integrated approach (human and environmental protection) for conducting radiological risk assessments.

It provides a highly significant scientific basis for a complex decision-making process in the interdisciplinary context of environmental issues. The use of Kds within this tool is heavily reliant on large international compendia. [17, 18] The ability for this tool to accurately characterise the distribution of Kds under varying environmental conditions may be a key limitation.

This study focuses on the effect of water movement on Pu transport in soils with the advection, dispersion and diffusion of Pu in the liquid phase considered. Convection and conduction for heat flow (temperature) is not taken into account. The highly variable rainfall typical of arid and tropical environments is simulated in a set of laboratory-based Pu transport column experiments under controlled conditions. A duration of 21 days enables the investigation of any temporal changes. A direct comparison of differing soil types under these conditions will increase our knowledge of gross edaphic factors related to Pu transport and migration. We aim to identify the effect of rainfall events on Pu transport, via determination of partition coefficients (Kd), in two different soil types, sandy and clay. The best practice for use of site-specific and measured Kd values with environmental transport models will also be investigated.

2. Materials and Methods

2.1. Soil samples

Two soil types found at sites with Pu contamination, sandy and clay soils [1, 6, 7, 19, 20], were used in a column transport experiment under conditions replicating arid and tropical rainfall regimes. The sandy soil was classified as a Tenosol and was sampled from Maralinga in central Australia, a former nuclear test site; the clay soil was classified as a Vertosol [21] and was sampled from Echuca, in southern Australia. The sandy has been geochemically characterised including an activity concentration of 5300 ± 800 mBq/g $^{239+240}$Pu and confirmed presence of Pu hot particles [8, 22]. It has been subjected to nearly 30 years of environmental exposure in a harsh arid environment where mechanical weathering of soils is expected. The samples was then stored in ambient, dry conditions prior to use in this study. Using a soil from a previously contaminated site as well as an uncontaminated soil allows investigation into the impact of water movement on aged versus recent contamination. The soils were homogenised prior to being subjected to one of four treatments.

Table 1 Sandy and clay soil variables (dd is decimal degrees)

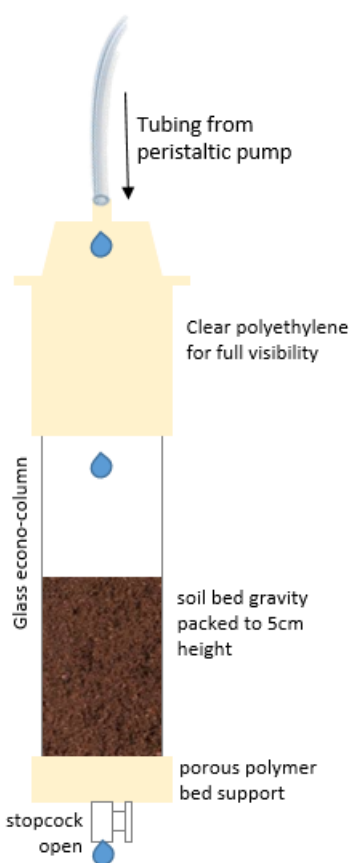|	Units	Sandy Maralinga	Clay Echuca
Latitude Longitude	dd	-31.2069, 131.4500	-36.1549, 144.6918
Sand	%	66.02	31.6
Silt	%	20.7	12.8
Clay	%	13.28	50.6
pH	-	8.97	7.01
EC	$\mu S.cm^{-1}$	78.8	166
Organic Matter (OM)	%	8.3	2.0

2.2. Experimental Design

Figure 1. Column setup

For the column setup, small 2.5 x 10 cm glass columns with a porous polymer bed support were established. The polymer bed at the bottom of the column retained fine particles, and translucent polypropylene end fittings allowed for observations of the entire column bed. Each set of columns was filled to 5 cm height with soil and connected to a peristaltic pump for controlled release every 231 or 32 hours in the low and high rainfall treatments, respectively (Table 1). Raindrop effects could be replicated in the remaining headspace of the column. Treatments were defined by rain rates (mm/hour) [23-25]. In the low rainfall treatment, the columns were subjected to 4.3 mm of simulated rainfall per hour, 10.2 mm rainfall per event with each event occurring for 5.1 hrs. In the high rainfall treatment, the columns were subjected to 2.2 mm of simulated rainfall per hour, 21.3 mm rainfall per rain event with each event occurring for 18.6 hours. To accurately simulate surface deposition of fallout Pu, 0.5g of each soil type was spiked with 4.8 Bq of ^{238}Pu, oven-dried and added on top of each dry-packed column (Figure 1). The mass of spiked soil (0.5g) was approximately 1% of the total column mass to replicate surface soil contamination replicating the conditions within 2km of Taranaki detonation site at Maralinga, Australia. The activity of ^{238}Pu spike used (4.8 Bq) ensures that trace level elutions can be measured for the duration of the experiment whilst replicating medial to distal fallout conditions.

Table 2. Rainfall climatologies

	Units	Low (arid)	High (tropical)
Rainfall per day	mm	93.5	177.6
Rainfall per event	mm	10.2	21.3
Rainfall per hr	mm	4.3	2.2
Total number of rainfall events	-	2.1	10
Average lifetime of a rainfall event	hr	5.1	18.6
Minimum inter-event time rainless	hr	231.0	32.0
Total rainfall per event	mm	21.9	40.9
Total rainfall over duration of study	mm	46.8	407.6

The experimental period totalled 21 days following a consistent pattern of rainfall events and rainless periods for each treatment. Therefore, 10 rainfall events were simulated for high frequency rainfall, and two rainfall events were simulated for the low frequency rainfall (Figure 2).
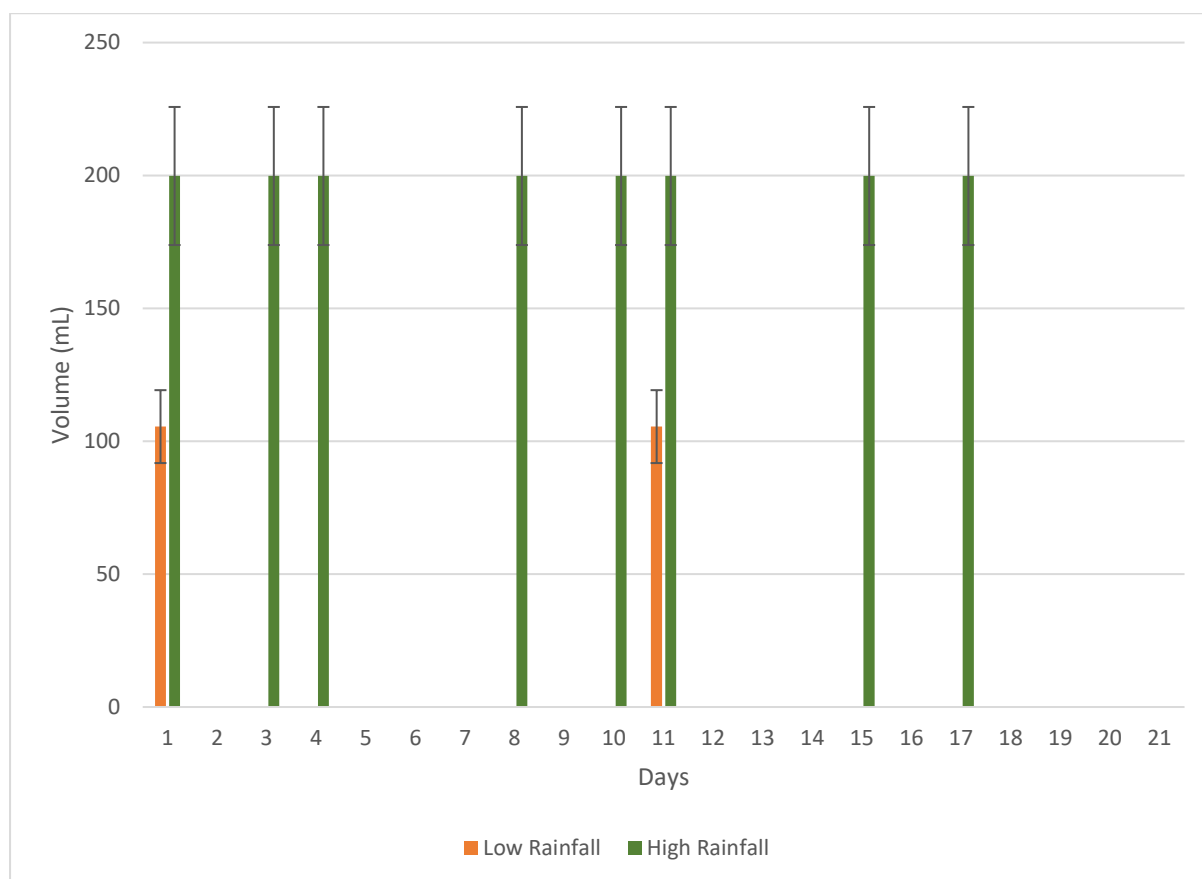
Figure 2 Column rainfall events

The flow rate of the water from the peristaltic pump was determined by taking the hourly rainfall mm/hr and converting it to mL/min. This was then gravimetrically verified with six replicates of elution rates resulting in a 13% variation overall. Using ^{238}Pu as a tracer ensures

quality control over the experiment and that any $^{239+240}$Pu present in the Maralinga soil samples do not introduce extraneous variables. Analyses were all conducted in triplicate. All analysis of Pu in soil and rainfall elutions were completed using the alpha spectrometry method by Cook [26].

2.3. Calculation of Kd

After each elution, the Kd was calculated using the concentration of Pu in the soil (mg kg–1 dry solid) and the concentration of Pu in the porewater (mg L–1), giving final units of mL g–1 using equation 1.

$$Kd\ (mL.g) = \frac{concentration\ of\ Pu\ in\ soil\ (mg.kg\ dry\ solid)}{concentration\ of\ Pu\ in\ pore\ water\ (mg.L)} \qquad (1)$$

3. Results

The column transport experiments showed that Pu interactions with each soil type (sandy or clay) varied with rainfall intensity and rainless periods. Figure 2 accurately portrays the large differences in frequency, minimum inter-event rainless periods and volume of each simulated climatology.

3.1. Pu elution

Figure 3a shows increased Pu elution for sandy soils in the low rainfall (arid) treatment, in comparison to clay soils under the same conditions (Figure 3b). In the high rainfall (tropical) treatment, sandy soils showed increased Pu elution over the duration of the study (Figure 3a). Clay soil under the same conditions showed varied Pu elution throughout the experiment (Figure 3b).
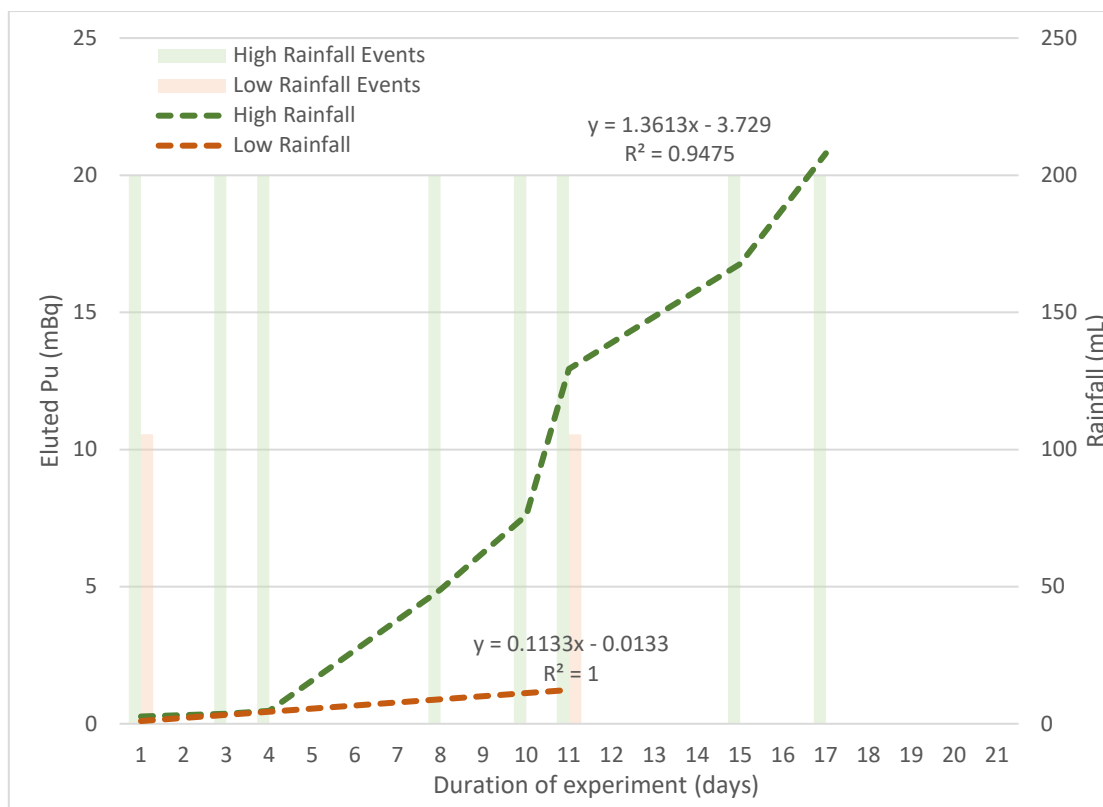
Figure 3a Cumulative Pu elution (mBq) in sandy soil
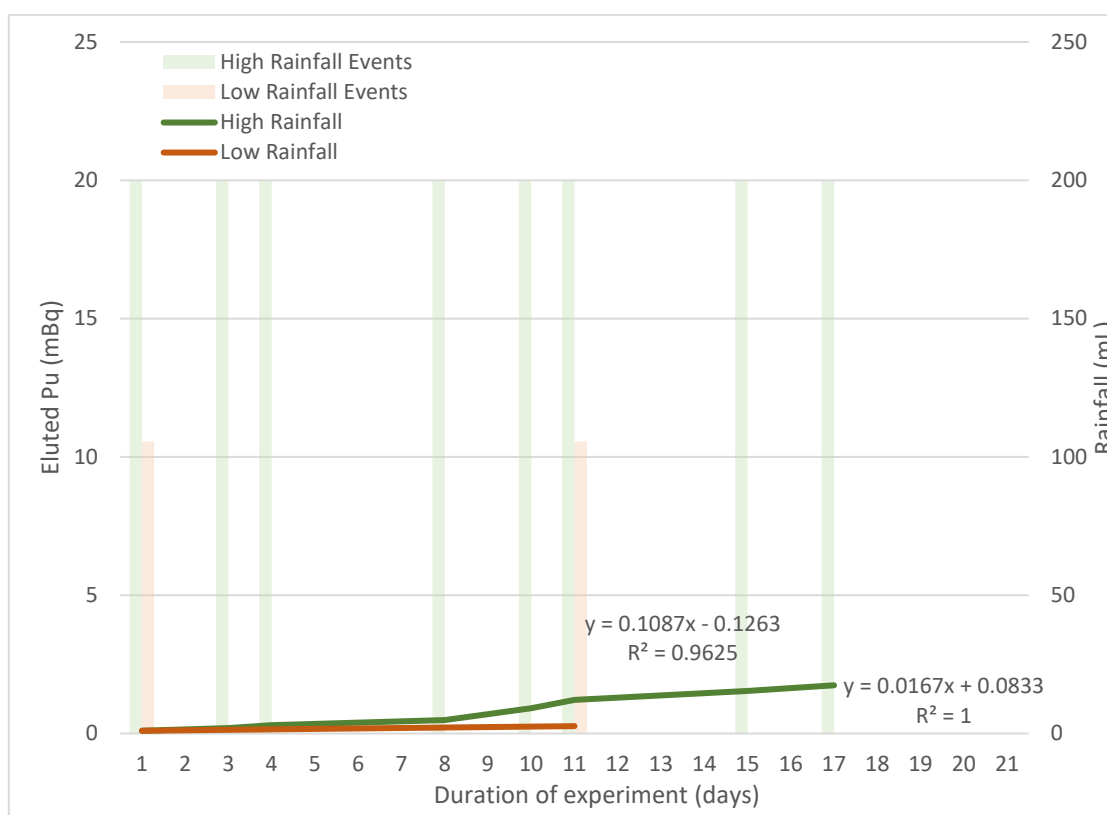
Figure 3b Cumulative Pu elution (mBq) in clay soil

Increasing amounts of Pu in both soil types were eluted with increasing volumes of water in the high rainfall treatments. The sandy soils in the low rainfall (arid) treatment elute at the same rate (0.2 ± 0.03 mBq per rainfall event averaged over the study) as clay soils in the high rainfall (tropical) treatment over the same period.

3.2. Kd determination

Using measured activity concentrations to determine the Kd using equation 1 at each elution provides an indication of the degree of Pu sorption and the biogeochemical effect of each rainfall treatment. Sandy soils in the high rainfall (tropical) treatment began with a Kd at an average of 98,000 mL g^{-1} and decreased two orders of magnitude over the duration of the experiment. A steep decrease (98%) occurred at day 8 (Figure 4a) to a Kd of less than 6,000 mL g^{-1} and remained in that range for the remaining five rainfall events. The Kd in sandy soils in the low rainfall (arid) treatment began higher than the high rainfall (tropical) treatment at an average of 130,000 mL g^{-1}, then followed a similar pattern with a steep decrease (91%) to less than 13,000 mL g^{-1} at day 11 (Figure 4a and b) resulting in a comparable decrease in Kd.
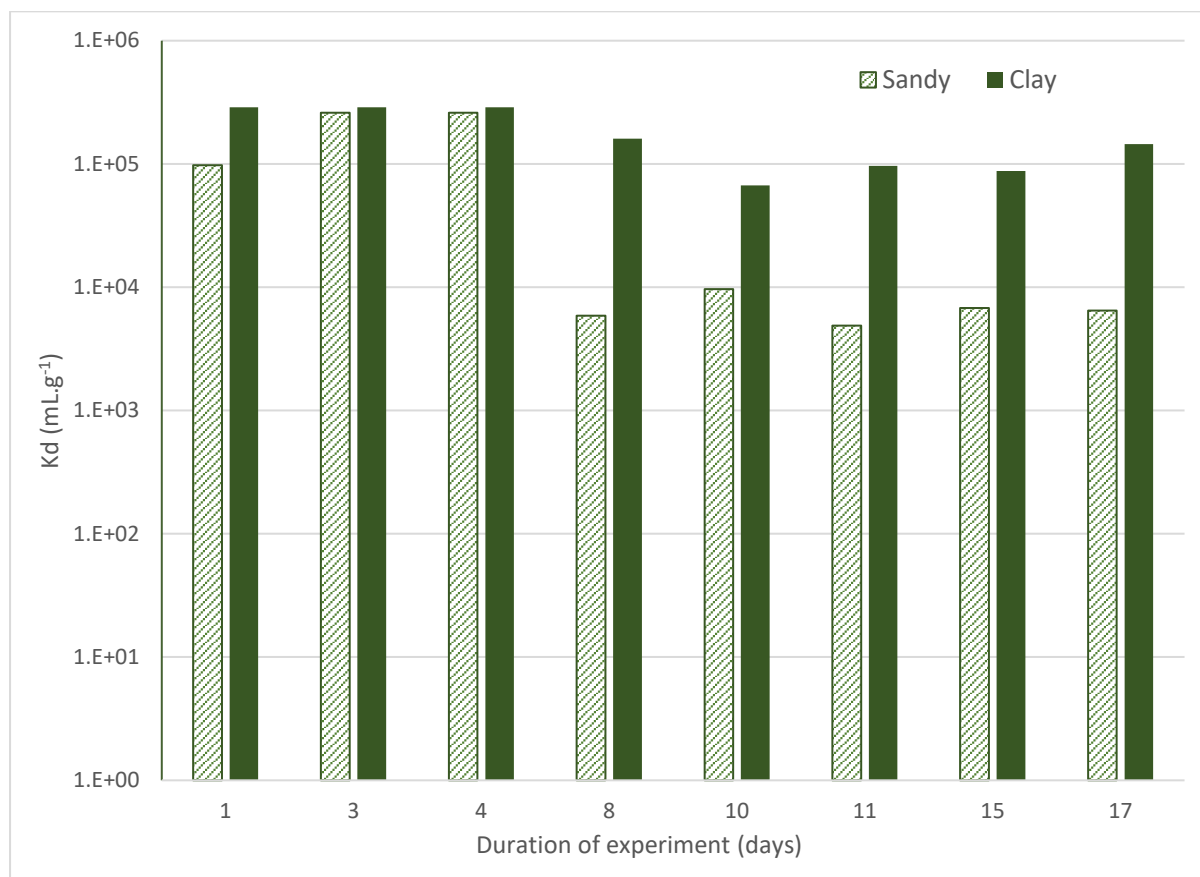
Figure 4a Kd of Pu in sandy and clay soil for high rainfall treatment
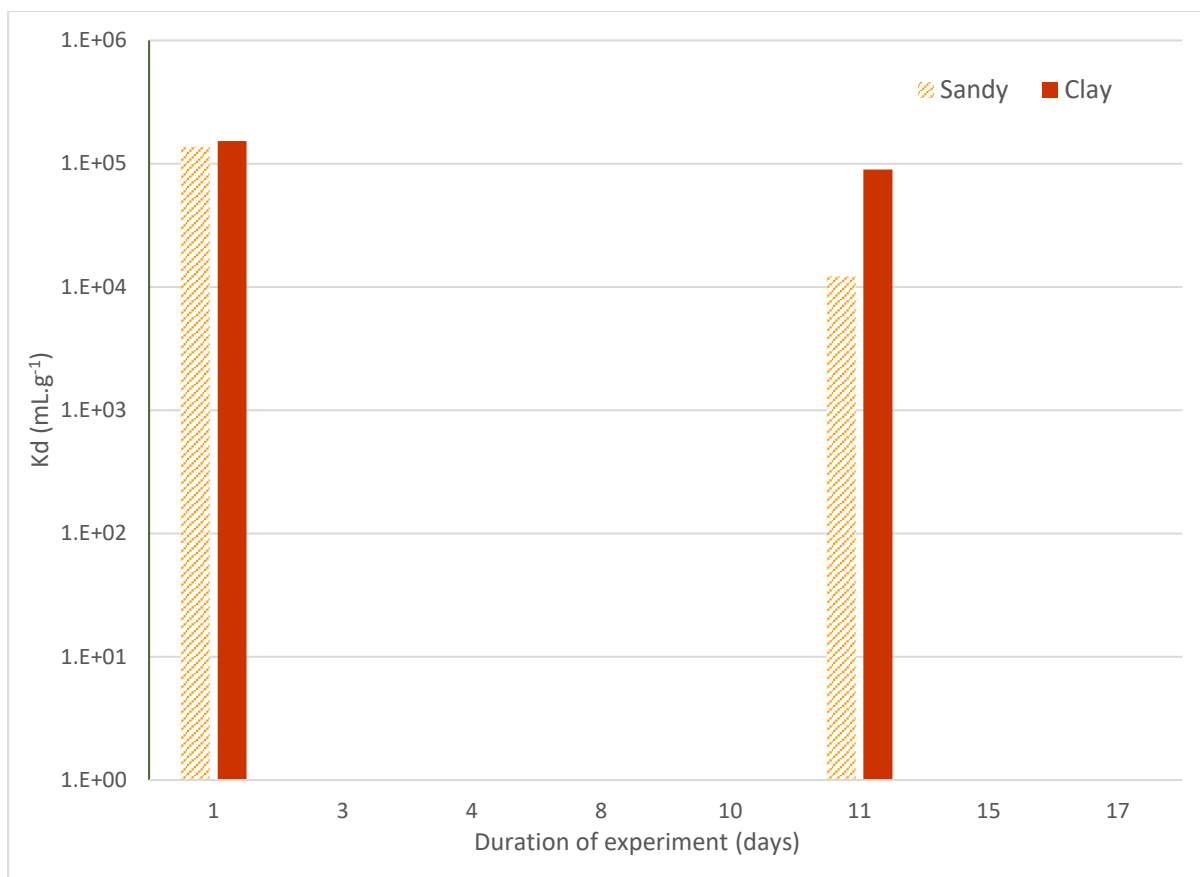
Figure 4b Kd of Pu in sandy and clay soil for low rainfall treatment

The Kd of the clay soils in the low rainfall (arid) treatment started at a similar magnitude as the sandy soils in the same treatment at 150,000 mL g^{-1}; however, the decrease in Kd was smaller at only 41% to an average of less than 90,000 mL g^{-1}. The clay soils in the high rainfall treatment had the highest Kd at an average of 290,000 mL g^{-1} which was sustained for three high rainfall events. A decrease of 44% to 160,000 mL g^{-1} occurred at day 8 which decreased again by a further 59% to 67,000 mL g^{-1} by day 10 (Figure 4a, 5). The sorption of Pu then changes to slowly increase to 140,000 mL g^{-1} by the end of the experiment. The clay soil in the high rainfall treatment is the only treatment that showed this response.
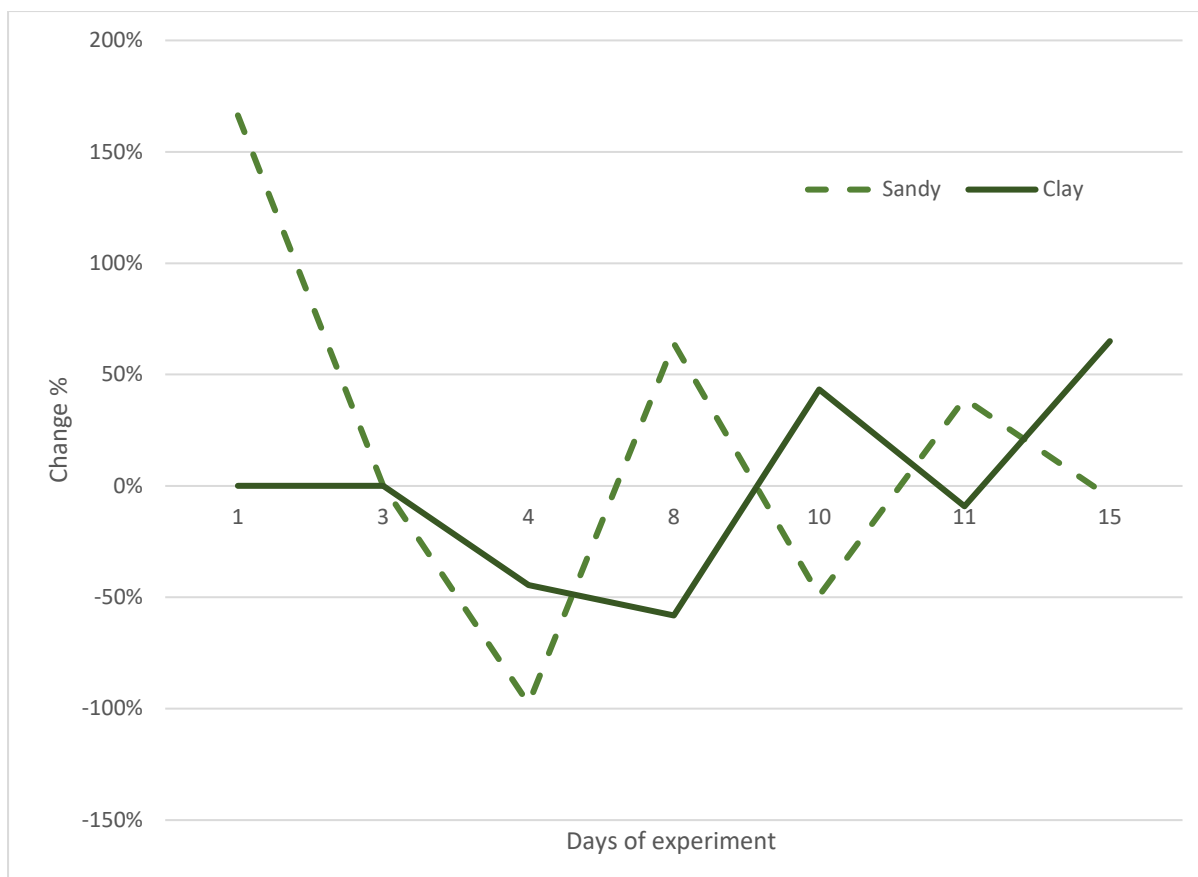
Figure 5 Temporal change for sandy and clay soil under high rainfall treatment

3.3. Contaminated soil extracted from natural systems

The known activity concentration of $^{239+240}$Pu in this soil allows the investigation of surface deposition (^{238}Pu) versus distributed contamination ($^{239+240}$Pu) as well as recent deposition versus aged contamination. The high rainfall treatment of the aged distributed contamination began with a sandy soil Kd of 13,000 mL g^{-1} indicating reduced mobility. This quickly decreased (-99%) to 73 mL g^{-1} after the first rainfall event (Figure 6). This magnitude of Kd was maintained for the remaining seven rainfall events. The low rainfall treatment of the aged, distributed contamination also began with a Kd of 6,700 mL g^{-1} and followed a similar trend to the high rainfall treatment falling to 96 mL g^{-1} (Figure 6).
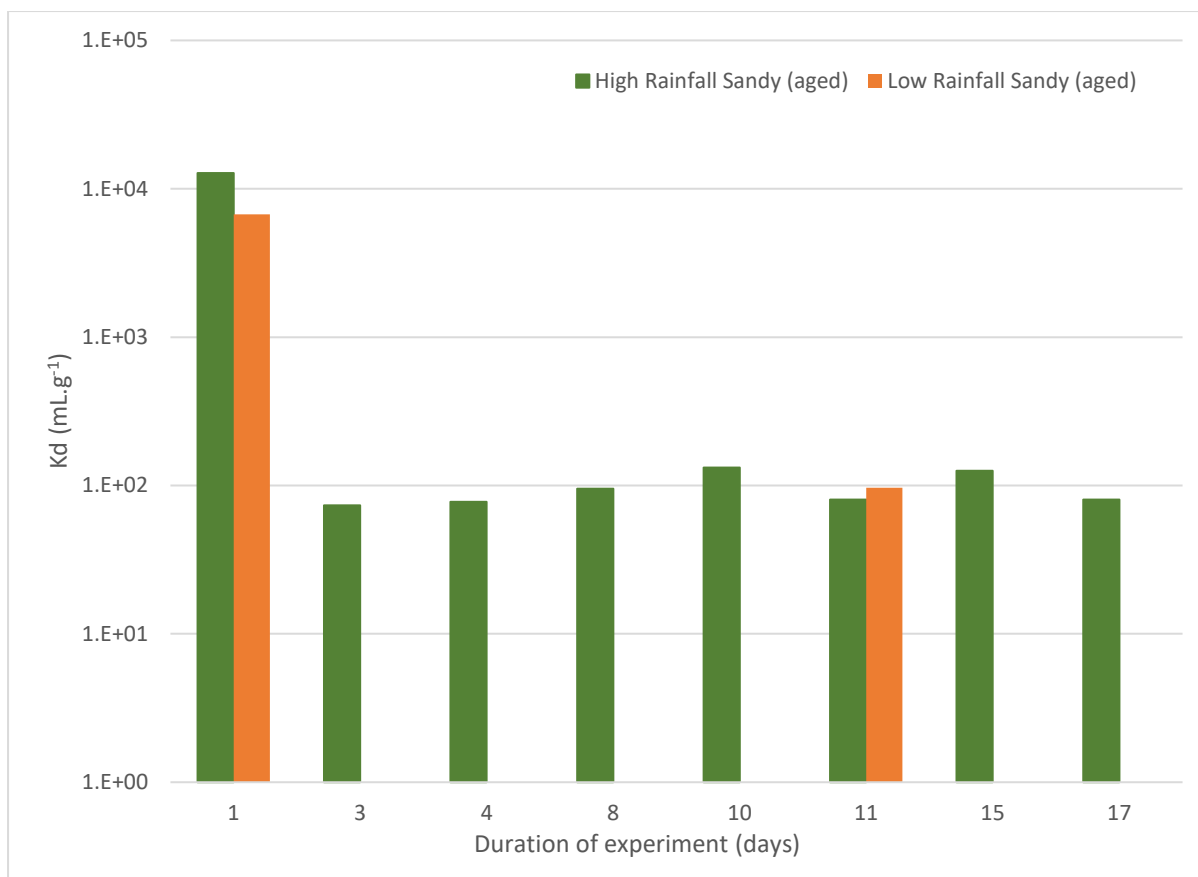
Figure 6 Kd of aged Pu contamination ($^{239+240}$Pu) in high and low rainfall treatments

In comparison with the recent surface deposition samples, the aged distributed contamination had a consistently lower Kd, by several orders of magnitude (Figure 7). The relatively consistent Kd following high rainfall events appears to be characteristic of the sandy soil, however, this occurs after one rainfall event for the aged distributed contamination sample. It takes four rainfall events for the recent surface deposition contamination to achieve this attribute (Figure 7).
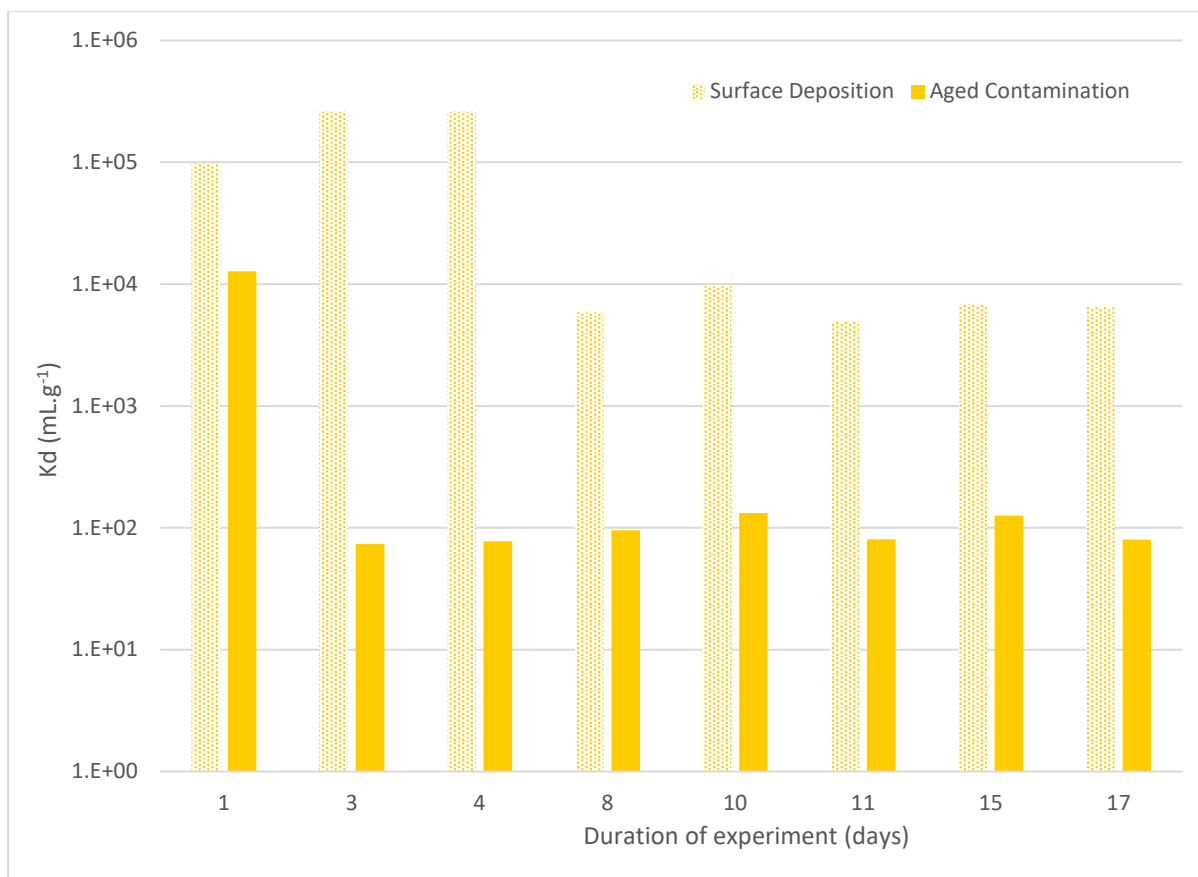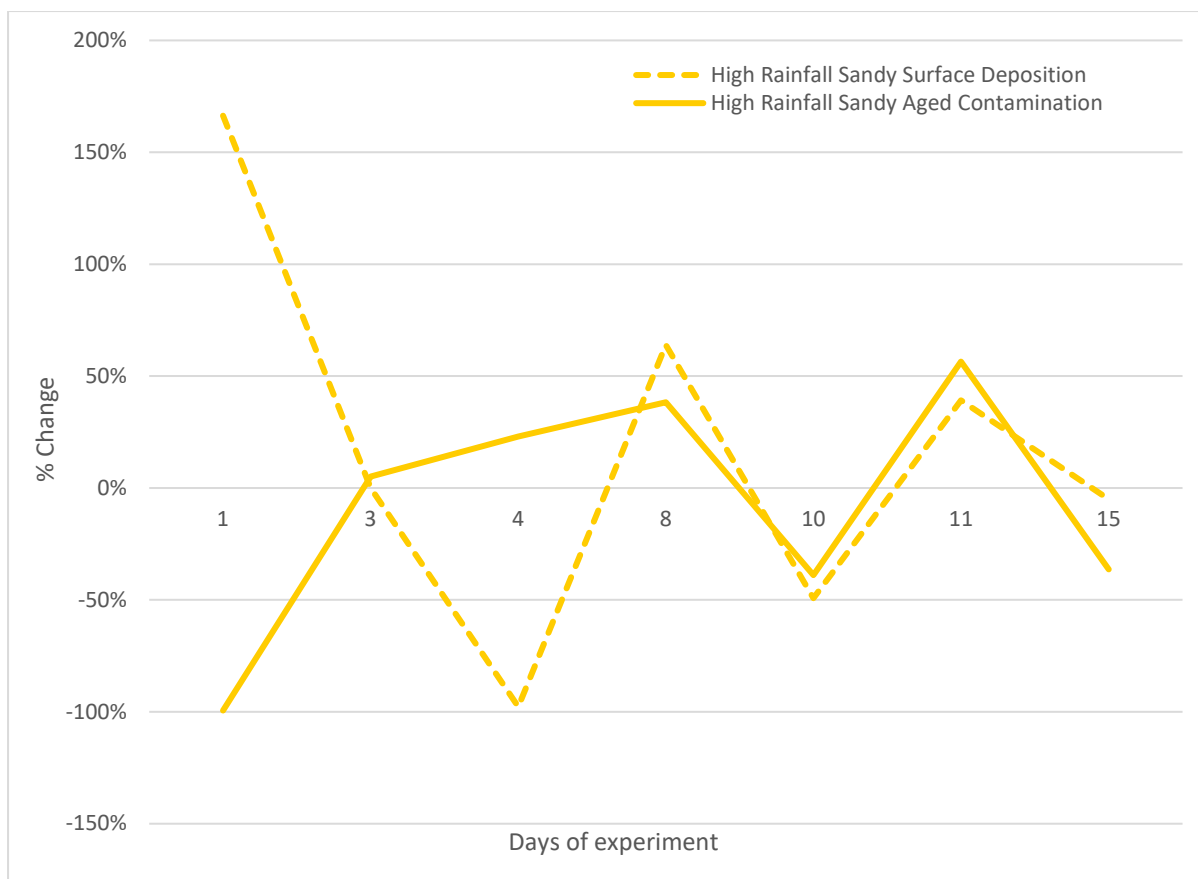
Figure 7 Kd of sandy soil under high rainfall treatment; surface deposition (^{238}Pu) versus aged contamination ($^{239+240}$Pu)

The temporal change of Kd in the sandy soil for both contamination types (surface deposition versus aged contamination) followed a similar trend (Figure 8). The opposite relationship was shown for the clay soil (Figure 5). The high rainfall sandy soil, after the fourth rainfall event, shows a +50% to -50% temporal change in a stepwise fashion for both the surface deposition and distributed aged contamination samples. Overall, the rate of change of the Kd (slope of the line) for aged contamination was ten times greater than that of the surface deposition samples.

Figure 8 Temporal change for sandy soil in high rainfall treatment; surface deposition (^{238}Pu) versus aged contamination ($^{239+240}Pu$)

4. Discussion

4.1. Kd variability

Understanding the fate and transport of Pu in the surface and subsurface environment is essential for protective actions or remediation of contaminated sites as well as the development of safety cases for nuclear waste disposals. Sorption processes in natural environments represented by default Kd values found in the literature can result in significant errors when used to predict the impacts of site-specific radionuclide migration or site-remediation options. [27] Therefore, it is becoming increasingly accepted that site-specific Kd values are essential for site-specific conditions and impact assessments. The reported high and low rainfall experimental Kd values, in comparison with Kd values centrally reported by IAEA, [28] fall within the bounds of anticipated values (approximately 10 - 300,000 mL g^{-1}). However, the large range means that Pu transport in tropical and arid systems can shift from immobile (100,000 mL.g^{-1}) to moderately mobile (1,000 mL.g^{-1}). [29] Importantly, the high rainfall sandy soil system has the potential to produce a Pu Kd of increased mobility (6,000 mL.g^{-1} for surface deposition) over shorter periods of weeks, and not years. A typical

objective for radiation protection at sites contaminated with long-lived radionuclides such as Pu is to detect changes and evaluate long-term trends in radiological conditions. Understanding that Pu transport at these sites can occur over a period of weeks requires implementing a more stringent monitoring plan to detect these changes. If this is not recognized, the resulting risk characterisation will be inadequate.

An important trend revealed by this study is the decrease in Kd of greater than 90% for both rainfall treatments in the sandy soils and greater than 40% for both rainfall treatments in the clay soils after the first extended rainless period (>24 hours). This exhibits the underlying physical and/or chemical properties of each soil that are affected by rainfall intensity and duration. Many mineral phases have been studied for Pu de/sorption processes (e.g. montmorillonite [30], goethite [31], kaolinite [32], illite [33]) to determine diminutive soil properties controlling these processes. Key geochemical properties of soils (silt %, clay %, organic content %, pH etc.) and complex chemical processes affecting Kd (aqueous complexation, redox reactions, adsorption, precipitation etc.) have been investigated and can be incorporated using a look-up table, parametric or mechanistic Kd approach. [34, 35] These Kd approaches are limited by the availability of site-specific data, limited environmental ranges of application, discrete chemical variables and the heterogeneity of solid and aqueous systems. [34] The distribution of soil types and mineral phases across landscapes is highly heterogeneous and presents a major challenge for predictive models [36] extending to the use of site-specific Kd values. The variability in geochemical properties and chemical processes can vary Kd values by six orders of magnitude. [37] This study shows that in addition, the uncontrollable environmental variables such as rainfall climatology can exert significant effects (up to four orders of magnitude) on these geochemical properties and chemical processes and should be considered in any modelling approach.

The replication of two different rainfall distributions that simulate arid and tropical climates has revealed several points for further investigation. The inter-event rainless periods, especially the longer periods >48 hours, have the effect of creating a stepwise response (Figure 3a and 3b). In a constraint-driven process, rainfall intensity and duration in this case, stepwise patterns can be generated in a system in which there is an underlying long-term trend. From this, we deduce that Pu sorption changes occurring during the rainless periods are exaggerated at the arrival of the next rain event and an increase in Pu transport occurs. Similarly, the clay soil affected by the high rainfall (tropical) treatment undergoes an increase

in sorption effects after day 10. To account for these changes in a risk characterisation or environmental impact assessment, a time- or event-dependent Kd is required.

4.2. Surface deposition versus distributed contaminant

Comparison of the surface deposition (^{238}Pu) and aged distributed ($^{239+240}$Pu) contamination in this experiment provides the ability to determine the effects of rainfall alone on the transport of Pu through sandy soil. Both high and low rainfall climatologies start and finish at a similar magnitude of Kd, and therefore Pu mobility, showing that the rainfall events alone trigger a change in Pu sorption or movement of colloidal particles. The increased Pu transport of $^{239+240}$Pu (ten times greater) can be attributed to the weathering/ageing of the soil and sorbed Pu alongside the weathering of Pu hot particles. [22] Climate plays a definitive role in the weathering and breakdown of soils, which in turn affects the leaching of soil contaminants. The episodic rainfall events in arid climates and higher frequency of rainfall events in tropical climates leads to faster leaching of radionuclides from the soil profile and is therefore, less likely to remain at the soil surface. The same conditions can enhance the ageing effect, which reduces bioavailability [38]. The ageing phenomenon in soils, which produces changes in material state over time, is associated with significant modification of mechanical and physical soil properties. The combination of high temperatures and heavy rainfall means that tropical climates experience the highest rate of soil weathering [38] and therefore, as shown by this study, increased transport.

Temporal changes are not currently included in radioecological modelling. The parallel temporal changes shown in Pu surface deposition and aged contamination after day 8 (Figure 8) is indicative of a long-term trend in the underlying geochemical properties or chemical processes effected by rainfall and inter-event rainless periods alone. Further investigation to validate this structured change would make it possible to account for this relationship via a time- or event-dependent Kd.

4.3. Application to environmental modelling

Decision-making on activities, facilities, existing sites and contaminated areas of potential, perceived or actual environmental concern are governed by an environmental impact assessment. A number of scientifically well-founded and credible systems for assessing the environmental impact of ionising radiation exist; contaminant transport models, surface complexation models, thermodynamic sorption models, and radioecological models. Distribution coefficients are a vital input to each of these systems. Generic contaminant

transport models utilise a simplified binary exchange mechanism to describe adsorption and desorption of a contaminant. The distribution of a contaminant between water and soil, sediment or sludge compartments is dependent upon the characteristics of the contaminant as well as the matrix; it may be additionally influenced by external environmental factors. An equilibrium constant Kd would not realistically characterise Pu soil interaction. [39] Equilibrium constant Kd values, which are typically used in transport models, assume that partitioning between the solid and aqueous phases occurs linearly (Kd does not change as a function of Pu concentration) and reversibly (that the rates of adsorption and desorption are equal). Surface complexation modelling allows quantitative comparison of the influence of complexing ligands and salts on Pu sorption and speciation. [40] Thermodynamic sorption models offer the potential to improve the incorporation of sorption in environmental modelling of contaminant migration describing radionuclide sorption to mineral surfaces using Kd. These models provide a scientific basis for the range of Kd values and for assessing the response of Kd to changes in chemical conditions. [41] Each of these models focuses on the chemical interactions of Pu with soil parameters without consideration of gross edaphic or climatic factors.

Radioecological modelling, specifically the ERICA tool, allows dynamic modelling for rapidly changing releases of radioactive contaminants and makes estimates of dose under changing radionuclide conditions. [16] This is achieved with the use of probabilistic calculations performed through the application of Monte Carlo simulations. Kd values are incorporated with the use of a probability distribution function (exponential, log/normal, log/triangular, log/uniform). Kds are often well fitted by lognormal distributions with singular values least biased distribution being an exponential one. [42] Fitting the distribution of Kds from this work reveals that none of the available distributions accurately describes this data (See Supplementary Material). This further supports the requirement for the development of a time- or event-based Kd as increased variability in rainfall infiltration is expected to increase Pu dispersion.

The use of Kd to explain Pu reactivity in this study reflects the simplified kinetic sorption process alongside gross edaphic and climatic factors but does not take into account the effects of convection and conduction for heat flow caused by temperature variations. Further focussed research is required in this area, taking into account the chemical properties of Pu alongside the impacts of different climate regimes including variations in temperature. It should be noted that the higher reported Kd values in this study may also reveal a unique

aspect of the transport processes of fallout Pu in that the concentration of Pu added to the column, dried onto a small aliquot of soil, can potentially become immobile by precipitation processes as opposed to absorption [27]. Elucidating the different factors (e.g. effects of initial water content, rainfall intensity, rainfall duration, saturation-infiltration relationships, saturation-permeability relationships, etc.) that influence the water movement through an unsaturated soil is crucial to understanding Pu transport and migration in a range of climates.

5. Conclusion

The following effects must be considered to reduce the uncertainties in environmental impact assessments of existing or future tropical and arid Pu contaminated sites: 1) the large range of Pu Kd values (three orders of magnitude) demonstrates that Pu movement in these sandy and clay soil systems under different rainfall regimes can shift from immobile to moderately mobile; 2) that this shift can occur over short time periods suggests that monitoring plans need to be modified to capture changes as they occur; 3) the rainless periods create a stepwise response in increasing Pu mobility which requires a time- or event-dependent rate equation Kd to capture the transformation kinetics occurring; 4) the distribution of Kd values determined herein cannot currently be accurately represented in radioecological models. Furthermore, physical and/or chemical properties of soils that are influenced by the rainfall intensity and duration have a role in the transport of Pu.

Knowledge gained from this study suggests that Pu will migrate at sites in arid and tropical climates and that variation in rainfall rates (mm/hour), minimum inter-event time, rain and rainless durations and differences in the initial source and soil characteristics are profoundly important in controlling its transport. This work will aid in determining the appropriateness of global Kd values for modelling these sites, if further defensible and conservative Kd values are required and the impact on Pu transport processes at sites represented by these climatologies.

6. References

1.   Kersting, A.B., *Plutonium transport in the environment.* Inorg Chem, 2013. **52**(7): p. 3533-46.
2.   Kersting, A., et al., *Migration of plutonium in ground water at the Nevada Test Site.* Nature, 1999. **397**(6714): p. 56.
3.   Charles T. and J. Garten, *A Review of Parameter Values Used to Assess the Transport of Plutonium,Uranium and Thorium in Terrestrial Food Chains.* Environmental Research 1978. **17**: p. 437-452.

4.   Francis, A.J. and C.J. Dodge, *Microbial mobilization of plutonium and other actinides from contaminated soil.* J Environ Radioact, 2015. **150**: p. 277-85.

5.   Cusnir, R., et al., *Probing the Kinetic Parameters of Plutonium-Naturally Occurring Organic Matter Interactions in Freshwaters Using the Diffusive Gradients in Thin Films Technique.* Environ Sci Technol, 2016. **50**(10): p. 5103-10.

6.   Begg, J.D., et al., *Plutonium sorption and desorption behavior on bentonite.* J Environ Radioact, 2015. **141**: p. 106-14.

7.   Boggs, M.A., et al., *Plutonium(IV) sorption to montmorillonite in the presence of organic matter.* J Environ Radioact, 2015. **141**: p. 90-6.

8.   Cook, M., Caritat, P. de, Kleinschmidt, R., Brugger, J., Wong, V. N. L., *Future migration: key environmental indicators of Pu accumulation in terrestrial sediments of Queensland, Australia.* Journal of Environmental Radioactivity, 2020. **Under Review**.

9.   Grifoll, J. and Y. Cohen, *Contaminant migration in the unsaturated soil zone: the effect of rainfall and evapotranspiration.* Journal of Contaminant Hydrology, 1996. **23**(3): p. 185-211.

10.   Marshall, J.D., B.W. Shimada, and P.R. Jaffe, *Effect of temporal variability in infiltration on contaminant transport in the unsaturated zone.* Journal of Contaminant Hydrology, 2000. **46**(1): p. 151-161.

11.   Kaplan, D., et al., *Influence of Sources on Plutonium Mobility and Oxidation State Transformations in Vadose Zone Sediments.* Environmental Science and Technology, 2007. **41**(21).

12.   Puls, R.W. and R.M. Powell, *Transport of inorganic colloids through natural aquifer material: implications for contaminant transport.* Environmental science & technology, 1992. **26**(3): p. 614-621.

13.   Twining, J.R., *Tropical radioecology.* 1st ed. ed. 2012, Amsterdam: Amsterdam : Elsevier.

14.   Uchida, S., *Radionuclides in tropical and subtropical ecosystems*, in *Radioactivity in the Environment*. 2007. p. 193-209.

15.   Meteorology, B.o. *Average annual & monthly days of rain*. 2016 November 2016 [cited 2019 November]; Available from: http://www.bom.gov.au/jsp/ncc/climate_averages/raindays/index.jsp?period=an&product=1mm#maps.

16.   Brown, J.E., et al., *The ERICA Tool.* Journal of Environmental Radioactivity, 2008. **99**(9): p. 1371-1383.

17.   IAEA, *Handbook of parameter values for the prediction of radionuclide transfer in terrestrial and freshwater environments.* 2010, International Atomic Energy Agency.

18.   Howard, B.J., et al., *The IAEA handbook on radionuclide transfer to wildlife.* J Environ Radioact, 2013. **121**: p. 55-74.

19.   Seaman, J.C. and K.A. Roberts, *Radionuclide Fate and Transport in Terrestrial Environments*, in *Encyclopedia of Sustainability Science and Technology*, R.A. Meyers, Editor. 2012, Springer New York: New York, NY. p. 8597-8634.

20.   Mahara, Y. and A. Kudo, *Plutonium mobility and its fate in soil and sediment environments*, in *Radioactivity in the Environment*. 2001, Elsevier. p. 347-362.

21.   Isbell, R., *The Australian soil classification.* 2016: CSIRO publishing.

22.   Cook, M., Estchmann, B., Ram, R., Ignatyev, K., Gervinskas, G., Conradson, S. D., Cumberland, S., Wong, V. N. L., Brugger, J., *The Nature of Plutonium Hot Particles.* Environmental Science & Technology, 2020. **Under Review**.

23.   Dunkerley, D., *How does sub-hourly rainfall intermittency bias the climatology of hourly and daily rainfalls? Examples from arid and wet tropical Australia.* International Journal of Climatology, 2019. **39**(4): p. 2412-2421.

24.   Dunkerley, D., *Intra-event intermittency of rainfall: an analysis of the metrics of rain and no-rain periods.* Hydrological Processes (Online), 2015. **29**(15): p. 3294-3305.

25.   Belachsen, I., et al., *Convective rainfall in a dry climate: relations with synoptic systems and flash-flood generation in the Dead Sea region.(Report)(Author abstract).* Hydrology and Earth System Sciences, 2017. **21**(10): p. 5165.

26.   Cook, M., *Agile fusion method for the determination of Pu isotopes in diverse sediments.* Journal of Radioanalytical and Nuclear Chemistry, 2020. **Under review.**

27.   Krupka, K.M., et al., *Understanding variation in partition coefficient, Kd, values.* Volume II: Review of Geochemistry and Available Kd Values, for Cadmium, Cesium, Chromium, Lead, Plutonium, Radon, Strontium, Thorium, Tritium (3H), and Uranium. EPA, 1999.

28.   IAEA-TECDOC-1616, *Quantification of radionuclide transfer in terrestrial and freshwater environments for radiological assessments.* 2009: IAEA.

29.   Sheppard, S., et al., *Solid/liquid partition coefficients (Kd) for selected soils and sediments at Forsmark and Laxemar-Simpevarp.* 2009, Swedish Nuclear Fuel and Waste Management Co.

30.   Begg, J.D., M. Zavarin, and A.B. Kersting, *Desorption of plutonium from montmorillonite: An experimental and modeling study.* Geochimica et Cosmochimica Acta, 2017. **197**: p. 278-293.

31.   Zhao, P., et al., *Plutonium (IV) and (V) sorption to goethite at sub-femtomolar to micromolar concentrations: redox transformations and surface precipitation.* Environmental science & technology, 2016. **50**(13): p. 6948-6956.

32.   Marsac, R., et al., *Modeling plutonium sorption to kaolinite: Accounting for redox equilibria and the stability of surface species.* Chemical Geology, 2015. **400**: p. 1-10.

33.   Banik, N., et al., *Sorption and Redox Speciation of Plutonium at the Illite Surface.* Environ. Sci. Technol., 2016. **50**(4): p. 2092-2098.

34.   Krupka, K., et al., *Understanding variation in partition coefficient, Kd, values. Volume I: The Kd model, methods of measurement, and application of chemical reaction codes.* Washington, DC: US Environmental Protection Agency, 1999.

35.   Krupka, K., et al., *Understanding Variation in Partition Coefficient, Kd, Values. Volume II: Review of Geochemistry and Available Kd Values for Cadmium, Cesium, Chromium, Lead, Plutonium, Radon, Strontium, Thorium, Tritium (3H), and Uranium.* Rep. No. EPA-402-R-99-004A, Office of Air and Radiation, Office of Solid Waste and Emergency Response, US Environmental Protection Agency, Washington, DC, 1999.

36.   Caritat, P.d. and M. Cooper, *National Geochemical Survey of Australia: The Geochemical Atlas of Australia.* Geoscience Australia Record, ed. G. Australia. Vol. 2011/20 2011: Department of Resources, Energy and Tourism.

37.   Sheppard, S.C., *Robust Prediction of Kd from Soil Properties for Environmental Assessment.* Human and Ecological Risk Assessment: An International Journal, 2011. **17**(1): p. 263-279.

38.   Tagami, K., et al., *Terrestrial Radioecology in Tropical Systems*, in *Tropical Radioecology*, M.B. J R Twining, Editor. 2012, Elsevier. p. 155-230.

39.   Voegelin, A., et al., *Multicomponent transport of major cations predicted from binary adsorption experiments.* Journal of contaminant hydrology, 2000. **46**(3-4): p. 319-338.

40.   Emerson, H.P., D.I. Kaplan, and B.A. Powell, *Plutonium binding affinity to sediments increases with contact time.* Chemical Geology, 2019. **505**: p. 100-107.

41.   Payne, T.E., et al., *Guidelines for thermodynamic sorption modelling in the context of radioactive waste disposal.* Environmental Modelling and Software, 2013. **42**(C): p. 143-156.

42.   Brown, J.E., et al., *A new version of the ERICA tool to facilitate impact assessments of radioactivity on wild plants and animals.* Journal of Environmental Radioactivity, 2016. **153**: p. 141-148.

The nature of plutonium at Maralinga: significance for predicting the environmental fate of hot particles

Authors: Megan Cook[1*], Barbara Etschmann[1], Rahul Ram[1], Joël Brugger[1], Konstantin Ignatyev[3], Gediminas Gervinskas[4], Susan Cumberland[2], Vanessa NL Wong[1]

Affiliations

[1]School of Earth, Atmosphere & Environment, Monash University, Australia

[2]The University of Strathclyde, Glasgow, UK

[3]Diamond Light Source, Oxford, UK

[4]Ramaciotti Centre for Cryo-Electron Microscopy, Monash University, Australia

*Correspondence to: megan.cook@monash.edu

Highlights

- Hot particles are characterised at the micro-, nano- and atomic scale
- Particles reveal complex heterogeneous polymetallic melts with varied internal structures and textures exhibiting a fragile nature
- Aged hot particles show external weathering and internal alpha decay damage providing evidence of the mechanisms of physical breakdown
- Plutonium is present in nanoparticulate (≤ 1 µm) form in all studied particles identifying a secondary contaminant form and possible augmentation to the hot particle risk assessment approach

Abstract

The high-energy release of plutonium (Pu) from the Maralinga nuclear testing and safety trials (1953-1963) resulted in the wide dispersion of Pu in the form of µm-sized, highly radioactive 'hot' particles that persist in soils. By combining non-destructive multi-technique synchrotron-based micro-characterization with the first nano-scale imaging of the internal composition of six Maralinga particles, we find that all particles show a far more intricate *physical* and *chemical* architecture than previously assumed. The hot particles show remarkably complex physical/chemical composition predicting increased reactivity, and resulting from cooling of polymetallic melts within the detonation plume. Moreover, some of the particles contain low valence plutonium-uranium-carbon compounds; such phases are typically pyrophoric at these sizes and are expected to spontaneously oxidize in contact with air or water. Nano-scale imaging of dissected particles shows that these low valence domains are protected by their inclusion in metal alloys, resulting in their preservation in soils over decades. At Maralinga, breakdown of the hot particles via mechanical fragmentation (due to phase heterogeneity and evolving porosity) and chemical weathering may result in the release of reactive plutonium-rich nanoparticles, increasing dispersion and causing long-term risks. It is notoriously difficult to predict the long-term environmental behavior of hot particles, and the example of Maralinga shows that nano-scale characterization of a particle population is required to understand their chemical and textural diversity; identify on-going weathering processes, their mechanisms, and kinetics; and provide the necessary information for prediction of the long-term (>100 years) stability of hot particles.

One Sentence Summary

Advanced multi-method characterisation of hot particles from Maralinga, Australia, reveals that plutonium is present in nano-particulate form and may be released into the atmosphere or groundwater over time due to the fragile nature of these particles.

Introduction

Plutonium (Pu) particles dispersed in the environment as a result of nuclear fuel cycle, weapons testing, and nuclear accidents are likely to be refractory and unreactive in their native state [1].

However, they may be susceptible to chemical weathering and/or physical breakdown [2]. Plutonium can then become mobile and bio-available in the environment in water-soluble or particulate forms, resulting in a long-term radiological risk to ecosystems and human health [3]. At Maralinga, South Australia, the British nuclear testing program (1952-1963) involved seven nuclear weapons tests as well as numerous minor subcritical tests designed to investigate the performance of weapons components and safety issues [4] (Table S4). The principal contamination is due to the Vixen B trials that dispersed 22.2 kg of Pu across the 260 km^2 'Taranaki' test site [5]. Plutonium uptake by wildlife appears to have remained constant for the last ~30 years, leading to the suggestion of slow Pu release from hot particles as a result of on-going weathering at Maralinga [6].

Maralinga hot particles were shown to be highly heterogenous based on bulk radionuclide contents and µm-scale chemical mapping of five particles by proton induced X-ray emission (PIXE) micro-spectrocopy [5, 7]. This reflects the varied nature of the tests and associated devices [7]. Recently, Ikeda-Ohno et al.[2] studied a single particle from the Vixen B trials using Synchrotron micro-X-ray fluorescence (µSXRF) and micro-X-ray absorption spectroscopy (µXAS). This work confirmed that the Pu-U distribution was inhomogeneous, showed that Pu is present in the form of Pu(IV) (oxy)hydroxide compound(s), and speculated that the particle forms a "core-shell" structure with a Pu(IV) oxyhydroxide core surrounded by an external layer containing Ca, Fe, and U. It is determined that this core-shell is linked to significant weathering of the particle following 50 years exposure.

The aim of this study is to assess the long-term fate of the hot particles released during the trials, and evaluate the potential pathways of Pu liberation and bioavailability. We characterized the chemical and physical nature of six hot particles at the µm- to the atomic-scales using non-destructive synchrotron µ-X-ray-based techniques followed by dissection of selected particles with focused-ion beam-SEM (nominal resolution <4 nm).

The multi-scale characterization revealed an unexpected heterogeneity in the chemical and physical properties of all the investigated particles, resulting in a paradigm shift in our understanding of the nature of Maralinga hot particles. We use the new information to (i) decipher mechanisms that led to the formation of hot particles with highly complex and varied internal composition at Maralinga; (ii) revisit the evidence for on-going weathering processes affecting Pu

and U in the hot particles; and (iii) explore the pathways for long-term Pu release from the hot particles. The Maralinga particles are models for hot particles released during subcritical nuclear incidents, and this knowledge can be applied to nuclear forensics applications. Overall, these new results corroborate that particle inhomogeneity, morphology [2, 3, 8] and internal architecture are as, if not more, important than the speciation of Pu in the environment to determine its fate, and demonstrate that the accuracy of predictive models depends on the inclusion of these parameters obtained from experimental measurements.

Hot Particles: Description and Chemical Composition

Six particles were extracted from proximal and distal soils sampled at Taranaki (Maralinga; Figs. SI1) ground zero during 1984 remediation efforts, and archived since at the Australian Radiation and Nuclear Safety Agency in sealed containers under ambient conditions (details in Supplementary Information (SI)). In keeping with the Australian tradition of informality, particles named *Potatohead* and *Bruce* were extracted by Burns, Cooper [9]; Cooper, Burns [5], whereas *CeresI*, *CeresII*, *CeresIII*, and *Chip* were extracted during this study from archived soil samples. A dry extraction procedure ensured minimal perturbation of the surface of the particles during their recovery from the soils. (see SI for details). Based on synchrotron µ-X-ray fluorescence (µSXRF) data, obtained at beam line I18 at the Diamond Synchrotron, Oxfordshire, UK (details in SI), the particles are classified into three different chemical groups (Table 1; elemental maps in Fig SI2; bulk spectra in Fig. S3): (i) relatively homogeneous co-location of Pu+U (*Potatohead* from the NW plume), (ii) highly heterogenous distribution of Pu+U (Bruce from the NE plume), and (iii) Pb-rich particles with discrete Pu ± U inclusions (CeresI-III + Chip from the northern plume). These groupings correlate with each distinctive detonation phenomenology.

Potatohead and Bruce were further characterized by µSXRF-fluorescence tomography (Fig. 1a,b), µ-X-ray Absorption Near Edge Structure (µXANES) (Fig. SI-5), µ-Extended X-ray Absorption Fine Structure (µEXAFS) (Fig. SI-6) and µ-X-Ray Diffraction (µXRD) (Fig. SI-7, SI-8) to provide information on Pu-U oxidation states and identify mineral phases present in the particles (details in SI-Hot particle composition).

Table 1. Hot particle characterization using SXRF, XAS, and XRD techniques.

Particle Name and Locality	Description	Major elemental composition	Oxidation state Pu and U	Major mineral composition
Bruce (GNE*) North-east plume	Irregular, uneven oblong particle with bumpy surface Length = 518 µm	Pu, U, Fe, Al	Pu(0)+Pu(IV)+Pu(III), U(IV/VI)	Pu, PuO_{2+x}, UO_{2+x}/U_3O_7, Al-Fe alloy/Al
Potatohead (ZD600*) North-west plume	Irregular trapezoidal shape with uneven surface. Length = 336 µm	Pu, U, Al, Fe	Pu(IV), U(IV/VI)	PuO_{2+x}, UO_{2+x}/U_3O_7
Ceres I (K480i) 100m north GZ	Spherical, slightly oval particle with smooth surface containing slight imperfections Length = 218 µm	Pb	Pu(IV), U(IV)	Native lead.
CeresII (K480ii) 100m north GZ	Irregular, somewhat spherical particle with square protrusion on surface Length = 216 µm	Pb	n/a	Native lead.
Ceres III (K480iii) 100m north GZ	Spherical particle with smooth surface containing slight imperfections Size = Length = 222 µm	Pb	n/a	Native lead.
Chip (K480iv) 100m north GZ	Irregular, oblong particle with smooth surface length = 110 µm	Pb	n/a	Native lead.

* Particles from study of Burns, Cooper [9]; Cooper, Burns [5]

The phenomenology of hot particle formation is incredibly unique. The thermochemical environment during hot particle formation assumes that the device components are exposed to a variable oxidising environment as atmospheric oxygen is secluded from or drawn into the fireball upon detonation [10]. The high temperature allows volatile elements to escape, while refractory

elements remain. The high pressure of the detonation also influences the crystallographic structure within the particle [11].

Composition and Texture

µSXRF-tomography

µSXRF-fluorescence tomography further highlighted the differences between *Potatohead* and *Bruce*. (Fig. 1). Whereas the concentrations of U and Pu are generally positively correlated in *Potatohead*, they are decoupled in *Bruce*; *Bruce's* framework is Pu-rich, but *Bruce* also contains particles of a U-rich phase varying in size from ≤2 µm to 10 µm (Fig. 1). Both particles contain volumes characterized by low total X-ray attenuation (Fig. 2); FIB-SEM data (see below) reveal that these volumes correspond to empty pores in Potatohead, but consist of light elements in Bruce. (Fig. 3). These may be empty pores or consist of light elements (e.g., Be, Al); the characteristic X-rays of light elements are fully absorbed by a few µm of U/Pu-rich material.

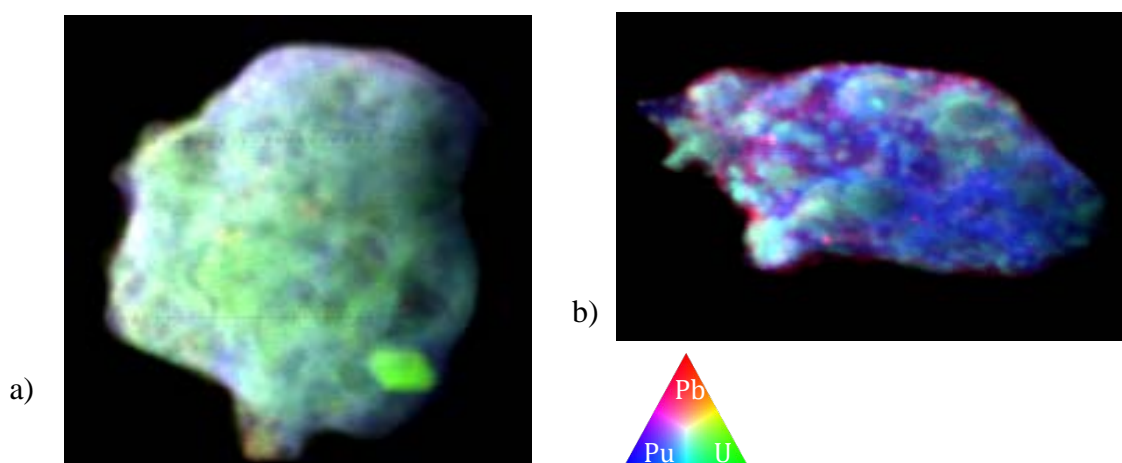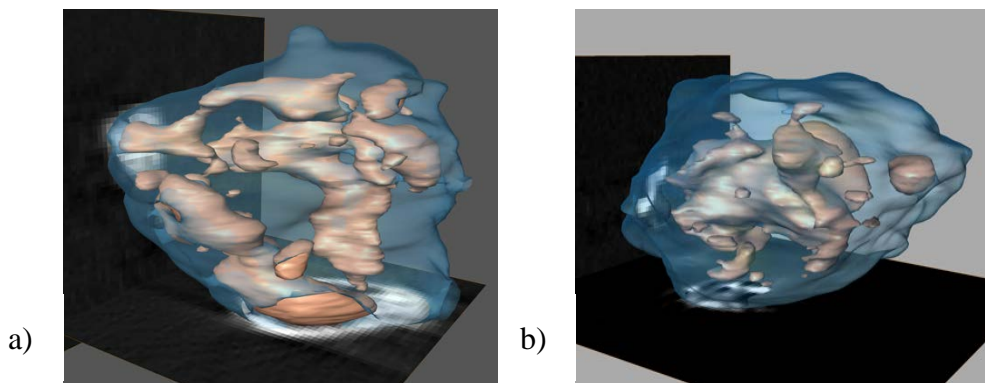*Figure 1. µSXRF Pu, U, Pb distribution in a) Potatohead and b) Bruce*

Figure 2. µSXRF-tomography images highlighting porosity of a) Potatohead and b) Bruce. The darker blue colour represents areas of Pu+U, while the lighter orange colour represents porosity in Potatohead and low-Z elements in Bruce.

Focused-Ion Beam-Scanning Electron Microscopy (FIB-SEM)

The characteristic X-rays of light elements are fully absorbed by less than a µm of U/Pu-rich material, which limits the information that can be gathered via non-destructive X-ray fluorescence. Hence, FIB-SEM was used to dissect *Potatohead, Bruce*, and *CeresIII* (Figs. 3 and 4). High resolution electron imaging and X-ray spectroscopy of the freshly exposed surfaces reveal the significant complexity of the internal textures of the grains and the micro (<5 µm) to nanoparticulate (1-450 nm) nature of the Pu-rich phases; we follow the definition of nanoparticle of Salbu et al.[3].

The extensive porosity of *Potatohead* is distinctive to gas entrapment pores and thermal cracks. This structure is representative of the high burnup structure of fast reactor mixed oxide fuels with high Pu content agglomerates, showing small, submicron sized grains surrounding porosity [12]. Aside from a U-rich inclusion, the Pu and U concentrations are highly correlated in *Potatohead* according to µSXRF and fluorescence tomography data (Figs. 1 and SI4). The nm-scale SEM characterisation reveals that *Potatohead* comprises of Pu/U+O particles, which synchrotron-XRD confirmed to be $(Pu/U)O_{2-x}$, that are up to ~1 µm in diameter, and are embedded in an Al-rich matrix (Fig. SI-7). We assume the incorporated Al is from the bomb casing or support structure, although no information is available in public records (Table SI-4). The FIB-SEM imaging also reveals that the porosity observed via tomography (size down to 2µm) consists of abundant spherical pores that go down in size to ~1 µm.
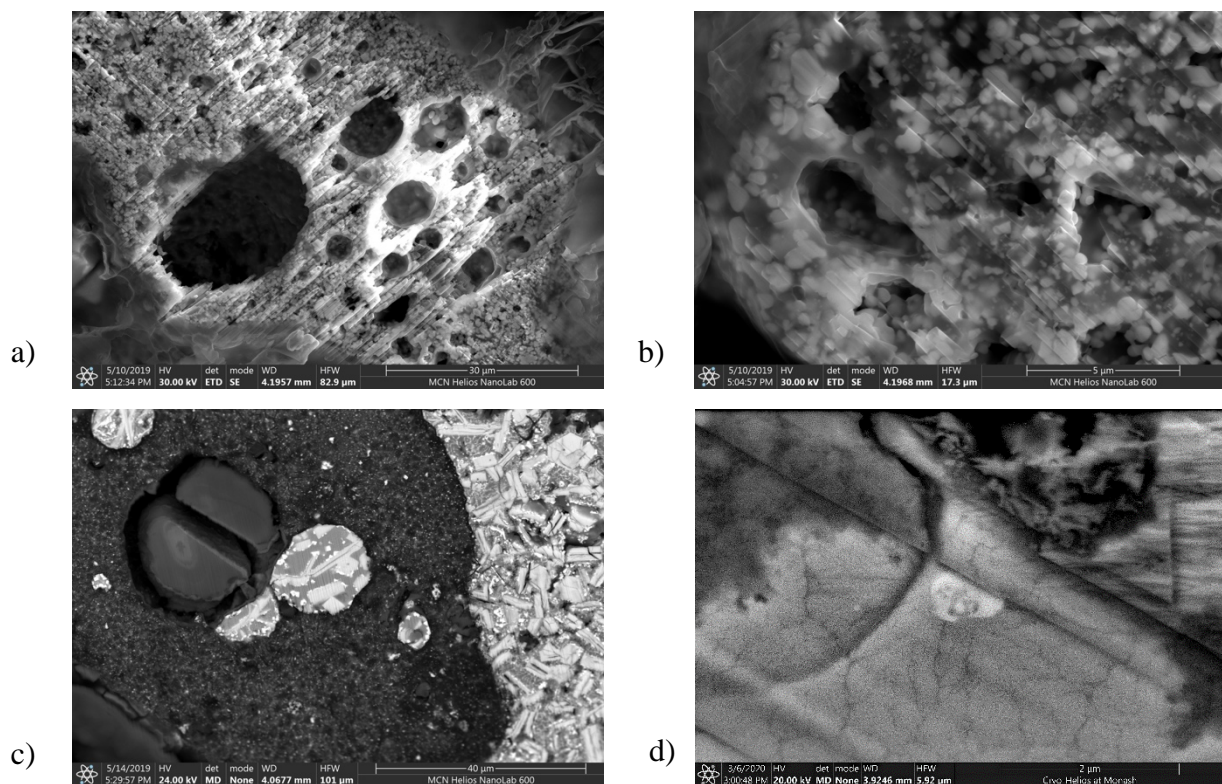
Figure 3. BSE images of a) Potatohead exhibiting popcorn-like texture of Pu-U phase and pores due to gas entrapment b) submicron Pu particles in Potatohead c) complex multi-phase composition of Bruce d) Pb matrix of CeresIII with Pu (light-coloured) creating alpha decay damage plus weathering evident at the perimeter.
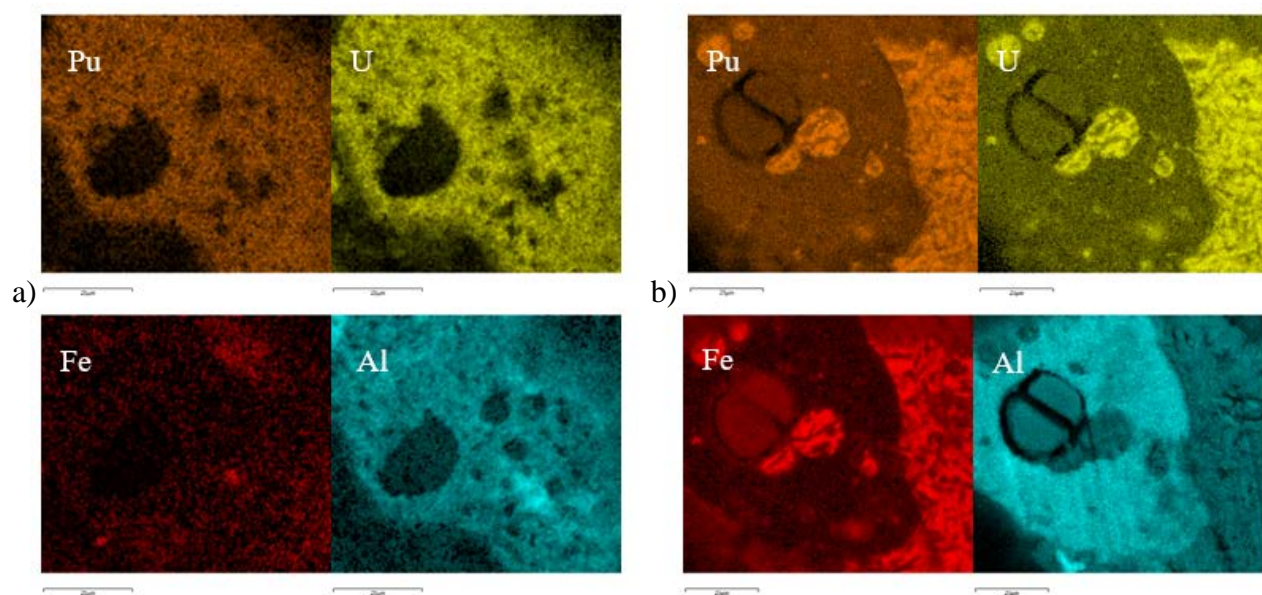

Figure 4. FIB-SEM elemental distribution in a) Potatohead and b) Bruce

FIB-SEM exposed a side of *Bruce* and revealed a number of internal phases and exceptional chemical and textural heterogeneity (Fig. 3c, 4b). The heterogeneity of *Bruce* is distinct with the lighter-coloured crystalline formations of fissile material and aggregates of darker non-fissile fragments. The agglomeration has created thermal cracks, which are the result of internal stress relaxation when the particle cooled external to the detonation fireball. The textures are consistent with a coexistence of two immiscible melts in Figure 4b, spherical inclusions of the Pu-U-Fe rich composition float with the Al-rich composition. Similar to Al, Fe likely originates from the structures supporting the test devices or the bomb casing. These Al-rich compositions correspond to the low-density areas in the tomogram (Fig. 2), and contain numerous, sub-µm-sized inclusion of a Pu-U rich phase (light spots in Fig. 3c).

The FIB-SEM cut confirms that *CeresIII* (Fig. 3d) was predominantly composed of metallic Pb. A rim of small (wt%) amounts of Pb-O-Fe were present with an outer layer of Ca and Si, minimal Pu or U was detected in the cut. There are small distinct micron-sized particles of Pu/U, both in the metallic Pb and oxidised Pb-O layers. *CeresIII* displays a thin (5-10 µm thick) rim of Pb-O replacing metallic Pb (Fig. 3d), indicating localized oxidation (weathering). Two types of porosity are present: the Pb-O weathering rim contains numerous cracks that extend into the metallic lead core and cracks emanating from the Pu-U particle in the metallic Pb area are indicative of radiation damage (Fig. 3d). These structural peculiarities are crucial for understanding the effect of weathering on these particles as they enter the environment.

Evolving hot particle fate and transport

Radioactive particles from fallout of nuclear material can carry substantial amounts of radioactivity, and represent point sources of radioactive contamination of potentially long-term environmental and ecological significance. Knowledge on particle characteristics and a comprehensive understanding of particle microstructures and their chemical and physical properties is necessary to extrapolate and assess long-term impacts from radioactive particle contamination [12]. The potential for Pu to migrate through the soil environment and enter the food chain can be defined using complex radioecological models to assess the risk to humans and non-human biota

Source Term

The initial conditions of Taranaki, the site at the focus of this study, are required to determine the full consequences of Pu particle contamination. Taranaki is 30 km north of Maralinga village, approximately 800 km NW of Adelaide in southern Australia (Fig. SI-1). The site was utilized for both major and minor trials resulting in extensive Pu contamination; the largest contamination plume showing easily detectable contamination 18 km from ground zero. These trials consisted of one balloon-supported nuclear detonation and five series totalling 12 safety trials. The nature of these trials was subcritical hydronuclear tests combining nuclear material, 4 TBq of plutonium in each series (approximately 22 kg in total), and high explosives that purposely resulted in negligible yield in order to study nuclear materials under conditions of explosive shock compression. The explosions dispersed plutonium along particular directions and carried finely divided plutonium in the direction of prevailing winds [13].

Measurements throughout the 1980s and 1990s [5, 9, 13-16] showed that most of the contamination remained within 10-20 cm of the soil surface (due to the arid climate) and consisted of three components: (i) visibly identifiable fragments of plutonium-contaminated debris, (ii) approximately uniformly distributed finely divided material (potentially inhalable), consisting of grains of plutonium oxide or contaminated soil, and (iii) heterogeneously distributed sub-millimetre size 'hot' particles of soil or other material. [17]

Physical breakdown

Maralinga hot particles have long been recognized to be friable; for example, Ikeda-Ohno's [2] particle broke into smaller pieces during gentle handing, as did our *Chip* particle. FIB-SEM data demonstrate that *Bruce* and *Potatohead* are intrinsically friable as a result of their chemical and physical heterogeneity down to the nm-scale. This phase heterogeneity results in joints and fractures providing points of mechanical weakness within the particle. (Figs. 2, 3 and SI9). Mechanical weathering is expected to predominate in deserts; the Maralinga nuclear test site is a hot, arid environment, with large diurnal fluctuations in temperature. The porosity and thermal cracks present in *Bruce* and *Potatohead* impart low mechanical properties and friability. Dislocations, impurities, interstitials, vacancies and Frenkel pairs are some of the crystal lattice defects present in PuO_2 material [18]. Frenkel pairs are caused by internal radiation damage (e.g. alpha particles 3×10^9 alpha emissions per gram per sec in ^{239}Pu; each 5 MeV alpha particle travels ~10 micron in the crystal causing damage along its path.) [18] (Fig. 3d)

The decreasing size of Pu particles as a result of mechanical breakdown has associated risks, in that particles less than 10 µm have been identified as a respirable risk, and the increased surface area of small particles makes them more amenable to chemical weathering.

Chemical weathering

Our results confirm the mostly refractory nature of Pu in these hot particles [3]. (Bio)chemical weathering in a semi-arid zone such as Maralinga is expected to be episodic, since water is absent most of the time [23]. A core-shell style chemical weathering was observed in *CeresIII* (Figs. 3d), replacing the Pb alloy with a Pb-O phase. This oxidation increased porosity, and Pu speciation changed from low-valence Pu in the core to Pu-O compounds in the weathered rim, concomitant with a decrease in size of the Pu-rich particles. Hence, in this case, chemical weathering clearly increases the probability of Pu release from the particle.

Further, a significant portion of Pu is present in low valence form in *Bruce* and *CeresIII*. This is the first report of Pu-carbide and Pu-bearing alloys in hot particles retrieved from the environment. Low valence Pu-U-carbide phases are typically pyrophoric at µm-grain size in contact with water or molecular oxygen [19], yet these phases were retained despite ~30 years exposure to an arid environment and then another ~30 years stored at ambient conditions. These highly reactive phases were likely protected by their inclusion in Fe-Al alloy (*Bruce*) and metallic Pb (*CeresIII*). In *CeresIII*, Pu-U-carbide exists within metallic Pb, but a Pu-U-oxide is predominant within the oxidized rim (Fig. 3d). The properties of actinide carbides are strongly dependent on minor or trace elements in the crystal structure [19]; this may further stabilize the carbide phases.

In general, the environmental behaviour of Pu is governed by its oxidation state: soil pH, solubility, hydrolysis, complexation, sorption and nanoparticle (colloid) formation reactions (all possibly catalyzed by microbiota [20]) differ significantly from one oxidation state to another [21, 22]. However, in the case of hot particles, Pu-rich phases can persist in chemical states that are far from equilibrium with their environment (water, air), as a result of the composition of these hot particles.

Prevalence of particulate transport

The processes affecting the fate of Pu in particulate form discussed above result in the release of Pu-rich particles ≤ 5 µm from bulk particulate form. Pu exists in micro- to nano-particulate form in all of the studied particles despite their heterogeneity, liberation of Pu does not require a

chemical process; simple mechanical breakdown will release nanoparticles. There is a paradigm emerging that Pu nanoparticles are less toxic than dissolved Pu species but more toxic than bulk hot particles. Nanoparticle-facilitated transport of Pu in groundwaters was first identified at the Nevada test site [22, 23] and at the weapon producing site at the Mayak Production Association, Urals, Russia [24]; Rocky Flats, Colorado, USA [25] and Hanford, Washington, USA [26]; (ii) at the nuclear power sites at Sellafield/Windscale, UK; Chernobyl, Ukraine; and Marcoule, France [26]; and (iii) in rivers waters related to the Grimsel test site, Switzerland [26]. The arid environment at Maralinga is conducive to both dust and waterborne nano-particulate transport; although rainfall is limited (~240 mm/year), it is often of a convective nature and characterized by high-intensity, short-duration events ($\geq$3 days with >10 mm rainfall per year [27]). Although direct evidence of nanoparticle transport is still lacking at the trace level conditions at Maralinga, direct imaging of the nature of the Pu-rich phases in the hot particles and their behavior during weathering suggest that this may be a primary cause for wildlife exposure [28].

Discrete hot particles resulting from nuclear critical (e.g., nuclear explosions) and subcritical (e.g., fires, corrosion etc.) destruction of nuclear materials such as fuel or weapon matrices, nuclear or radiological sources have been well studied using synchrotron x-ray techniques and imaging (Table SI-1). Utilising multi-scale characterisation for this work enabled the first nanoscale imaging and the first report of the presence of Pu nanoparticles within hot particles retrieved from the environment. Recently, it was found that Pu(IV) stabilization onto mineral surfaces may result in Pu surface precipitation in the form of PuO_2 nanoparticles [29-32]. Therefore, the study of PuO_2 nanoparticles becomes increasingly important, and it is actively being conducted [33-36].

Consequences for exposure pathways

The potential for Pu to migrate through the soil environment and enter the food chain, and the resulting risk to biota can be estimated using complex radioecological models. These models need to consider not only the amounts of radioactive material released to the environment following an accident, but also the physical and chemical characteristics of the contaminant and their potential changes through time in order to determine the long-term impacts arising from contamination [12, 22, 37-39]. Based on non-destructive micro-analytical characterization, hot particles from sub-critical nuclear incidents across the globe are chemically and texturally heterogeneous (Table SI-

1). This heterogeneity is hindering their inclusion in radioecological models that are used to predict long-term risks [40].

At Maralinga, the particles contain Pu (and U) in the form of high temperature, anhydrous phases, which are far from equilibrium with respect to environmental conditions. Textural and phase relationship considerations reveal that all studied particles formed via cooling of polymetallic melts resulting from fissile material mixing with the scorching detonation environment. The Pb, Fe and Al present in the particles reflect the composition of the individual devices and detonation structures [17]. Most Pu is hosted in nano-phases that crystallized during the cooling of these polymetallic melts, and, consequently, the micro- to nano-particulate nature of the Pu in these hot particles, regardless of their bulk composition, is an intrinsic result of their formation via cooling of micro-droplets of polymetallic melt [41] (Fig. 3c, 4b). The hot, anhydrous micro-environment under which the particles condense also accounts for the crystallization of phases that contain Pu (and U) in low valence state (carbides; Pu in Fe-(Al)-alloys). Sub-solidus reactions (e.g. *Bruce*; Fig. 3c, 4b; Fig SI-9) and weathering (*CeresIII*, Fig. 3d) further contributed to the generation of fine Pu-rich nanoparticles (<100 nm) subsequent to cooling.

The recognition of the nature and internal composition of the hot particles has important consequences for the cycling of Pu in the arid environment at Maralinga. Liberation of micro- to nano-particulate Pu is promoted over time via mechanical breakdown, facilitated by the heterogenous and/or highly porous nature of the particles and thermal cycling in the environment. In addition, near-surface particles have a high probability of ingestion by soil biota and higher animals. Compared to the parent hot particles, these micro- (<<5 µm) and nanoparticles have additional toxicity risks due to their small sizes, the low-valence state of Pu and their mobility in dust and groundwater.

The Vixen B trials at Maralinga were designed to simulate sub-critical nuclear incidents, i.e. accidents where energy is released from external fires or conventional explosives. Since these tests, the world has documented a few instances of such incidents (Table SI-1), including the B-52 accidents that resulted in the conventional detonation of thermonuclear weapons near Palomares, Spain [42] and Thule, Greenland [42, 43]; and the explosion of an armed nuclear missile and subsequent fire at the McGuire Air Force Base, USA [44]. Hot particles from these sub-critical nuclear incidents share the chemical and textural heterogeneity of the Maralinga particles as a

result of the similar mode of formation from polymetallic melts. In particular, the distinctive texture of *Potatohead* (Fig. 3a, b, 4a) is remarkably similar to that of the particles from Palomares [42] and Thule [43]; and hot particles from the McGuire Air Force Base accident have µSXRF images and Pu-U correlations similar to either *Bruce* and *Potatohead* [44]. In summary, hot particles released via high energy sub-critical incidents acquire their compositions and textures at high temperature within the explosion cloud, and this mode of formation sets the scene for their long-term environmental behavior [39]. We note that hot particles released following high energy failure of containment in nuclear reactors, such as Chernobyl [41, 45, 46] and Fukushima [47], also show heterogeneous compositions, with U±Pu associated with Zr and other metals from the reactor cladding [47-49]. These particles share a formation via cooling of high temperature melts, however in this case melting occurs in the nuclear fuel rather than in the explosion cloud.

Between 1950 and 1988 alone, there were more than 230 recorded nuclear weapon accidents, including at least 10 with documented release of radioactive particles into the environment [50]. Yet, there is currently no international best practice for the inclusion of Pu-U rich hot particles released during sub-critical incidents in environmental impact assessment or risk characterization. The new observations on the hot particles from the Maralinga tests provide a clear explanation for the heterogeneous behavior of different hot particles with respect to chemical and physical weathering [45, 51] that has hindered predictive modelling. Bulk characterization of the hot particles provides limited information about the nature and heterogeneity of the particles [2]. This issue is alleviated by the use of FIB-SEM nanoscale chemical and textural characterization. It exposes the diversity of hot particles; allows quantification of the different weathering pathways in historic particles; and provides the fundamental information for predicting the future behavior of the particles and the radioecological risk to humans and non-human biota. Future research in the area should be focussed on defining an empirical parameter that quantifies the interaction of (nano-) particulate Pu in soil in order to address the specific behaviour of the contaminant. There is a developing consensus that Pu nanoparticles may pose a relatively low environmental risk but uncertainty and a lack of data in many areas means definitive conclusions cannot be drawn. There have been pronounced developments in metrology, transformations, bioavailability and mechanisms of Pu toxicity where continued research is required to fill knowledge gaps, increase

integration of technological innovation and risk assessments to judiciously apply the precautionary principle.

Author contributions:

Megan Cook: concept, sample preparation, sample analysis, data collection, data analysis, writing first draft and finalising manuscript;

Barbara Etschmann: concept, data analysis, input into manuscript, finalising manuscript;

Rahul Ram: data analysis, finalising manuscript;

Joël Brugger: data analysis, input into manuscript, finalising manuscript;

Konstantin Ignatyev: sample analysis, data collection, data analysis;

Gediminas Gervinskas: sample analysis;

Susan Cumberland: sample analysis, data collection, finalising manuscript;

Ross Kleinschmidt: finalising manuscript;

Vanessa NL Wong: sample analysis, finalising manuscript.

Competing interests: Authors declare no competing interests.

Data and materials availability: All data is available in the main text or the supplementary materials.

References

1.   Salbu, B., *Radioactive particles released from different nuclear sources: With focus on nuclear weapons tests*, in *Nuclear Risks in Central Asia*. 2008, Springer. p. 7-17.

2.   Ikeda-Ohno, A., et al., *Fate of plutonium at a former nuclear testing site in Australia.* Environmental science & technology, 2016. **50**(17): p. 9098-9104.

3.   Salbu, B., et al., *Challenges associated with the behaviour of radioactive particles in the environment.* Journal of environmental radioactivity, 2018. **186**: p. 101-115.

4.   Symonds, J.L., *A history of British atomic tests in Australia*, ed. R. Australia. Department of, Energy, and L. Nijelo Pty. 1985, Canberra: Canberra : Australian Govt. Pub. Service.

5.   Cooper, M., et al., *Characterization of plutonium contamination at the former nuclear weapons testing range, at Maralinga in South Australia.* An International Journal Dealing with All Aspects and Applications of Nuclear Chemistry, 1994. **177**(1): p. 161-184.

6.   Johansen, M.P., et al., *Plutonium in wildlife and soils at the Maralinga legacy site: persistence over decadal time scales.* J Environ Radioact, 2014. **131**: p. 72-80.

7.   Burns, P.A., et al., *Properties of plutonium-contaminated particles resulting from British Vixen B trials at Maralinga*. 1990, Australian Radiation Lab.

8.   Batuk, O.N., et al., *Multiscale Speciation of U and Pu at Chernobyl, Hanford, Los Alamos, McGuire AFB, Mayak, and Rocky Flats.* Environmental science & technology, 2015. **49**(11): p. 6474.

9.   Burns, P.A., et al., *Plutonium-contaminated fragments at the Taranaki site at Maralinga*. 1986, Australian Radiation Lab.

10.   Cassata, W.S., et al., *When the dust settles: stable xenon isotope constraints on the formation of nuclear fallout.* Journal of Environmental Radioactivity, 2014. **137**: p. 88-95.

11.   Salbu, B. and O.C. Lind, *Analytical techniques for charactering radioactive particles deposited in the environment.* Journal of Environmental Radioactivity, 2020. **211**.

12.   Parrish, R. and A. Aitkaliyeva, *A review of microstructural features in fast reactor mixed oxide fuels.* Journal of Nuclear Materials, 2018. **510**: p. 644-660.

13.   MARTAC, *Rehabilitation of former nuclear test sites at Emu and Maralinga (Australia) 2003.* The Maralinga Rehabilitation Technical Advisory Committee: Canberra, Australia, 2003.

14.   Johnston, P.N., et al., *Isotopic ratios of actinides used in British nuclear trials at Maralinga and Emu.* 1988, Australian Radiation Lab.

15.   Lokan, K.H., *Residual radioactive contamination at Maralinga and Emu, 1985*. 1985, Australian Radiation Lab.

16.   Johnston, P., et al., *Plutonium contamination in the Maralinga Tjarutja lands*. 1989, Australian Radiation Lab.

17.   MARTAC, *Rehabilitation of former nuclear test sites at emu and maralinga (Australia)*, B. Williams and Themeda, Editors. 2003.

18.   Villa-Aleman, E., et al., *Raman microspectroscopy of PuO2 particulate aggregates.* Journal of Nuclear Materials, 2019. **515**: p. 140-149.

19.   Manara, D., et al., *Thermodynamic and Thermophysical Properties of the Actinide Carbides.* Comprehensive Nuclear Materials, Vol 2: Material Properties/Oxide Fuels for Light Water Reactors and Fast Neutron Reactors, 2012: p. 87-137.

20.   Newsome, L., K. Morris, and J.R. Lloyd, *The biogeochemistry and bioremediation of uranium and other priority radionuclides.* Chemical Geology, 2014. **363**: p. 164-184.

21.   Clark, D.L., *The chemical complexitites of Plutonium.* Los Alamos Science, 2000. **26**: p. 364-381.

22.   Kersting, A.B., *Plutonium transport in the environment.* Inorg Chem, 2013. **52**(7): p. 3533-46.

23.   Kersting, A., et al., *Migration of plutonium in ground water at the Nevada Test Site.* Nature, 1999. **397**(6714): p. 56.

24. Kazinskaya, I.E., et al., *Association of radionuclides with components of fulvic acids isolated from soils.* Radiochemistry, 2012. **54**(1): p. 87-91.

25. Santschi, P.H., K.A. Roberts, and L.D. Guo, *Organic nature of colloidal actinides transported in surface water environments.* Environmental Science & Technology, 2002. **36**(17): p. 3711-3719.

26. Geckeis, H., et al., *Environmental Chemistry of Plutonium*, in *Plutonium Handbook, 2nd edition.*, D.L. Clark, D.A. Geeson, and R.J. Hanrahan, Jr., Editors. 2019, American Nuclear Society. p. 1979-2118.

27. *Bureau Of Meteorology, http://www.bom.gov.au/jsp/ncc/climate_averages/raindays/ (retrieved 28/9/2020).*

28. Johansen, M.P., et al., *Plutonium in wildlife and soils at the Maralinga legacy site: persistence over decadal time scales.* Journal of Environmental Radioactivity, 2014. **131**: p. 72-80.

29. Kirsch, R., et al., *Oxidation state and local structure of plutonium reacted with magnetite, mackinawite, and chukanovite.* Environ Sci Technol, 2011. **45**(17): p. 7267-74.

30. Romanchuk, A.Y., et al., *Behavior of plutonium in the environment.* Russian Chemical Reviews, 2016. **85**(9): p. 995-1010.

31. Zhao, P., et al., *Plutonium (IV) and (V) sorption to goethite at sub-femtomolar to micromolar concentrations: redox transformations and surface precipitation.* Environmental science & technology, 2016. **50**(13): p. 6948-6956.

32. Schmidt, M., et al., *Surface-Mediated Formation of Pu(IV) Nanoparticles at the Muscovite-Electrolyte Interface.* Environmental science & technology, 2013. **47**(24): p. 14178-14184.

33. Powell, B.A., et al., *Stabilization of Plutonium Nano-Colloids by Epitaxial Distortion on Mineral Surfaces.* Environmental science & technology, 2011. **45**(7): p. 2698-2703.

34. Romanchuk, A.Y., et al., *Redox-mediated formation of plutonium oxide nanoparticles.* Dalton Trans., 2018. **47**(32): p. 11239-11244.

35. Kvashnina, K.O., et al., *A Novel Metastable Pentavalent Plutonium Solid Phase on the Pathway from Aqueous Plutonium(VI) to PuO2 Nanoparticles.* Angewandte Chemie International Edition, 2019. **58**(49): p. 17558-17562.

36. Gerber, E., et al., *The missing pieces of the PuO 2 nanoparticle puzzle.* Nanoscale, 2020. **12**(35): p. 18039-18048.

37. Haschke, J.M., T.H. Allen, and L.A. Morales, *Surface and corrosion chemistry of Plutonium.* Los Alamos Science, 2000. **26**(2): p. 252-273.

38. Hecker, S.S., *The Plutonium challenge- environmental issues.* Los Alamos Science, 2000. **26**(2000): p. 36-47.

39. Salbu, B., et al., *Challenges associated with the behaviour of radioactive particles in the environment.* J Environ Radioact, 2018. **186**: p. 101-115.

40. IAEA, *Quantification of Radionuclide Transfer in Terrestrial and Freshwater Environments for Radiological Assessments (978–92–0–104509–6). Retrieved from https://www-pub.iaea.org/MTCD/Publications/PDF/te_1616_web.pdf.* 2009.

41. Tooth, B., et al., *Bi-melt formation and gold scavenging from hydrothermal fluids: An experimental study.* Geochimica Et Cosmochimica Acta, 2011. **75**(19): p. 5423-5443.

42. Lind, O.C., et al., *Characterization of U/Pu particles originating from the nuclear weapon accidents at Palomares, Spain, 1966 and Thule, Greenland, 1968.* Sci Total Environ, 2007. **376**(1-3): p. 294-305.

43. Lind, O.C., et al., *Characterization of uranium and plutonium containing particles originating from the nuclear weapons accident in Thule, Greenland, 1968.* J Environ Radioact, 2005. **81**(1): p. 21-32.

44. Batuk, O.N., et al., *Multiscale Speciation of U and Pu at Chernobyl, Hanford, Los Alamos, McGuire AFB, Mayak, and Rocky Flats.* Environmental Science & Technology, 2015. **49**(11): p. 6474-6484.

45. Salbu, B., et al., *Hot Particles in Accidental Releases From Chernobyl and Windscale Nuclear Installations.* Analyst, 1994. **119**: p. 125-130.

46. Burakov, B.E., S.I. Shabalev, and E.B. Anderson, *Principal Features Of Chernobyl Hot Particles: Phase, Chemical And Radionuclide Compositions*, in *Role of Interfaces in Environmental Protection. NATO Science Series, IV. Earth and Environmental Sciences. Vol. 24.* 2003, Barany, S. p. 145-151.

47. Ochiai, A., et al., *Uranium Dioxides and Debris Fragments Released to the Environment with Cesium-Rich Microparticles from the Fukushima Daiichi Nuclear Power Plant.* Environ Sci Technol, 2018. **52**(5): p. 2586-2594.

48. Admon, U., *Single particles handling and analyses*, in *Radioactive Particles in the Environment*, D.H. Oughton and V. Kashparov, Editors. 2009, Springer. p. 15-55.

49. Kurihara, E., et al., *Particulate plutonium released from the Fukushima Daiichi meltdowns.* Sci Total Environ, 2020. **743**: p. 140539.

50. Gregory, S. and A. Edwards, *The hidden cost of deterrence - nuclear-weapons accidents 1950-88.* Bulletin of Peace Proposals, 1989. **20**(1): p. 3-26.

51. Cooper, M.B., et al., *Characterization of plutonium contamination at the former nuclear weapons testing range, at Maralinga in South Australia.* Journal of radioanalytical and nuclear chemistry, 1994. **177**(1): p. 161-184.

52. Symonds, J., *A history of British atomic tests in Australia.* 1985.

53. Holton, J.M., *A beginner's guide to radiation damage.* Journal of synchrotron radiation, 2009. **16**(2): p. 133-142.

54. Solé, V., et al., *A multiplatform code for the analysis of energy-dispersive X-ray fluorescence spectra.* Spectrochimica Acta Part B: Atomic Spectroscopy, 2007. **62**(1): p. 63-68.

55. Coelho, A.A., et al., *The T OPAS symbolic computation system.* Powder Diffraction, 2011. **26**(S1): p. S22-S25.

56. Ravel, B. and M. Newville, *ATHENA, ARTEMIS, HEPHAESTUS: data analysis for X-ray absorption spectroscopy using IFEFFIT.* Journal of synchrotron radiation, 2005. **12**(4): p. 537-541.

57. Rehr, J.J., et al., *Parameter-free calculations of X-ray spectra with FEFF9.* Physical Chemistry Chemical Physics, 2010. **12**(21): p. 5503-5513.

58. Conradson, S.D., et al., *Higher order speciation effects on plutonium L(3) X-ray absorption near edge spectra.* Inorganic chemistry, 2004. **43**(1): p. 116.

59. Conradson, S.D., et al., *Local and Nanoscale Structure and Speciation in the PuO{sub 2+x-y}(OH){sub 2y} ·zH₂O System.* Journal of the American Chemical Society, 2004. **126**(41).

60. Syverson, D.D., et al., *Oxidation state and coordination environment of Pb in U-bearing minerals.* Geochimica et Cosmochimica Acta, 2019. **265**: p. 109-131.

61. Atwood, R.C., et al., *A high-throughput system for high-quality tomographic reconstruction of large datasets at Diamond Light Source.* Philosophical transactions. Series A, Mathematical, physical, and engineering sciences, 2015. **373**(2043): p. 20140398.

62. Hund, F., *Fluoritmischphasen der Dioxide von Uran, Thorium, Cer und Zirkonium mit Wismutoxid.* Zeitschrift für anorganische und allgemeine Chemie, 1964. **333**(4-6): p. 248-255.

63. Zachariasen, W., *Crystal chemical studies of the 5f-series of elements. X. Sulfides and oxysulfides.* Acta Crystallographica, 1949. **2**(5): p. 291-296.

64. Ellinger, F. and W. Zachariasen, *The crystal structures of PuGa4 and PuGa6.* Acta Crystallographica, 1965. **19**(2): p. 281-283.

65.   Ellinger, F.H., C. Land, and V. Struebing, *The plutonium-gallium system.* Journal of Nuclear Materials, 1964. **12**(2): p. 226-236.

66.   Larson, A., D. Cromer, and C. Stambaugh, *The crystal structure of PuAl3.* Acta Crystallographica, 1957. **10**(7): p. 443-446.

67.   Osán, J., et al., *Study of the oxidation state of uranium and plutonium in Pu/U hot particles released to the environment.* 2005.

68.   Lind, O., et al., *Characterization of U/Pu particles originating from the nuclear weapon accidents at Palomares, Spain, 1966 and Thule, Greenland, 1968.* Science of the Total Environment, 2007. **376**(1-3): p. 294-305.

Conclusion

Understanding and quantifying the behaviour of Pu in the soil environment and the environmental variables affecting its transport and migration improves and validates radioecological models of interest for Australian exposure situations such as Maralinga and Montebello Islands. This thesis investigated the transport and migration of Pu isotopes in soils/sediments using Queensland sediments as a model system; established model inputs (Kd) describing the transport of Pu in different soil and rainfall regimes; and revealed the microstructure of Pu hot particles and the impact of particle structure and composition on Pu fate and transport. Here, the results are summarised and applied to current radiation protection practices.

6.1 Trace level analysis of Pu isotopes in varied soils

The capability to analyse trace levels of Pu isotopes in varied soils as routine analysis is applicable to environmental baseline characterisation, radioecological studies and emergency response scenarios. In chapter 1, an agile method for the analysis of Pu isotopes in soils/sediments was developed utilizing fusion with an oxidative catalyst, TEVA extractive chromatographic resin and alpha spectrometry. A larger sample mass, complete dissolution and greater than 70% tracer recoveries resulted in a trace-level detection limit of 0.04 mBq g^{-1}. The method has improved on the commonly used acid leaching processes with a focus on refractory fallout particles whilst addressing the capacity to employ an increased sample size and the removal of interfering elements for ease of analysis. This method was utilized throughout all laboratory experiments for the analysis of Pu isotopes.

6.2 Impacts for radioecological modelling of Pu

Mechanisms leading to transport and migration of radionuclides in soil (physical and chemical processes) are found globally. To address the features of environmental transport of Pu in Australian soils, a large-scale approach was initially taken. In Chapter 3, Queensland was used as a model system to obtain empirical Pu data to assess the extent of impact of the detonation plumes from the British nuclear testing program. The key environmental indicators (KEI) identified by the modified PCA of the data showed that the physical and chemical processes affecting the surrounding soils control Pu transport and migration. Overall, trace level Pu accumulations are associated with the coarse, refractive components of Australian soils, and are more likely regulated by the climate of the region and overall soil type. A database of the baseline Pu contamination and soil exposure across the north-east of the Australian continent was established as an output of this work. In applying radiation protection principles, the identification of KEIs plus baseline Pu activity concentrations enable this work to be utilised in emergency or existing exposure situations. These are situations where a rapid response for protective actions is required followed by possible remedial actions for situations in which Pu soil contamination may occur (e.g. nuclear accident in

the region via neighbouring country or visiting nuclear powered warship etc.). Knowledge of the current baseline Pu levels together with the identification of areas of radioecological sensitivity through KEIs, any intervention or remedial actions are well informed and provide a first step for risk characterisation.

In Chapter 4, the soil types and rainfall regimes of tropical and arid climates identified that dynamic abiotic soil parameters and contaminant sorptio kinetics should be analysed when performing assessments for non-temperate sites. The use of site-specific inputs to reduce uncertainties for radioecological models must be considered when performing an environmental impact assessment. As an indication of Pu transport capacity, the soil-water partition coefficient (Kd) was determined for sandy and clay soils under high and low rainfall regimes representing tropical and arid climates, respectively. The Kd trends showed a step-wise response for arid samples caused by the rainfall intensity and the extended rainless periods. An arid rainfall climatology allows the soils to dry prior to the next rain event, which increases the mobility of Pu at the next rainfall event. Importantly, the tropical sandy soil system has the potential to produce a Pu Kd of moderate mobility (6,000 mL.g^{-1}) within weeks, not years as previously suspected. Current radiological models cannot accurately represent the Kd probability distribution produced here therefore confirming that Pu Kd will continue to change over time, and the thermodynamic constant concept should be replaced with a time- or event-dependent Kd.

Highly heterogeneous hot particles incorporating Pu become long-term sources of contamination and defy many of the radioecological models and risk concepts currently used in radiation protection practices. In Chapter 5, Pu particles from Maralinga nuclear test site were characterised at the micro-, nano- and atomic scale to determine the physical and chemical properties that determine their long-term radiological risk to ecosystems and human health alike. All particles showed a complex heterogeneity resulting from the polymetallic melt at high temperatures in the detonation plume. Complex and varied internal structures including high porosity from gas entrapment, thermal cracks and amorphised zones along areas of structural weakness exhibit a fragile nature. The particles are coated in a Pu-carbide layer which lends its unreactive nature, however, external weathering and internal alpha decay damage is evident. Pu exists predominantly in nanoscale form within the fragile particles, indicating that chemical or physical breakdown or ingestion by higher animals will likely result in the release of Pu nanoparticles into the soil ecosystem to pose significant environmental and anthropogenic risks.

6.3 Concluding remarks

To justify and optimise radiation protection effectively, it is necessary to understand all the variables of concern. Having qualitative and quantitative data from an assessment of the site in hand means a risk characterisation can be performed. The objective of a risk characterisation is to

identify the potential for adverse effects to occur based on the hazard and exposure assessments. The qualitative and quantitative data presented here will reduce the uncertainty of radioecological modelling, and impact assessments, and ensure these are realistic and not excessively conservative. High quality environmental impact assessments for Pu contaminated sites must take into consideration the components reported: site-specific environmental transfer processes, seasonality of the transfer of Pu, the distinctive soil characteristics of the site, and the presence and form of particulate Pu.

Future research in this area should focus on the following:

- A controlled investigation of the identified KEIs at a range of Pu contamination levels to confirm and investigate the scope of impact of this environment on Pu transport and migration.
- Better mechanistic understanding of the biogeochemical processes that both facilitate and limit Pu transport in order to develop reliable transport models. Specifically, the susceptibility of Pu transport behaviour and environmental interactions to change in non-temperate environments.
- Further focussed experiments determining the chemical properties of Pu that are most affected by the different climate regimes.
- Inclusion of temperature as a variable of climate for column transport experiments to include biotic as well as abiotic parameters affecting Pu transport.
- Direct evidence of nanoparticle transport from Pu hot particle breakdown and particle behaviour during weathering
- Definition of an empirical parameter, for inclusion in modelling and impact assessments, that quantifies the interaction of nano-particulate Pu in order to address the specific behaviour of the contaminant

Appendices

Transport and migration of plutonium in different soil types and rainfall regimes

Megan Cook[a], Ross Kleinschmidt[b], Joël Brugger[a], Vanessa NL Wong[a]

[a]School of Earth, Atmosphere & Environment, Monash University, Australia

b Epic Environmental, PO Box 13058, Brisbane Queensland 4003, Australia

Supplementary Material

The MATLAB R2019 Distribution Fitter app interactively fits probability distributions to data. The app displays plots of the fitted distributions superimposed on a histogram of the data. Bin rules were set to a fixed number of 8 to reflect the event-dependency of the Kd and ensure the distribution of both climatologies were comparable. The probability distributions investigated were normal, lognormal, exponential, triangular (non-parametric), and uniform (non-parametric).
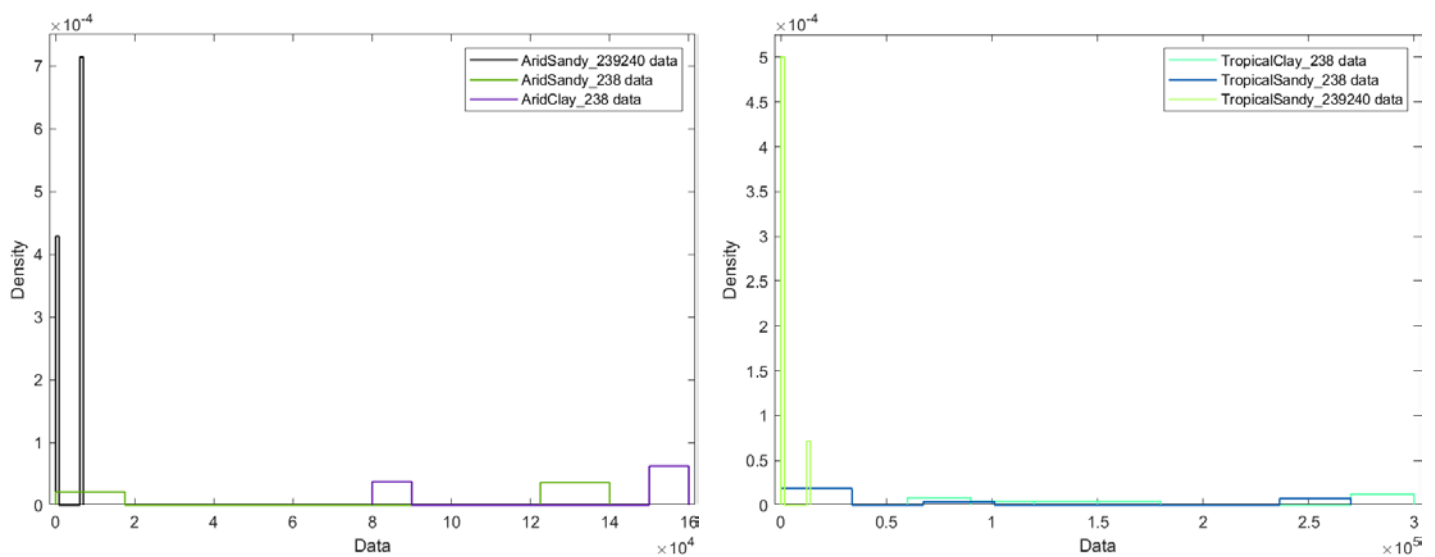

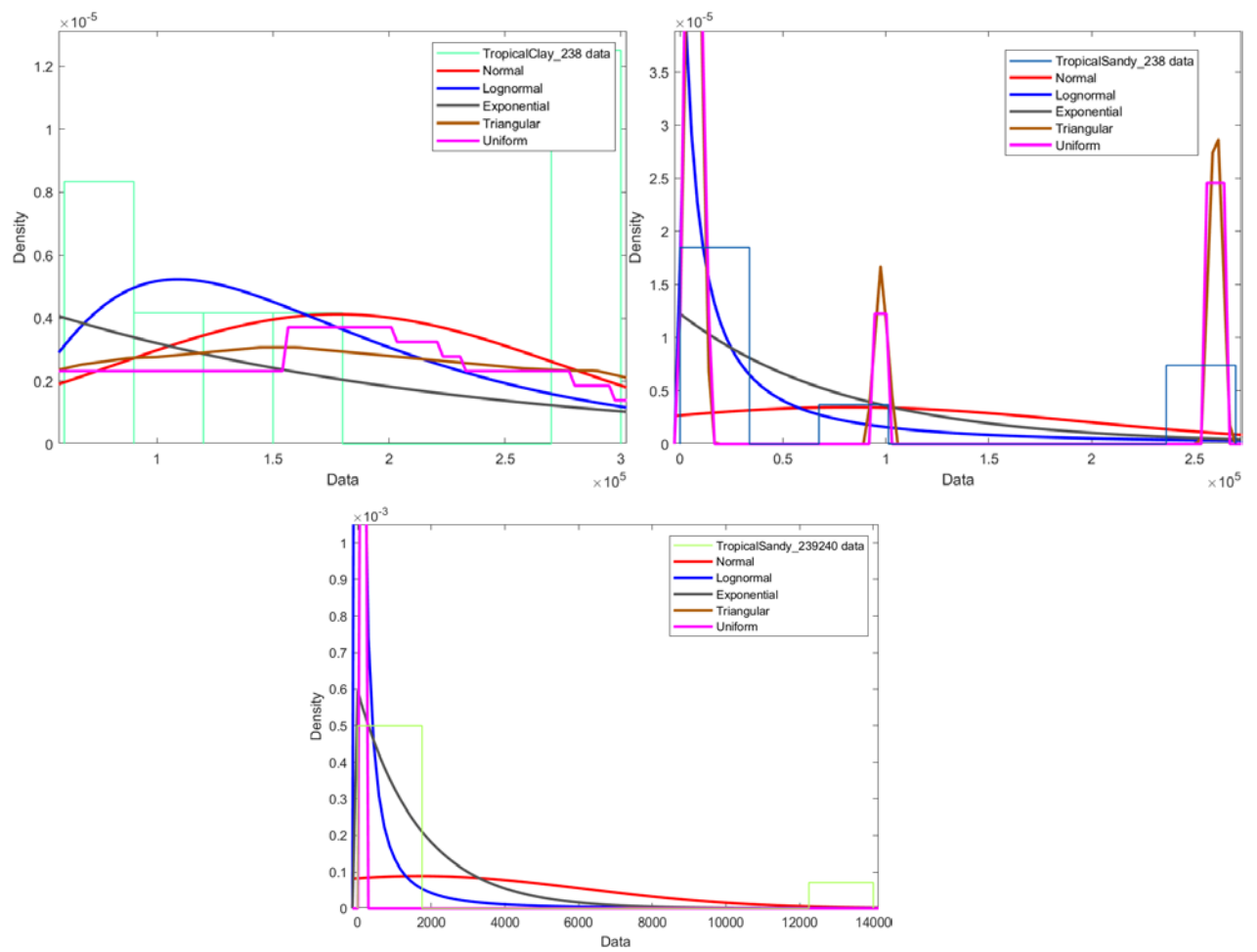*Figure S1 Kd probability distribution as determined in Matlab R2019 Distribution Fitter app*

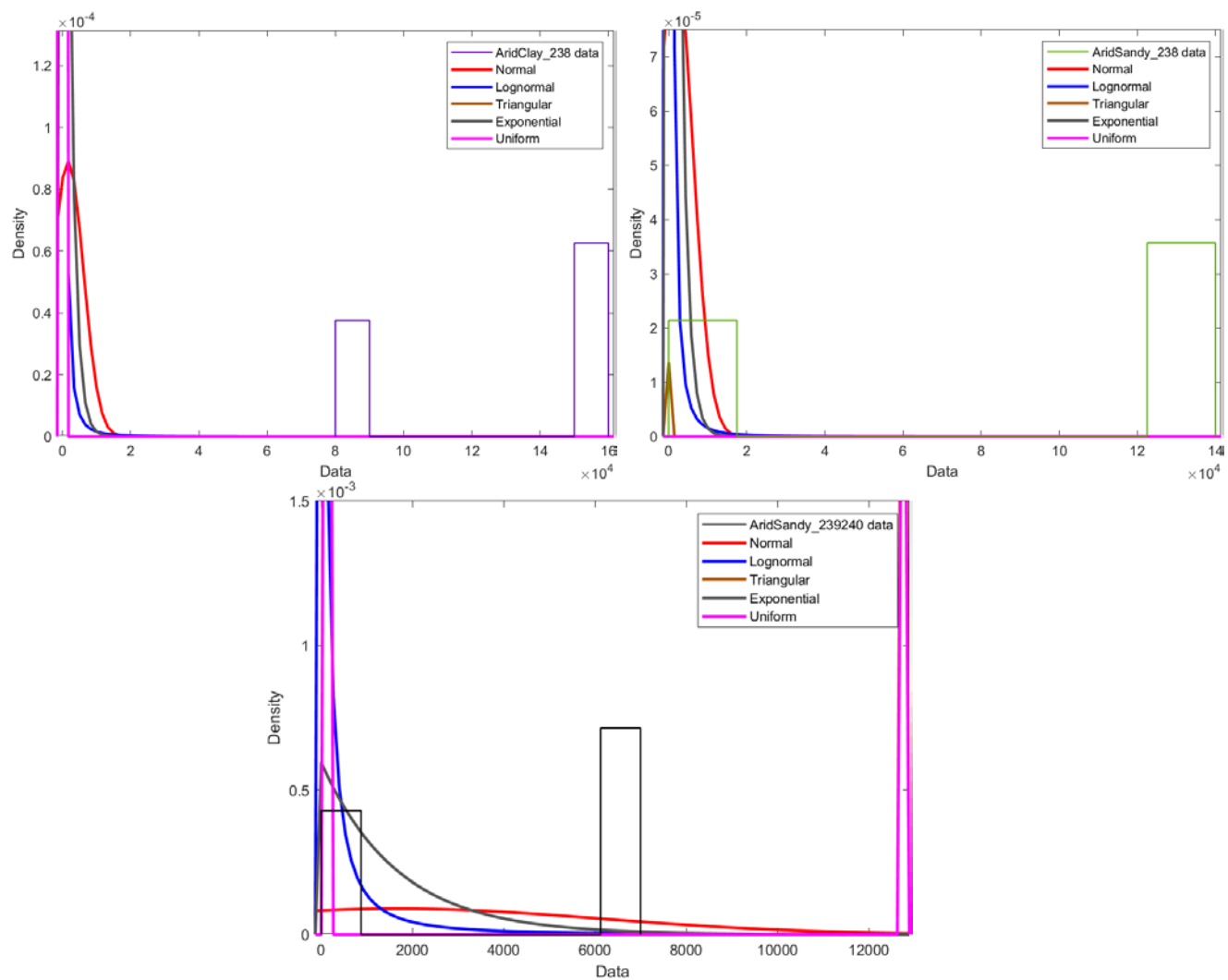*Figure S2 Kd probability distribution fits for high rainfall tropical climatology*

Figure S3 Kd probability distribution fits for low rainfall arid climatology

The nature of plutonium at Maralinga: significance for predicting the environmental fate of hot particles

Authors: Megan Cook[1*], Barbara Etschmann[1], Rahul Ram[1], Joël Brugger[1], Konstantin Ignatyev[3], Gediminas Gervinskas[4], Susan Cumberland[2], Vanessa NL Wong[1]

Affiliations

[1]School of Earth, Atmosphere & Environment, Monash University, Australia

[2]The University of Strathclyde, Glasgow, UK

[3]Diamond Light Source, Oxford, UK

[4]Ramaciotti Centre for Cryo-Electron Microscopy, Monash University, Australia

Supplementary Materials

Materials and Methods

Sample Site Description

The first contamination of Maralinga, an Australian nuclear test site with plutonium hot particles resulting from nuclear detonations occurred in September 1956 [52]. Twelve nuclear weapons tests and numerous minor trials investigating the performance of various components of a nuclear device took place as part of the British Nuclear Testing Program between 1952 and 1963. The secrecy surrounding the program at the time of the detonations and poor record keeping resulted in an incomplete account of the tests performed during the minor trials [52]. The incomplete account of these minor trials creates difficulty in linking particle characteristics to specific sources and in turn the prediction of interactions in the environment and a full understanding of environmental impacts and risks.

Soil sampling and extraction of hot particles

Soil samples were taken in 1984 (28 years after the trials) as part of a study [7] to aid in remediation of the site. More than 20 particles were extracted and analysed using gamma spectrometry and proton-induced x-ray emission (PIXE) spectroscopy [5, 7]. These samples were then archived and stored at the Australian Radiation and Nuclear Safety Agency (ARPANSA) under ambient conditions. The soil samples were stored in plastic ziploc bags, double sealed with tape and packed into and sealed in a 55 gallon drum. These were stored in an air-conditioned basement that is temperature controlled. There was no moisture present in the sample bag when it was retrieved. The separated particle (*Potatohead* and *Bruce*) were sealed with glue between two glass slides that have a central cavity, placed in plastic ziploc bags and stored in a separate sealed 55 gallon drum and stored in the same temperature controlled basement. Again, no moisture was present in the slide cavity when the sample was retrieved.

This study extracted proximal soil samples from the archived samples using gamma spectrometry to screen for the presence of hot particles. A high chance of the presence of hot particles was signified where overall gamma activity was greater than 100 kBq. From this region, a small aliquot (0.5 g) was sprinkled over an A4 page of thin cardboard covered in double-sided tape to achieve a single particle thin layer. This layer was then scanned systematically using a handheld RadEye gamma survey meter capable of detecting very low gamma energies (45 keV – 1.3 MeV, approximately 0.5 µSv/h lower detection limit), then 'hot spots' were removed with a scalpel. Further selection was assisted by means of an optical microscope and particles of interest were removed and examined using a small 2 cm^2 alpha pancake probe to confirm the presence of alpha emitters Pu, U and Am. Finally, selected particles were mounted on 10 µm kapton micromounts using superglue and doubly encapsulated with kapton tape.

This method of locating and extracting hot particles was developed to avoid altering the chemistry of the particle during preparation for analysis. Hot particles must be extracted from soil media prior to analysis to ensure interference-free analysis on the synchrotron beamline.

This study focuses on two hot particles, *Bruce* (one of 12 GNE particles) and *Potatohead* (one of 9 ZD600 particles) originating from the north-east and north-west plumes, see Figure S1, which were extracted by Burns, Cooper [7]. Unfortunately, it was not possible to equate *Bruce* and

Potatohead to the particle numbers attributed by [7]; Bruce is either GNE-1, 4, 7, 8 or 9; and Potatohead is either ZD600-1, 5, 6, or 9. Four additional particles were extracted from the stored soil samples according to the method described above; these particles originate from a soil sample taken 100 metres north of ground zero during remediation efforts (Figure 1); Ceres 1 (K480i), Ceres 2 (K480ii), Ceres 3 (K480iii) and Chip (K480iv).

Data collection at Diamond synchrotron

The chemical composition and physical nature of the particles were determined using SXRF (synchrotron X-ray fluorescence), XANES (X-ray absorption near edge structure), EXAFS (extended X-ray absorption fine structure), XRD (X-ray diffraction) and µSXRF-tomography, collected at the I18 beam line at the Diamond Synchrotron, Oxfordshire, UK. I18 is an undulator beam line with a Si (111) monochromator with an energy resolution of 1.4×10^{-4} at 10 keV. Kirkpatrick-Baez mirrors were used to focus the beam to a spot size of ~2x2 µm^2. Fluorescence (SXRF, XANES, EXAFS) and µSXRF-tomography data were collected with a Si-Drift detector with 130 eV resolution. A charge coupled device (CCD) detector was used to collect transmission diffraction (XRD) data. SXRF maps were collected at 18.2 keV; XAS (XANES and EXAFS) spectra were collected at both the Pu L_3 (18.057 keV) and U L_3 (17.166 keV) edges; XRD data were collected at 17 keV and µSXRF-tomography was collected at 18.2 keV. The energy for both U and Pu XAS edges were calibrated using a Zr foil (acquired simultaneously in transmission mode), such that the maximum of the first derivative of the Zr K-edge was at 17999.35 eV. Analysing Pu at the L_3-edge (fluorescence line $L_{\alpha1}$ 14 282 eV) is susceptible to overlapping peaks from greater concentrations of Zr ($K_{\alpha1}$ 15775 eV) and Sr ($K\alpha1$ 14165 eV) in the soil matrix.

Radiation damage caused by the synchrotron beam may occur at ambient temperature, the extent of damage being dependent on the photon flux incident on the sample [53], which is 2×10^{12} photons per second at I18. To minimise potential chemical changes induced by radiation damage, the time spent on each sample was limited to one to seven minutes per XANES analysis. Repeat measurements show non-significant changes for all particles.

SXRF data processing

SXRF data were processed using PyMCA 5.4.1 [54]; PyMCA enables full spectral fitting which is important when samples contain elements with overlapping X-ray lines (e.g. Pu, U, Sr). By fitting multiple X-ray transitions per element it is possible to distinguish between elements that have some overlapping X-ray lines.

XRD data processing

Due to the in-situ data collection using a micro-focused beam on a fixed point of the particles and the transmission geometry, the XRD data are not suitable for full quantification using the Rietveld method (limited amounts of mineral grains; significant absorption issues). XRD data were examined using Eva and Topas [55] which enabled phase identification and unit cell measurements.

XANES and EXAFS data processing

XANES and EXAFS data were processed using Athena and Artemis, part of the HORAE package [56] using FEFF v9 [57]. Pu standards are from Conradson (2004a, b) [58, 59] and U standards are from Syverson (2019) [60].

Fluorescence tomography data processing

µSXRF-tomography data were processed utilising Savu, a python framework developed at Diamond Light Source [61]. Data were further processed using Fiji and Avizo.

- Schindelin, J.; Arganda-Carreras, I. & Frise, E. et al. (2012), "Fiji: an open-source platform for biological-image analysis", *Nature methods* **9(7)**: 676-682, PMID 22743772, doi:10.1038/nmeth.2019 (on Google Scholar).
- https://www.thermofisher.com/au/en/home/industrial/electron-microscopy/electron-microscopy-instruments-workflow-solutions/3d-visualization-analysis-software/avizo-materials-science/avizo-2d-software-materials-characterization.html

FIB-SEM

Particles were sliced using a FEI Helios G4 UX cryo-FIB-SEM at the Ramaciotti Centre for Cryo-Electron Microscopy at Monash University, Victoria, Australia. The FIB-SEM is equipped with SE, BSE, EDX (Oxford X-Max-80-SDD) and mirror (an in-column) detectors.

Hot Particle Composition

In addition to µSXRF, Potatohead and Bruce were further characterized by µ-X-ray Absorption Near Edge Structure (µXANES) (Fig. SI5), µ-Extended X-ray Absorption Fine Structure (µEXAFS) (Fig. SI6, Table SI2) and µ-X-Ray Diffraction (µXRD) (Fig. SI7, Table SI3).

Group 1: Potatohead (single Pu form)

µXRD indicated the predominance of the crystalline phases $(Pu,U)O_{2+x}+(U,Pu)O_{2+x}$ in Potatohead; the asymmetry of the diffraction peaks suggests the presence of two distinct isostructural phases (one Pu-rich, the other U-rich), rather than a single mixed $(Pu+U)O_{2+x}$ (Fig. SI7B). The lattice parameters of the two phases were refined to be 5.448(2) Å and 5.418(3) Å, values that lie between those of the pure endmember UO_2 (5.466 Å [62]) and PuO_2 (a=5.397 Å [63]). The relatively large errors in the measured unit cells, derived from the average of seven measurements on different parts of Potatohead, reflect the difficulty in obtaining precise values due to the proximity of the two $(U/Pu)O_{2+x}$ phases. The refined unit cells are consistent with significant substitution of U and Pu in each endmember. µXANES results indicate that U is present mainly as U(IV), consistent with $(U,Pu)O_{2+x}$ phase. µSXRF and fluorescence tomography data indicate the presence of a U-rich, idiomorphic inclusion within Potatohead (Figs. SI2, SI4); a spectrum collected from this U-hot spot consisted of ~70% U(VI) and ~30% U(IV). EXAFS are consistent with UO_{2+x}, but the U hotspot is enriched in U(VI) (Table SI2) in uranyl form (U-O distances = 1.70(2) to 1.77(1) Å). Combined with the absence of U-U interaction in the second shell, this suggests the presence of a uranyl oxy-salt, although no such phase was detected in the µXRD data. Plutonium is present mainly as Pu(IV) (Figs. SI5-SI7). The bond lengths derived from EXAFS shell-by-shell fitting (Table SI2) are typical of those for PuO_{2+x}.

Group 2: Bruce (various forms of Pu)

Bruce presents with increased heterogeneity, agglomeration and irregular structure (Fig. 1b). The heterogeneity created joins and fractures providing points of weakness within the particle (Fig. 3c). μXRD analysis of Bruce showed a particularly complex phase makeup, with diffraction patterns varying from point to point, as shown in Fig. SI8. Pattern matching the XRD data, in conjunction with the μSXRF, μXANES and μEXAFS data, indicates that Bruce contains some $(Pu,U)O_{2+x}$, + $(U,Pu)O_{2+x}$, as well as bromellite (BeO), Al-Fe and Al-Mg alloys. The Pu XANES spectra were shifted to lower energy compared to Pu(IV), but the white line is less intense and broader than that expected for Pu(III) compounds [58, 59] and these spectra could be fitted as a linear combination of $Pu(0) + Pu(IV) \pm Pu(III)$. It should be noted that FIB-SEM (discussed below) indicated the presence of a Pu-U phase in a metallic Fe-Al alloy; there was no evidence for the presence of oxygen. (While the detection limits are on the order of wt%, and does not exclude the presence of minor amounts of oxygen, this does indicate the presence of more metallic-like Pu-U.) Note that the forms of Pu are difficult to distinguish from XANES alone, XRD plus SEM-FIB is key to verifying the validity of the XANES fitting model.

The Pu EXAFS spectrum #506 (Table S2; Fig. SI6) can be fitted with ~4.5 x O (Pu-O bond length = 2.37(1) Å) + 2 x Pu (Pu-Pu bond length = 3.74(5) Å), consistent with a structurally disordered PuO_{2+x}. An extra peak in R-space (phase un-uncorrected) is located at ~2.8 Å (Fig. SI6-A). This peak is not accounted for by adding small amounts of Pu_2O_3 into the fit, but can be fitted with a range of metals (Ga, Fe, Al, Pu) with bond lengths varying from 2.96 to 3.36 Å, suggesting the presence of some Pu-Ga/Fe/Al alloy. Pu-Ga alloys exist with bond lengths ranging from 3.01 Å [64] to 3.20 Å [65]; the Pu-Fe system has Pu-Fe bond at 2.98 Å and Pu-Pu bonds at 3.11 Å and Pu-Al has bond lengths at 3.02 Å ($PuAl_3$,[66] .

A second EXAFS spectrum (#398) measured at another point on Bruce had only one broad peak in R-space. This spectrum was modelled using a single Pu-O distance but with a rather large EXAFS Debye-Waller term, which suggests a range of Pu-O distances (Table S2). The absence of Pu-Pu or Pu-U contribution at large R (3.5−4.5 Å) demonstrates that Pu is not present as $(Pu/U)O_2+x$ crystals, but in monomeric form [8], e.g. dissolved in an amorphous or light metal alloy, for example in small amounts in the Al-rich alloy phase.

U XANES data indicate the presence of both U(IV) and U(VI), the U EXAFS spectra were too noisy to fit. Linear combination fitting of the XANES suggest approximately 50% U(IV) and 50% U(VI).

Group 3: Ceres 1 (predominantly Pb with heterogeneous distribution of Pu + U)

XANES data indicated that Pu exists as Pu(IV) and the U spectra closely match those of uraninite (i.e., UO_{2+x}, Fig. SI5); hence, U in CeresI is more reduced than in Potatohead and Bruce. The Pu EXAFS data (Fig. SI6, Table SI2) were fitted with 8 x O at a Pu-O bond length of 2.34(2) Å), as expected for PuO_{2+x}, and consistent with the Pu(IV) indicated by XANES. However, the further out electron density peak at 3.63(2) Å, while not typical of any known phase, can be fitted with 12 x Pb. Given the large amounts of Pb in/associated with this particle is does not seem unreasonable to postulate that this could be indicative of Pb atoms substituted into the PuO_{2+x} structure. The isostructural UO_{2+x} phase can incorporate up to 20 wt% PbO [60].

Results of previous studies of Pu containing particles

Ikeda-Ohno, Shahin [2] examined a particle from the Maralinga tests with SXRF and found that the Pu and U distributions were de-coupled. Batuk, Conradson [8] used SXRF imaging to show that particles from the McGuire Air Force Base accident have both homogenous and inhomogeous Pu+U distribution. Osán, Eriksson [67] using SXRF imaging and μSXRF-tomography found that in the particles collected from the Thule accident the Pu occurs predominantly where the U occurs, however the Pu/U intensity distribution varies. Lind, Salbu [68] demonstrated with SEM-EDX that the particles that they analysed from both the Thule and Palomares accidents had a homogeneous Pu+U distribution (Table S1).

These studies also characterised nature of Pu in these particles and found Pu to exist predominantly as Pu(IV), with evidence of Pu(III), P(V) and P(VI) as well and U to exist as a mix of U(IV) and U(VI). Lind, Salbu [43] studied three particles from Thule and found evidence of Pu(III)+Pu(IV) homogeneously distributed with U(IV). In, their later study, Lind, Salbu [68], examined 2 particles from Palomares and found a mixture of Pu(III)+Pu(IV)+Pu(V) co-existing with U(IV). Of the six particles from Thule analysed by Osán, Eriksson [67], contained predominantly Pu(IV) and two

particles were 33% Pu(IV)+ 67 % Pu(VI), and all were mixed heterogeneously with U(IV). Ikeda-Ohno, Shahin [2] examined five fragments from one particle from the nuclear test site at Taranaki, Maralinga and found a relatively insoluble $PuO_{2+x-y}(OH)_{2y} \cdot zH_2O$ phase coexisting with Pb surrounded by an external coating of Ca, Fe and U believed to be acquired from the soil. In one of the most comprehensive studies to date, Batuk, Conradson [8] characterised numerous hot particles and bulk soil & concrete samples from six different sites: Rocky Flats, McGuire Airforce Base, Chernobyl, Mayak, Los Alamos TA-21 and Hanford. Batuk, Conradson [8] showed the incredible complexity and variation of these particles. U varying from UO_{2+x} to U_2O_3 to U(UI) and Pu existing as both well ordered PuO_{2+x} and novel PuO_{2+x} type compounds incorporating additional elements; they concluded that the speciation may, but also may not, be associated with the source terms and histories of the samples.

Supplementary Figures

Figure SI-1: (a) Geographical location of Maralinga with location of major and minor trial sites (inset) (b) location of particles within contamination plume contours
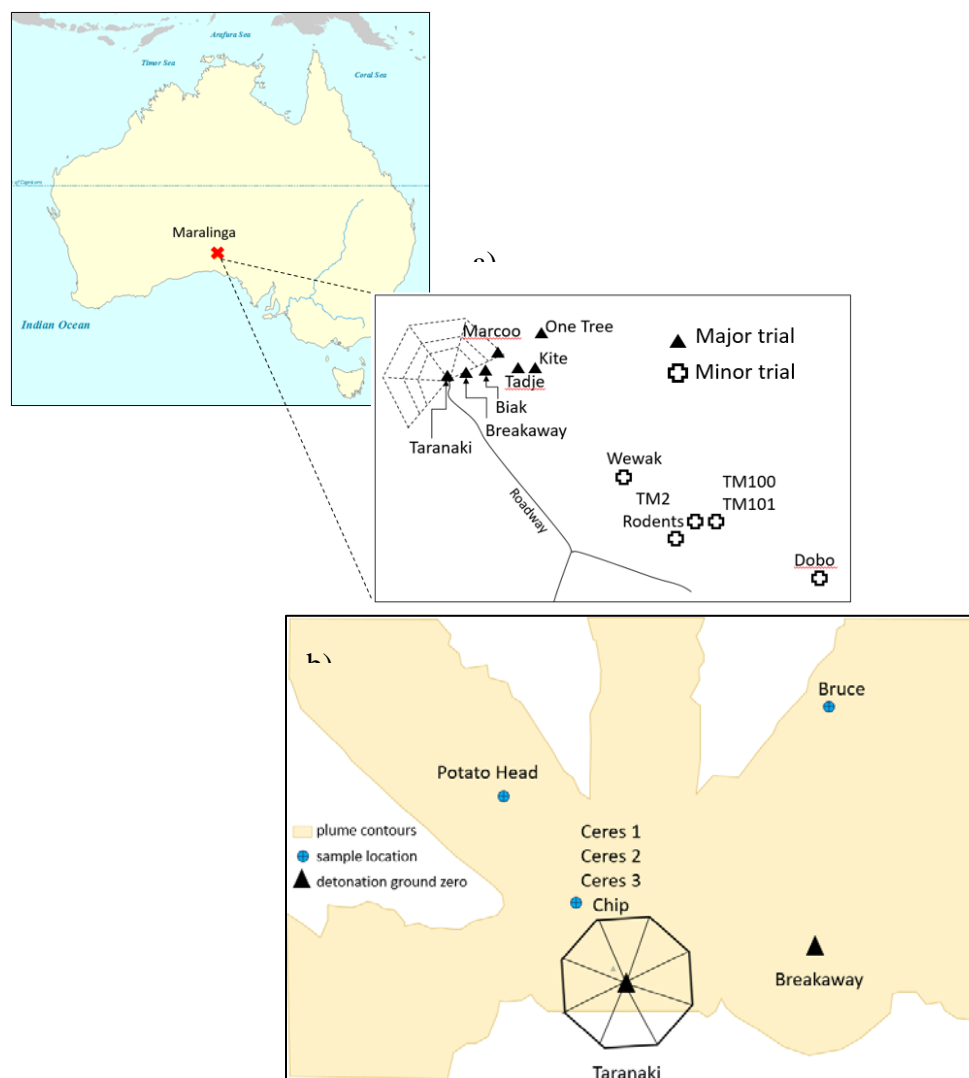
Figure SI-2. SXRF ROI mapping of all hot particles, Pu in blue, U in green, Pb in red.
a) Potatohead; b) Bruce; c) Chip; d) Ceres II; e) Ceres I; and f) Ceres III.
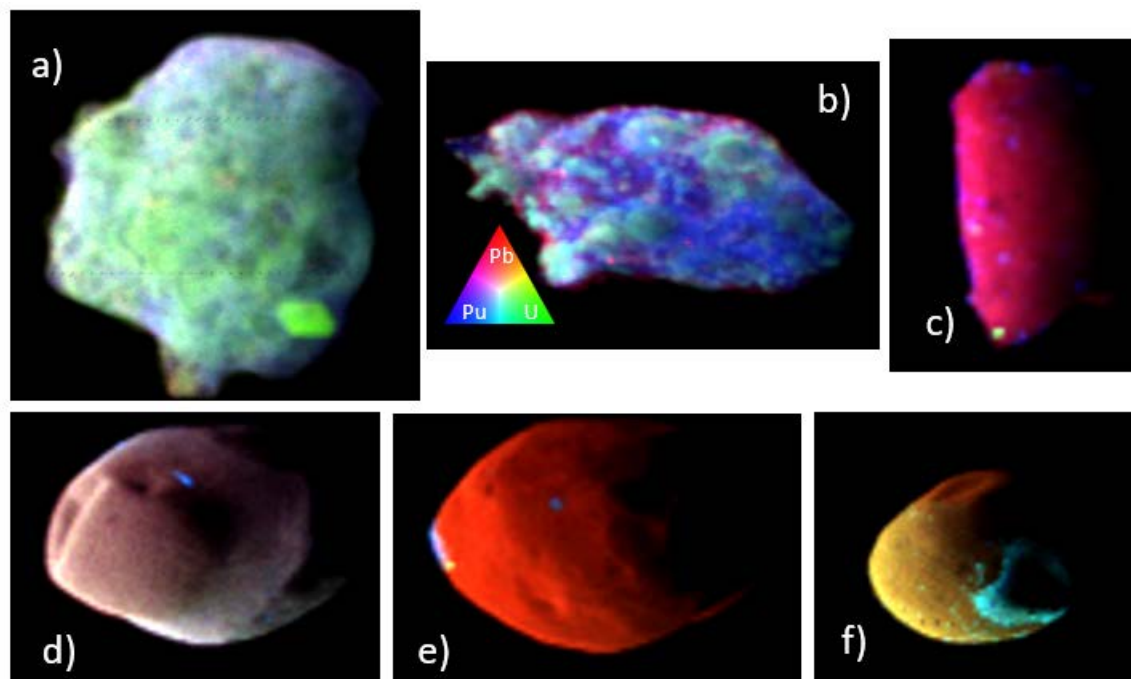
Figure SI-3. SXRF spectra of the six grains, qualitatively highlighting the similarity of Ceres1, CeresII, CeresIII and Chip and the difference of Bruce and Potatohead.
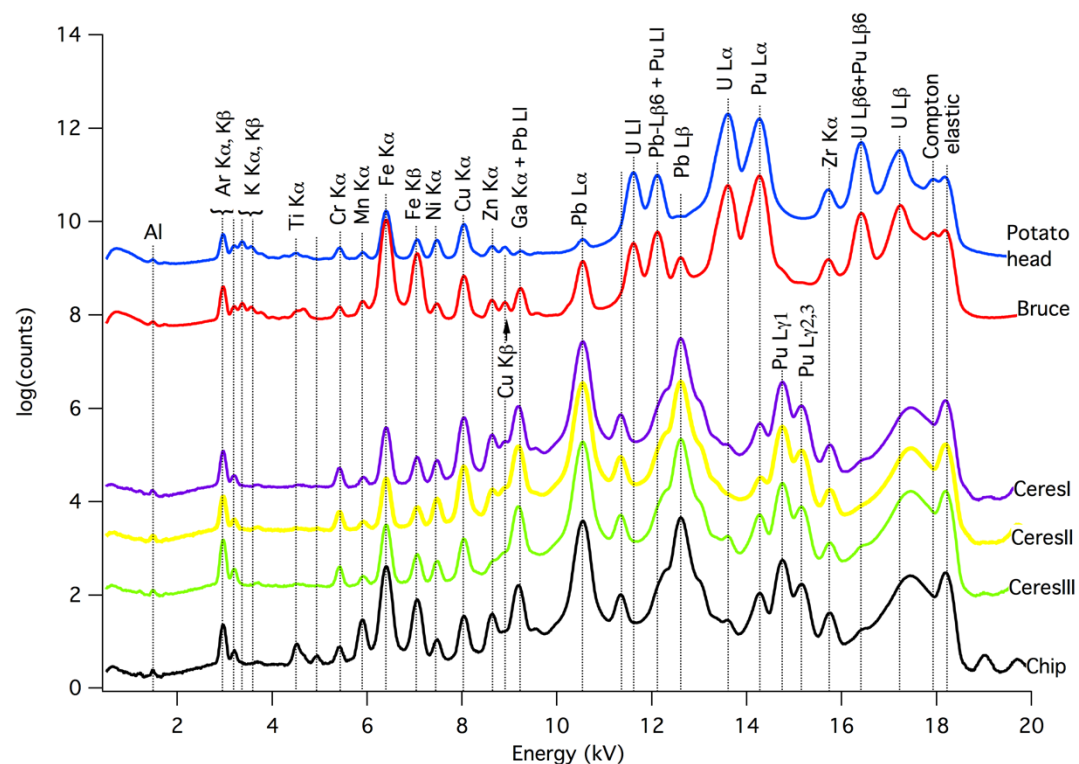
Figure SI-4. SXRF elemental ROI images of the six grains, and elemental correlation plots.

Bruce (131337): Pu	Bruce (131337): U	Bruce (131337): Pb	Bruce (131337): Fe
Chip (131418): Pu	Chip (131418): U	Chip (131418): Pb	Chip (131418): Fe
CeresII (131415): Pu	CeresII (131415): U	CeresII (131415): Pb	CeresII (131415): Fe
CeresI (131407): Pu	CeresI (131407): U	CeresI (131407): Pb	CeresI (131407): Fe

CeresIII (131419): Pu	CeresIII (131419): U	CeresIII (131419): Pb	CeresIII (131419): Fe

U-Pu scatter plot			
Potatohead (131476)	Bruce (131337)	Chip (131418)	ceresII (131415)
		ceresI (131407)	CeresIII (131419)

Pb-Pu scatter plot			
Chip (131418)	ceresII (131415)	ceresI (131407)	ceresIII (131419)

Figure SI-5. Pu and U XANES of Potatohead, Bruce and Ceres 1; (a) Pu XANES of particles shown with Pu XANES standards from Conradson et al. (2004a,b), (b) U XANES of particles compared to uraninite (predominantly U^{4+}) and uranyl nitrate (U^{6+}); (c) location of XAS measurements on Potatohead and (d) location of XAS measurements Bruce. (e) U-SXRF image divided by Pu-SXRF image and the associated line profile showing the U/Pu ratio throughout the potatohead. The point of interest is the high U concentration at edge of Potatohead and in the hotspot, where point XANES show higher U(VI) relative to other points measured on the sample.

(a) Pu XANES

(b) U XANES

(c) Location of XAS on Potatohead

(d) Location of XAS measurements on Bruce
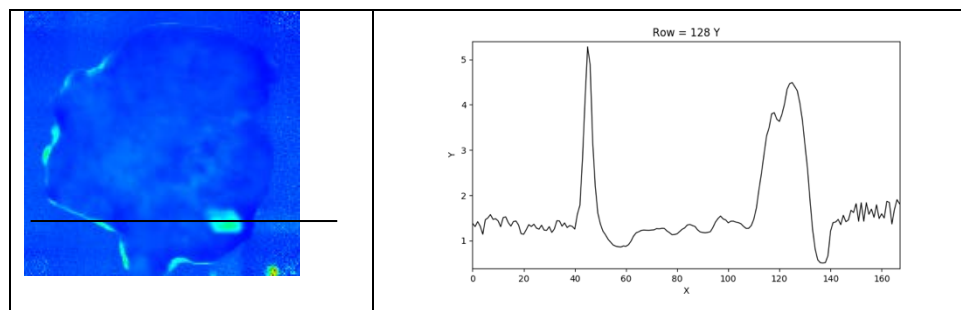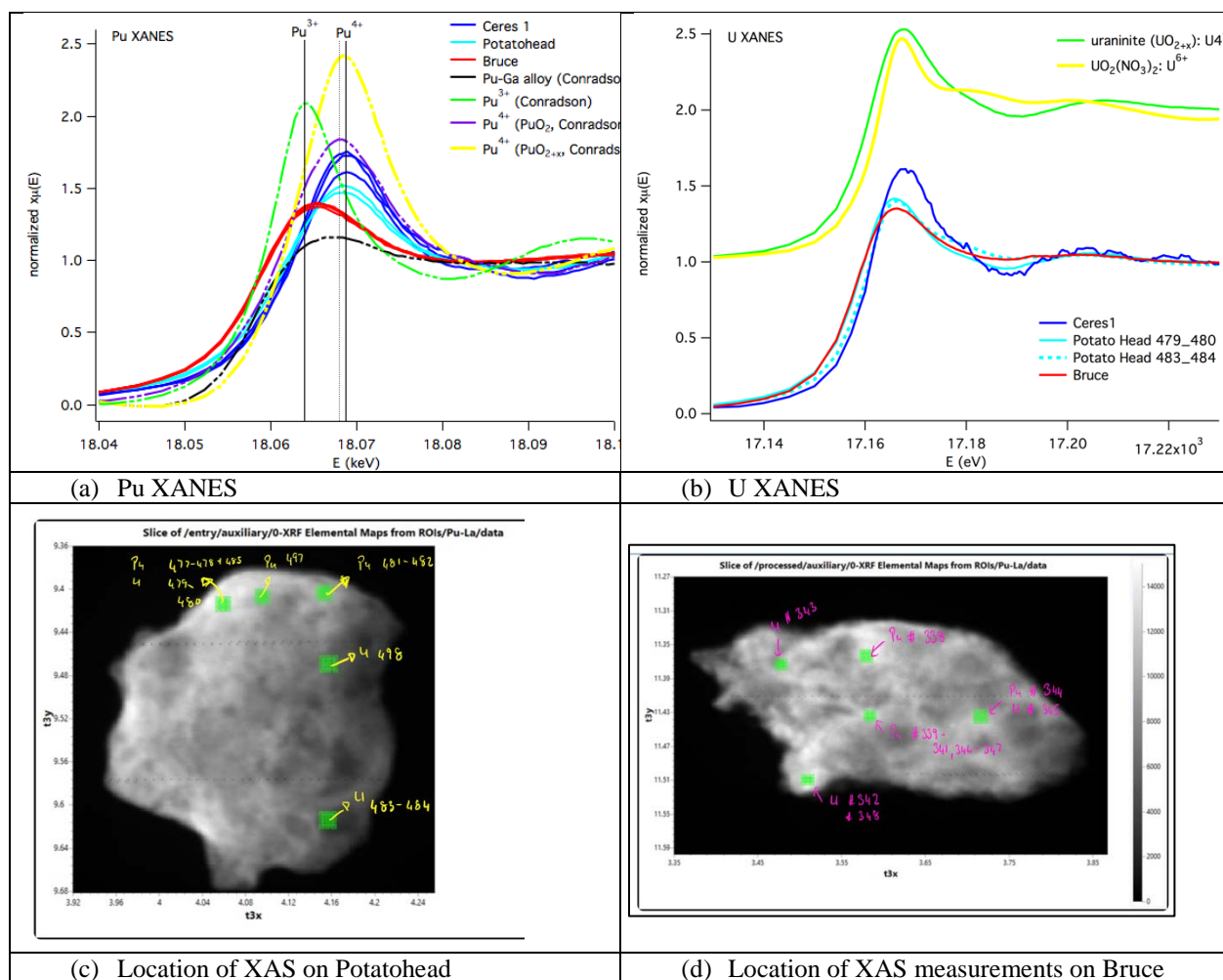
(e) SXRF of Potatohead: U/Pu	Line profile through hotspot (U in hotspot is more U(VI)

Figure SI-6. Pu and U EXAFS a) Fourier transform of Pu EXAFS b) Fourier transform of U EXAFS c) Pu and U EXAFS.

(A)

(B)

(C)
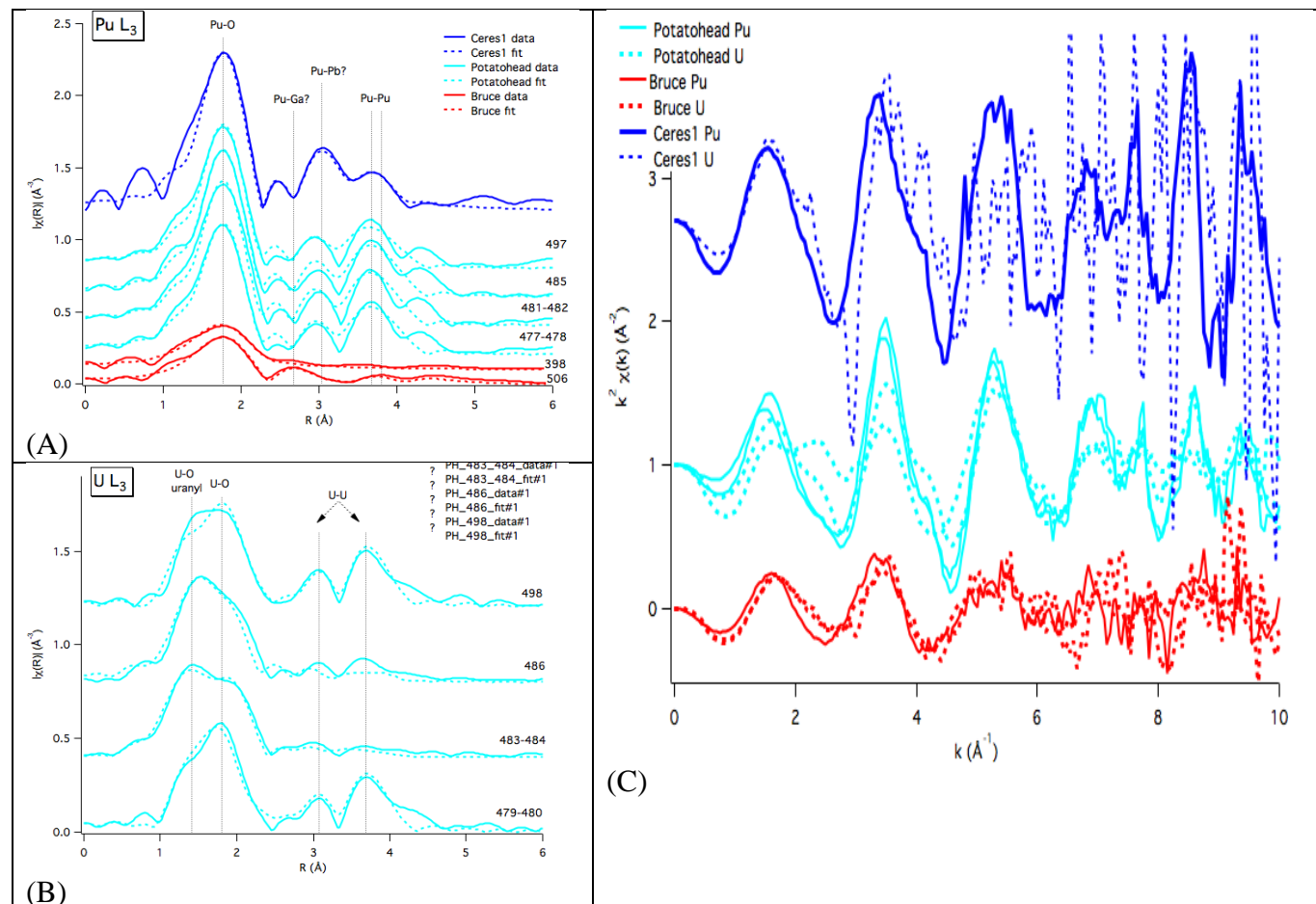
Figure SI-7. XRD of Potatohead (data in red, fits in blue). (A) Predominant phases for all spectra (taken at different points) are PuO_2+UO_2(C-phase). A few minor (unidenitifed) phases are also present.
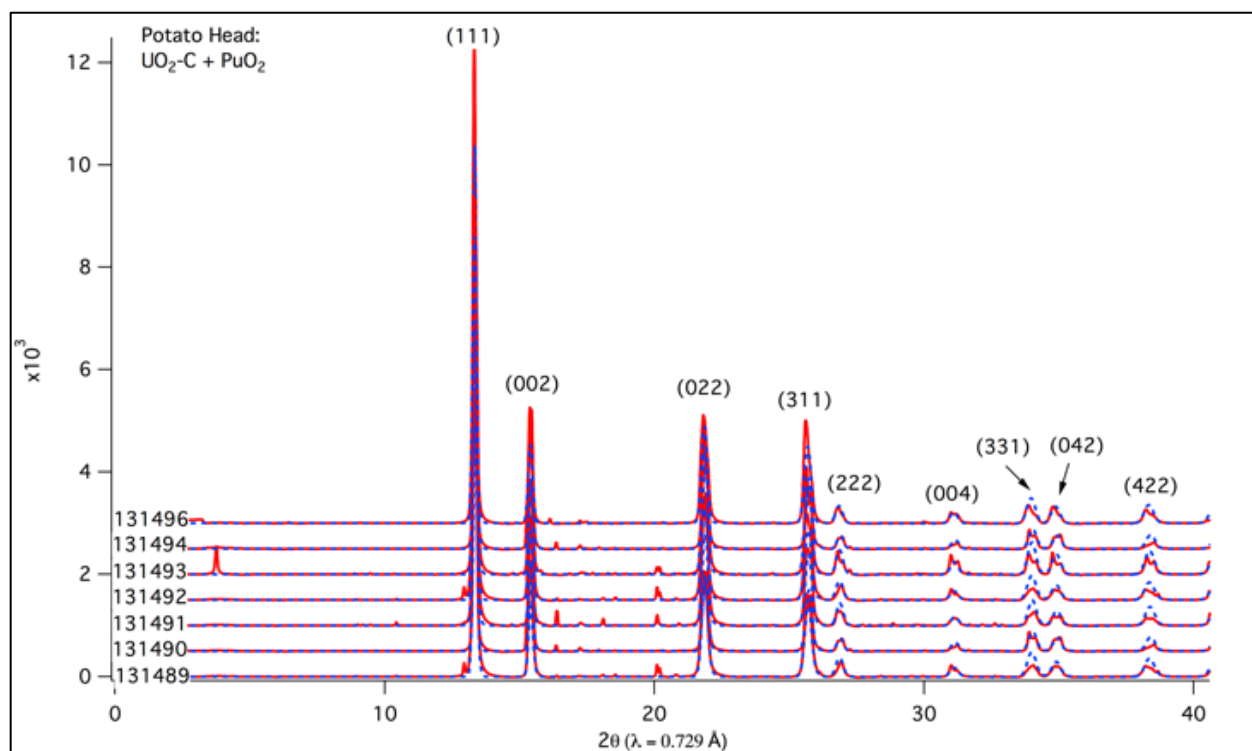
(B) Zoom in of spectrum # 131489 – showing splitting of peaks suggestive of both PuO_{2+x} and UO_{2+x} phases.

Figure SI-8. XRD of Bruce. The spectra are from different points on the particle, demonstrating heterogeneity of Bruce. Phases were ascertained by pattern matching, based on elements/phases from SXRF and SEM+FIB.
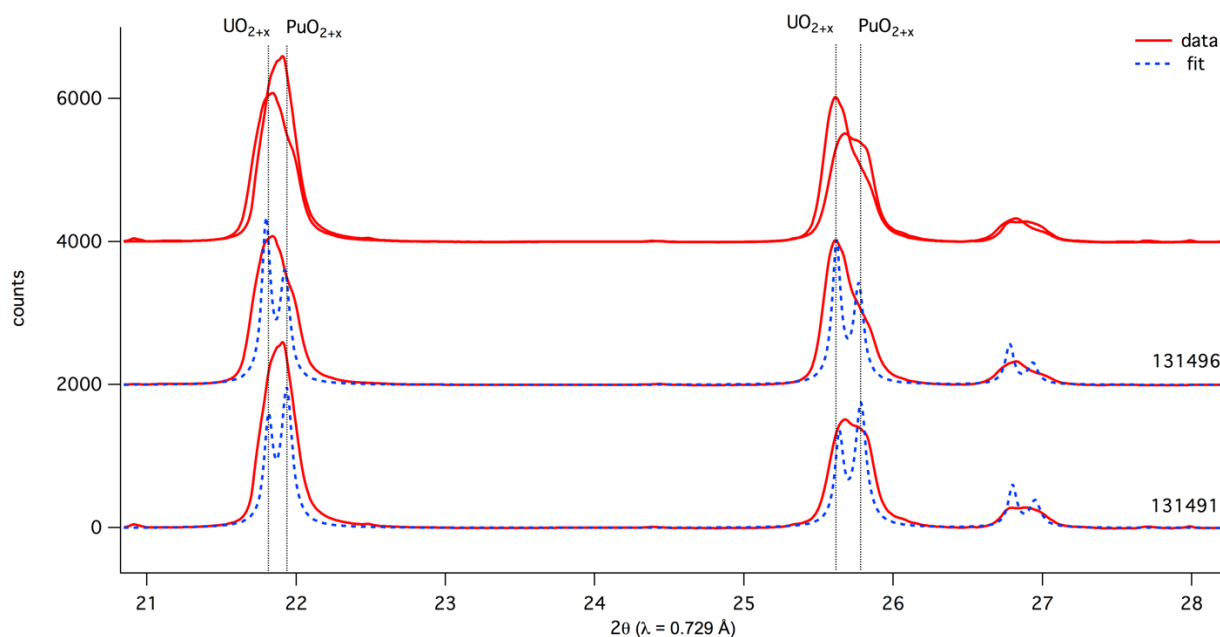
Figure SI-9. FIB-SEM images. These are BSE images collected using the in-column mirror detector. Bright phases indicate higher atomic number (Pu-U) and darker area are phases that are comprised of lower atomic number. Typically, the brightest phases are some form of Pu-U, the medium grey is dominated by a high concentration of Fe and the darkest area of the samples are Al-dominant. Note the small, sub-micron to nano-sized bright particles in the dark Al-rich area.

Bruce
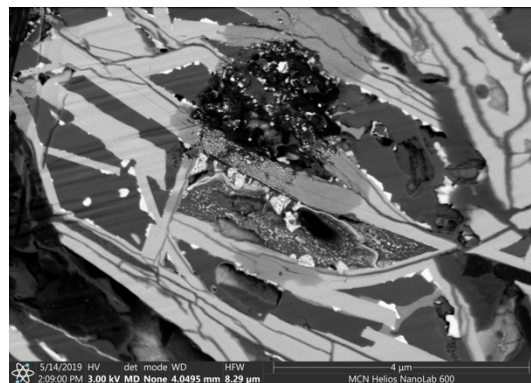
The very bright areas indicate Pu-U particles.

Alpha decay damage causing Frenkel pair formation. Note dusting of sub-micron to nano Pu-U particles in parts of the image.
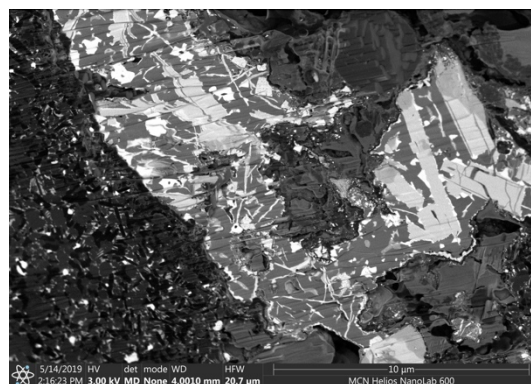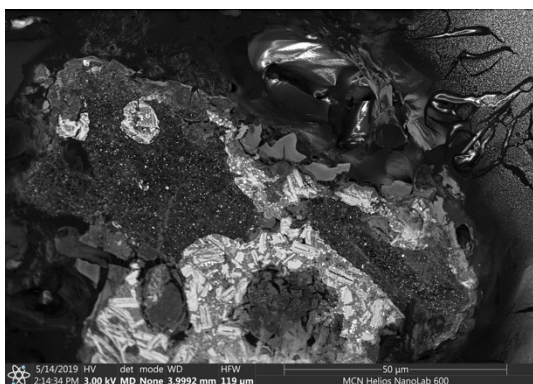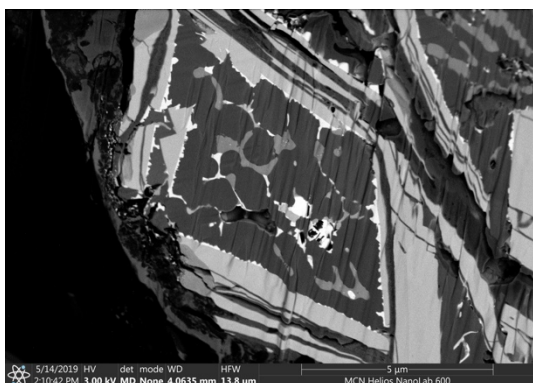
Potatohead
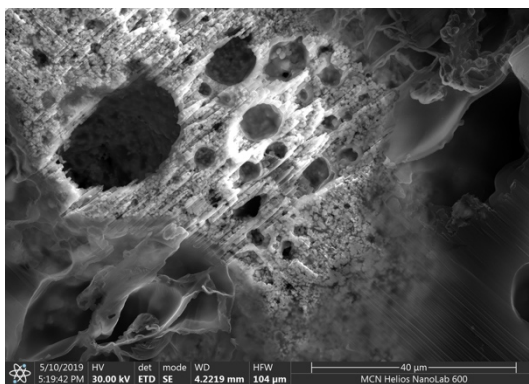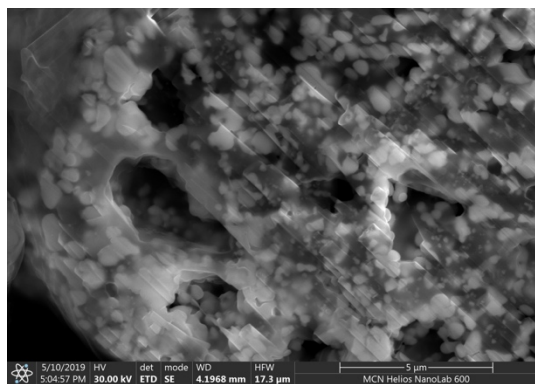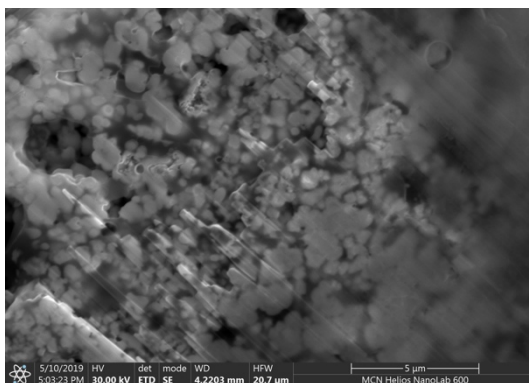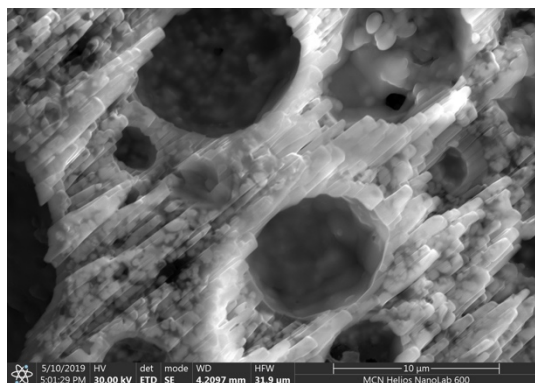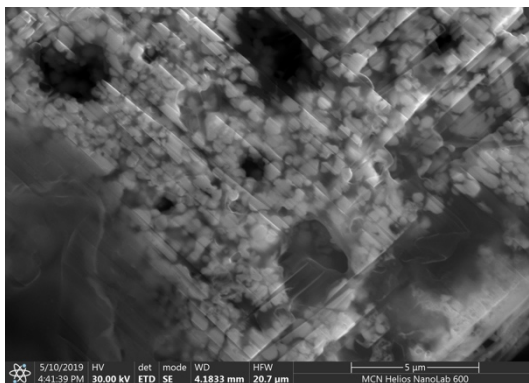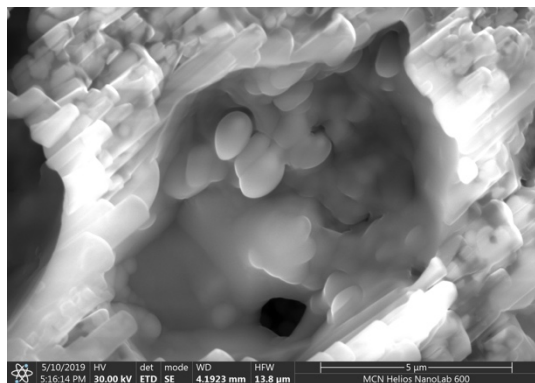
Supplementary Material: Tables

Table S1. Previous studies characterizing Pu-bearing particles/colloids with imaging and/or XAS techniques

Study	Site	Source/Transport	No. of 'hot' particles	Technique	Summary of results
Ikeda-Ohno et al., (2016)	Maralinga, Australia	Nuclear & partial to non-fission weapons tests	1 fragment -> 5 particles	SXRF XANES+EXAFS	Pu and U distributions were de-coupled $PuO_{2+x-y}(OH)_{2y} \cdot zH_2O$
Cooper et al., (1994) Burns et al. (1990)	Maralinga, Australia	Nuclear & partial to non-fission weapons tests	5	PIXE	Pu and U distributed homogeneously in 2 samples (not detected in others) –areas scanned are Pu dominant
Batuk et al. (2015)	McGuire Air Force Base, USA	Conventional/Non-critical nuclear weapon accident	2	SXRF XANES+EXAFS XRD	homogenous and heterogenous Pu+U distribution PuO_{2+x}, $PuUO_{2+x}$ and UO_{2+x} Fm3m diffraction pattern
Batuk et al. (2015)	Los Alamos TA-21 waste site, USA	R&D waste	2	SXRF XANES+EXAFS	Pu(IV) mononuclear species & Fe incorporated into PuO_{2+x}
Batuk et al. (2015)	Rocky flats	Operational release	2	XANES+EXAFS XRD	PuO_{2+x}, $Pu(U)O_{2+x}$
Batuk et al. (2015)	Hanford, USA	Waste disposal site: Z-9 + Z12 cribs	3	SXRF XANES+EXAFS XANES+EXAFS	P incorporated into PuO_{2+x} Pu(IV) mononuclear species
Kersting (2013)	Hanford, USA	Waste disposal site: Z-9 crib	3?	Nano-SIMS	Pu colloids
Buck et al., (2014)	Hanford, USA	Sediments Z9-4-5 and Z9-4-11 from Z (PFP) plant	2	SEM, TEM, EELS, EXAFS	Pu mainly present as PuO_2 + evidence for a nano-particulate Fe-Pu-phosphate phase. EXAFS shows P is O–bridged to the Pu in the PuO_2 lattice.

Felmy et al., (2010)	Hanford, USA	Discharge from Z-9, Z-12 and subsurface sediments (Plutonium Finishing Plant- Z-plant complex)	4	EXAFS + XRD	Largest Pu particles found to be $PuO_{2+x-y}(OH)_{2y}.(H_2O)_{2z}$. Pu from sediment samples was either monomeric or highly disordered, with potential of F incorporated into PuO_2 structure.
Kersting et al. (1999)	Nevada test site, USA	Atmospheric, ground & underground nuclear weapons tests	Solution	SEM XRD	Pu colloids in ground water
Varshney et al., (2018)	Clean Slate II, Nevada test site, USA	Safety (nuclear weapon destruction) tests with chemical explosives	7	SEM-EDS	The authors note that particles were rougher with sharper edges (not "popcorn" or sponge-like as other non-critical accidents/releases); however, the images presented do not corroborate their statements.
Aragon et al., (2008)	Palomares, Spain	Conventional/Non-critical nuclear weapon accident	7	SEM-EDX	Textures were typically massive and/or granulated with variable grain sizes to less than 0.5 um; some particles fragmented. EDX showed primarily Pu and U with minor Si, Al, Fe and Cr.
Lind et al. (2007)	Palomares, Spain	Conventional/Non-critical nuclear weapon accident	5	SEM-EDX+SXRF XANES	homogeneous Pu+U distribution Pu(III)+Pu(IV)+Pu(V) co-existing with U(IV)
Ranebo et al., 2007	Thule, Greenland	Conventional/Non-critical nuclear weapon accident	3	SEM-EDX, SIMS	Heterogeneous distribution of U and Pu in particles, with either a spongy or "popcorn" structure.
Lind et al., (2005)	Thule, Greenland	Conventional/Non-critical nuclear weapon accident	3	SEM-EDX XANES	homogeneous Pu+U distribution Pu(III)+Pu(IV) homogeneously distributed with U(IV)

Erkisson et al. (2005)	Thule, Greenland	Conventional/Non-critical nuclear weapon accident	5	SXRF imaging and u-SXRF-tomography XANES	Pu occurs predominantly where the U occurs, however the Pu/U intensity distribution varies 2 particles contained predominantly Pu(IV) and 2 particles were 33% Pu(IV)+ 67 % Pu(VI); all were mixed heterogeneously with U(IV)
Jernstrom et al., 2006	Runit Island, Enewetak atoll, Marshall Islands	Nuclear test program included 4xair drops and 35x barge + 13xtower + 10xsurface + 3xunderwater detonations.	6	SXRF SEM-EDX-WDX; SIMS	3xsmaller particles, containing mainly a Pu matrix, most likely from Quince safety test (based on ^{240}Pu/^{239}Pu & no ^{137}Cs). 3xlarger particles with a Si-O matrix containing heterogeneous distribution of Pu, most likely from the low-yield Fig test (based on ^{240}Pu/^{239}Pu & ^{137}Cs).
Erkisson et al. (2005)	Muraroa atoll	Atmospheric & underground nuclear weapons tests	1	u-SXRF-tomography	Pu "nugget" attached to coral
Wolf et al., 1997	Johnston Atoll	Three non-nuclear destructs of nuclear warhead-carrying THOR missiles in 1962	9	SEM-EDS+TEM-EDS Electron diffraction	Pu and U are present as discrete phases in hot particles and EDS+electron diffraction provides evidence of $(U/Pu)O_2$, $(U/Pu)O_2CO_3$ and $(U/Pu)O_3.0.8H_2O$ phases in the soil.
Conway et al., 2009	Semipalatinsk NTS, former USSR	Low-yield (240 t), Pu-fuelled fission devices exploded at ~30 m below ground	9	SEM	'Hot' particles typically 1 mm in size with a vitrified, glass-like structure, typical of fused soil containing small discrete units of high-Z elements (Pu,Am – based on α-spectroscopy).
Novikov et al. (2006)	Mayak, former USSR	Waste re-processing plant	Solution	nano-SIMS	Pu and U sorbed to iron-oxide colloids
Tamborini and Betti, 2000	"Staryi Vishkov", Novozybkov district, Russia	Certified soil IAEA-375 obtained from the International Atomic Energy Agency	2	SEM, SIMS	SIMS/SEM was used to characterise Pu-containing particles with respect to size, shape and isotopic ratios and identified two different kinds of Pu; platelets of PuO_2 and fibrous PuO_2 rods.

Table S2. Particle EXAFS refinements

nO is the number of oxygen atoms coordinated to the actinide of interest. RO is the Pu/U-O distance (Å). σ^2O (Å²) is the EXAFS Debye-Waller factor; nPu is the number of Pu atoms. RPu is the Pu-Pu distance (Å), σ^2Pu (Å²) is the EXAFS Debye-Waller factor; similarly for Pb and Ga.
Values in parentheses are the errors of the fitted values.

Potatohead data were fitted: $2 \leq k \leq 9.5$ Å^{-1}, $1 \leq R \leq 5$ Å.

	nO	RO (Å)	σ^2O (Å²)	nPu	RPu (Å)	σ^2Pu(Å²)	$\chi2_{red}$
Potato Head 477-478	8 (fix)	2.32(1)	0.008(1)	12 (fix)	3.83(2)	0.010(2)	140
Potato Head 481-482	8 (fix)	2.32(1)	0.007(1)	12 (fix)	3.83(1)	0.009(1)	140
Potato Head 485	8 (fix)	2.32(1)	0.006(1)	12 (fix)	3.83(2)	0.009(2)	140
Potato Head 497	8 (fix)	2.32(1)	0.007(2)	12 (fix)	3.83(3)	0.012(4)	140

Ceres 1 data were fitted: $2 \leq k \leq 8.75$ Å^{-1}, $1 \leq R \leq 4$ Å.

	nO	RO (Å)	σ^2O (Å²)	nPb	RPb (Å)	σ^2Pb (Å²)	nPu	RPu (Å)	σ^2Pu(Å²)	$\chi2_{red}$
K480 - 131408	8 (fix)	2.32(1)	0.004(1)	12 (fix)	3.63(2)	0.004(2)	6 (fix)	3.63(3)	0.010 (fix)	31

Bruce data were fitted: $2 \leq k \leq 8.0$ Å^{-1}, $1 \leq R \leq .24$ Å.

	nO	RO (Å)	σ^2O (Å²)	nGa	RGa* (Å)	σ^2Ga (Å²)	nPu	RPu (Å)	σ^2Pu(Å²)	$\chi2_{red}$
Bruce - 131506	4.9(7)	2.37(1)	0.017(4)	2.1(7)	3.36(3)	0.010 (fix)	2 (fix)	3.74(5)	0.010 (fix)	9
Bruce- 131398	6.4(9)	2.38(2)	0.024(4)†							

*This peak can be fitted with a range of elements (Al, Ga, Pu) at a range of distances 2.96 to 3.36 Å. This may appear strange, but it is difficult to pin-point precisely which phase(s) is/are contributing to this peak.

†The EXAFS Debye-Waller term is very large for a first-shell Pu-O distance, suggesting disorder, ie this peak could be fitted with a range of Pu-O distances.

U data were fitted with a combination of uraninite (predominantly U(IV)) and uranyl nitrate (U(VI)).
Potatohead data were fitted: $2 \leq k \leq 10 \ Å^{-1}$, $1 \leq R \leq 5 \ Å$)

	nO	RO (Å)	σ^2O (Å^2)	nU	RU (Å)	σ^2U(Å^2)	Phase %	$\chi 2_{red}$
Potato Head 479-480	8 (fix)	2.31(1)	0.014(1)	12 (fix)	3.87(1)	0.009(1)	75 U(IV)	125
	2 (fix)	1.69(3)	0.005 (fix)				25 U(VI)	
	2 (fix)	2.30 (fix)	0.014(1)					
	4 (fix)	2.48(3)	0.014(1)					
Potato Head 483-484	8 (fix)	2.37 (fix)	0.005(3)	12 (fix)	3.81(8)	0.021(16)	25 U(IV)	125
	2 (fix)	1.76(1)	0.005 (fix)				75 U(VI)	
	2 (fix)	2.40(2)	0.005(3)					
	2 (fix)	2.84(2)	0.005(3)					
	2xN (fix)	2.24(2)	0.005(3)					
Potato Head 486	8 (fix)	2.37 (fix)	0.005 (fix)	12 (fix)	3.85(7)	0.005 (fix)	10(8) U(IV)	125
	2 (fix)	1.78(1)	0.005(3)				90(8) U(VI)	
	2 (fix)	2.18(3)	0.005 (fix)					
	2 (fix)	2.34(6)	0.005 (fix)					
	2xN (fix)	2.42(8)	0.005 (fix)					
Potato Head 498	8 (fix)	2.35(1)	0.011(3)	12 (fix)	3.87(2)	0.007(3)	65(8) U(IV)	125
	2 (fix)	1.69(3)	0.005 (fix)				35(8) U(VI)	
	2 (fix)	2.17 (fix)	0.011(3)					
	4 (fix)	2.86 (fix)	0.011(3)					

*Phase% indicates the fitted amount of U(IV) (uraninite) U(VI) uranyl nitrate ($UO_2(NO_3)_2.6H_2O$).

Table S3. Potatohead XRD TOPAS "refinement".

scan	a((U,Pu)O$_{2+x}$) Å	a((Pu,U)O$_{2+x}$) Å	Δ	Refined wt% (UO$_2$)	Refined wt% (PuO$_2$)	R-factor
131489	5.44745(23)	5.41948(25)	1.56	48(1)	52(1)	Rwp = 61
131490	5.44679(21)	5.41594 (20)	1.72	45(2)	59(1)	Rwp = 62
131491	5.44860(22)	5.41865(23)	1.67	40(1)	60(1)	Rwp = 60
131492	5.44895(23)	5.42019(25)	1.60	47(1)	52(1)	Rwp = 61
131493	5.44930(16)	5.41438(23(	1.95	55(1)	45(1)	Rwp = 58
131494	5.44514(21)	5.41506(21)	1.68	42(1)	58(1)	Rwp = 62
131496	5.45252(18)	5.42156(25)	1.72	57(1)	43(1)	Rwp = 58
AVERAGE	5.4484(23)	5.4179(28)	1.70(13)			

*normalised to 100%, but did not fit minor components - from FIB-SEM expect these to be Al or Al-Fe compounds

Table S4: A history of British nuclear tests in mainland Australia

Major Test Trials						
Test Series	**Test Name**	**Location**	**Date**	**Yield**	**Explosion Conditions**	**Comments**
	Hurricane	Monte Bello (off Trimouille Island) 20.41°S 115.55°E	3rd Oct, 1952	25 kt	Ocean Surface burst (HMS Plym)	A British Blue Danube Design with a levitated pit plutonium implosion device (air gap between the uranium tamper and the plutonium core) was used. The bomb was exploded inside the hull of Plym, anchored 350 m off Trimouille Island. The fallout is unknown, although changes in wind pattern likely led to land contamination.
Totem	Test 1	Emu Field, South Australia 28.68°S 132.34°E	15th Oct 1953	10 kt	Steel Tower, 31m	A British Blue Danube design was used. The main purpose of the trial was to determine the acceptable limit on the amount of ^{240}Pu present in a bomb. Reports highlight a black mist generated from Totem-1 across the landscape at Wallatina and Welbourn Hill stations in Granite Downs, 175 km from the test site, and led to "unacceptably" high levels of radioactive contamination.
Totem	Test 2	Emu Field, South Australia 28.70°S 132.35°E	27th Oct 1953	8 kt	Steel Tower, 31m	A modified British Blue Danube design was used. The yield was much bigger than the expected 2–3 kt, however, was below the estimated maximum. High winds dispersed the radioactive cloud so that it had dissipated to the point where it could not be tracked.
Mosaic	G1	Trimouille Island in the Monte Bello Islands, Australia 20.23°S 115.55°E	16th May 1956	15 kt	Aluminium Tower, 31m	The first British test using a boosted fission weapon design with lithium deuteride fusion fuel. The fallout cloud initially moved out to sea as predicted, but then reversed direction and drifted across northern Australia.
Mosaic	G2	Alpha Island in the Monte Bello Islands, Australia 20.40°S 115.53°E	19th June 1956	98 kt	Aluminium Tower, 31m	A boosted fission weapon design with lithium deuteride fusion fuel and a Uranium tamper was used. It is the largest nuclear device ever detonated in Australia with the highest yield. The bulk of the fallout drifted over the Arafura Sea, but owing to different winds at different altitudes, part of it drifted over the mainland.
Buffalo	One Tree Site, Round 1	Maralinga (One Tree) 29.87°S 131.66°E	27th Sept 1956	15 kt	Aluminium Tower, 31m	A Red Beard un-boosted fission implosion weapon with a composite core (containing both weapons-grade plutonium and weapons-grade ^{235}U) was used. Two radioactive fallout clouds resulted from the test with rainfall depositing some fallout in the Brisbane-Lismore area.
Buffalo	Marcoo Site, Round 2	Maralinga (Marcoo)	4th Oct 1956	1.5 kt	Ground	A Blue Danube bomb equipped with low yield Mark I enriched uranium core was used. The weapon was lowered into a

		29.88°S 131.62°E				concrete pit and left a crater 49m wide and 12m deep. The fallout crossed the east coast 25 to 30 h after the detonation.
Buffalo	Kite Site, Round 3	Maralinga (Kite) 29.89°S 131.66°E	11th Oct 1956	3 kt	Air drop, 150m	This was Britain's first air drop test. It tested a low-yield Blue Danube core with less fissile material. Two clouds formed; a low-level one at 2,100m that dropped all its radioactive material inside the prohibited area, and a high-level one at 3,700m that deposited negligible amount of fallout over South Australia, Victoria and New South Wales.
Buffalo	Breakaway, Round 4	Maralinga (Breakaway) 29.89°S 131.60°E	22nd Oct 1956	10 kt	Aluminium Tower, 34m	This was the second test of a boosted Red Beard fission implosion weapon with a composite core (containing both weapons-grade plutonium and weapons-grade ^{235}U). The radioactive fallout reached 11,000m but soon became widely dispersed between Darwin and Newcastle.
Antler	Round 1	Maralinga (Tadje) 29.89°S 131.65°E	14th Sept 1957	1 kt	Aluminium Tower, 31m	The test of Pixie, a lightweight small diameter implosion device with a plutonium core was conducted using cobalt pellets as a test diagnostic for measuring yield. Later reports found personal handling of these pellets led to exposure of ^{60}Co. The results of the continental sticky paper survey showed that the fallout levels were low; the maximum observed was at Alice Springs, and most of the fallout occurred to the north-east and north-west of Maralinga. Small amounts of fallout, close to the detection limits were detected in Adelaide and Melbourne.
Antler	Round 2	Maralinga (Biak) 29.89°S 131.62°E	25th Sept 1957	6 kt	Aluminium Tower, 31m	A lightweight plutonium implosion device named Indigo Hammer, intended for a surface to air defence missile (Bloodhound) and thermonuclear primary applications was tested. A calculation immediately after firing using the observed height of the cloud predicted that the fallout would exceed out to a distance of about 240km.
Antler	Round 3	Maralinga (Taranaki) 29.89°S 131.59°E	9th Oct 1957	25 kt	Balloon-burst over land, 300m	A test of a primary for a megaton range thermonuclear device using plutonium surrounded by highly enriched uranium was conducted. The final predicted fallout showed that the expected contamination at many of the sites, including Breakaway, Marcoo and Mina, would exceed half-level B. Fallout from this round also fell on Adelaide, Melbourne and Sydney.

Minor Tests Trials*

Operation Kittens	Operation Kittens	Naya Area, Maralinga (94) & Emu Fields (5)	1953–1961	NA	NA	A total of 99 trails were conducted on the development and testing of neutron initiators. The initiator consisted of a radioactive substance brought into contact with beryllium by a chemical explosive. In later Kittens trials, the neutron output was used to assess the performance of the high explosive assembly that compresses the fissile material in the core. The experiments at Emu Fields dispersed 36g of beryllium and 15 TBq of ^{210}Po into the surrounding area. The Kittens experiments at Naya Area dispersed 259 TBq of ^{210}Po, 750 g of beryllium and 120 kg of natural and depleted uranium.
Operation Tims	Operation Tims, TM100 and TM101	Naya and Kuli Areas, Maralinga (321)	1955–1963	NA	NA	The Tims experiments were designed to measure the compression of a simulated core of an atomic weapon and the design of the high explosive component to achieve maximum compression. A total of 321 experiments were carried out in the Naya and Kuli areas to investigate uranium and beryllium tampers, and early subcritical hydro-nuclear tests. These experiments used and dispersed beryllium (77 kg), natural uranium ore (825 kg) and ^{238}U (6800 kg). In 1960, twelve Tims experiments carried out at TM100 and TM10l used about 1.2 kg of plutonium.
Operation Rats	Operation Rats	Naya and Dobo Areas, Maralinga (125)	1956–1960	NA	NA	The Rats experiments had a similar objective to the Tims experiments but used a different technique to determine the compression. A total of 125 trials of explosive dispersal of uranium were conducted; the materials used included ^{46}Sc (80 TBq), ^{238}U (180kg), ^{210}Po (15 TBq) and ^{212}Pb (4.4 TBq)
Vixen	Operation Vixen A	Wewak Area, Maralinga (31)	1959–1961	NA	NA	A total of 31 Vixen A trials were conducted to investigate the spread of radioactive and toxic materials that might result from an accidental fire on a nuclear weapon, and involved a total of 1kg Plutonium. Three kinds of experiments were conducted: combustion in controlled petrol fire (800-1200ºC) for Uranium and Beryllium, and 600-1000ºC for Plutonium; combustion in air in an electric furnace operating at 600-800ºC used only for uranium; and dispersion by high explosives consisting of the explosive implosion assemblies from nuclear weapons. The materials used during these trials included 6.0 kg of beryllium of which 4.2 kg was dispersed, 68 kg of natural and depleted uranium, 0.98 kg of plutonium of which 0.58 kg was dispersed, 3.6 TBq of ^{210}Po and 0.07 TBq of ^{227}Ac.

| Vixen | Operation Vixen B | Taranaki Area, Maralinga | 1960–1963 | NA | NA | A total of 12 Vixen B Trials were conducted to determine the effects of an accidental detonation of some of the high explosive in the weapon and involved 22 kg of Pu. All of the Vixen B rounds were carried out at Taranaki where they produced the worst of the contaminated areas at Maralinga. The materials used and dispersed in the Vixen B series included ^{239}Pu (22.2 kg), ^{235}U (22.4 kg), ^{238}U (24.9 kg) and beryllium (17.6 kg). At the time of Operation Brumby, there were 21 pits in the Taranaki area containing about 830 t of material contaminated by 20 kg of plutonium. The remaining plutonium, now estimated to be about 2 kg, was dispersed on the Range. |

* these minor tests were performed without formal Australian government approval, and without any advice being given to the Australian government by Australian or British scientists.

*1 TBq = 10^{12} Bq

UK Atmospheric Nuclear Weapons Tests in Australia, Oct 1952 – Oct 1957

OPERATION and Location	Date and TIME (GMT)	Site	Type	Height (m)	Measured Yield (kt)	Approx Yield (kt)	Yield Range
HURRICANE; MonteBello Is,WA	3 Oct 1952 0000Z*	Lagoon of 12m depth	CSB; in HMS Plym.	-2.7	25	25	Kiloton, or Low Intermediate.
TOTEM; EmuField, SA	14 Oct 1953 2130Z	T1.	NSB: MS Tower.	31	9.1 ± 0.4	10	Kiloton, or Low.
	26 Oct 1953 2130Z	T2.	NSB: MS Tower.	31	7.1 ± 0.3	8	Kiloton, or Low.
MOSAIC; MonteBello Is,WA	16 May 1956 0350Z	G1: Trimouille Is.	NSB: Al Tower.	31	13.5 ± 0.2	15	Kiloton, or Low
	19 June 1956 0214Z	G2: Alpha Is.	NSB: Al Tower.	31	56 ± 0.8	60	Kiloton, or Low Intermediate.
BUFFALO; Maralinga Range, SA.	27 Sept 1956 0730Z	One Tree.	NSB: Al Tower.	31	12.9 ± 0.2	15	Kiloton, or Low.
	4 Oct 1956 0700Z	Marcoo.	CSB: at ground surface.	0.2	1.4	1.5	Kiloton, or Low.
	11 Oct 1956 0557Z	Kite.	Airburst: freefall.	150	2.88	3	Kiloton, or Low.
	21 Oct 1956 1435Z	Breakaway.	NSB: Al Tower.	31	10.8 ± 0.2	10	Kiloton, or Low.
ANTLER; Maralinga Range, SA.	14 Sept 1957 0505Z	Tadje.	NSB: Al Tower.	31	0.93 ± 0.12	1	Sub-kiloton, or Very Low.
	25 Sept 1957 0030Z	Biak.	NSB: Al Tower.	31	5.67 ± 0.12	6	Kiloton, or Low.
	9 Oct 1957 0645Z	Taranaki.	Airburst: Balloon System Borne.	300	26.6 ± 0.7	25	Kiloton, or Low Intermediate.

NSB: Near Surface Burst
CSB: Contact Surface Burst
MS: Mild Steel
Al: Aluminium Alloy

Ref: AWRE Classified Reports T1/77 and T2/80.

For most radiological protection, medical, health and safety, or nuclear weapons effects purposes the approximate yield will be sufficiently accurate.

* For clarity, this time is conventionally quoted as 0001Z on 3 October 1952 (GMT): the firing time was almost exactly midnight 2/3 October 1952 GMT.

W N SAXBY
SFS/AWRE

X

Copy..4. of .14. copies

S.T.D.
S.S.T.D.
S.S.T.P.
S.S.R.D.
S.S.I.D.
S.S.P.D.
S.P.T.

Antler General Arrangements 0236 IA
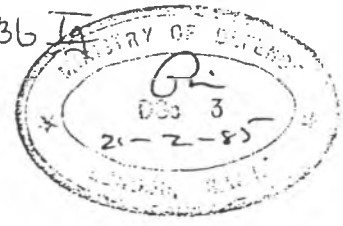
Antler - Weapon Identification

Some confusion has arisen over the numbering of the Antler rounds. This is primarily because for Trials Planning purposes the reason for the numbers is to conceal information about weapon details whereas for design and contruction purposes the numbers are required to indicate certain details.

It has been agreed that the best way to eliminate the confusion is to have a new series of Trials numbers, which will be the only ones used for trials planning purposes and to retain the existing numbers for design and contruction purposes.

The numbers are:

Trials Number	E1	=	Redbeard	=	Round C1A or C1B
"	"	E2	=	Pixie	=	" C2
"	"	E3	=	Blue Fox	=	" C3
"	"	E4	=	Blue Fox Boosted	=	" C4
"	"	E5	=	Tom	=	" C5B
"	"	E6	=	Radiation Round	=	" C6A

Any variations in design may be reflected in changes in the 'C' series but will not affect the 'E' series.

Copies No 1
2
3
4
5
6
7
8
9
10

R. PILGRIM
S.S.T.D.

Building D3   11
A.F.R.E.   + D 27. 3. 61

14th June, 1957   13
                  1 v Spare D 27 3. 61

Reference C/H/711

S.S.T.D.,
Building D3.   Antler General Arrangements 0236 1g

YIELDS EXPECTED AT ANTLER

You may like to have my latest estimates of the yields which are likely and also those which are the maximum conceivable for the weapons to be fired at Antler.

Round 1 = Trial E3 = Weapon C3.   The explosive for this weapon has not yet been chosen.   Even with the better explosive I do not see how the yield can exceed 15 Kilotons.   For the likely yield I favour 5 Kilotons in view of the recent TM trials on this weapon.

Round 2 = Trial E4 = Weapon C4.   I think the maximum conceivable is 30, and in view of results from Orange Herald I believe that the likely value is 15 Kilotons.

Round 3 = Trials E1 = Weapon C1A or C1B.   In either case I do not see how 20 Kilotons can be exceeded.   I think 15 Kilotons is a likely value.

Round 4 = Trial E5 = Weapon C5B.   I think this will give 30 Kilotons, and it is unlikely to exceed 35.

Round 5 = Trial E6 = Weapon C6A.   I do not know anything about this. I believe that Dr. Hulme has quoted a maximum yield of 80 Kilotons.
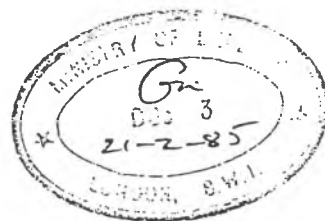
Round 6 = Trial E2 = Weapon C2.   I think the likely yield is 1 Kiloton, but here again the explosive is not yet settled.   Even with the better explosive I would not expect the yield to exceed 2 Kilotons.

(J. Corner)

SSPD.,
Bldg. E1.

18th June, 1957.

To: Geoff Williams/ARPANSA/Health@Health_gov_au
cc:

Subject: MARALINGA

Geoff

I have just received an AWRE report on the isotopic composition of
plutonium in the Vixen B trials. It seems that gallium was the principal
alloying material (1% by mass) and therefore the delta phase of plutonium
was used in these trials. This has no bearing on the origin of the material
but the figures and other data in the report may prove useful. One figure
of interest that I will have to work on is "% by alpha activity" for
Am-241.

It appears that we have both been operating under a minor misconception.

Regards
Alan Batchelor

- att1.htm

British Defence Research and Supply Staff

Anzac Park West Building Constitution Avenue Parkes
Canberra ACT 2600

Telex BDRSS CANBERRA   Telephone 48 2111 ext 2846

Dr G A Williams Commonwealth Department of Health Australian Radiation Laboratory Lower Plenty Road Yallambie VIC 3085	Your reference Our reference JAA/243/01/MAST Date 21 May 1986

Dear Dr Williams,

1.   I understand that you asked Dr Roger Allen for information about PU/AM ratio data. The following information has been received from AWRE Aldermaston and I trust that it will meet your needs.

2.   The AWRE radiochemical analytical data have been examined and for radiological protection, waste disposal, hazard/risk and safety assessment purposes we consider that the average data for all the tests will provide sufficient information of more than adequate accuracy. There are several scientific/technological reasons which make the only valid "birth dates", for the plutonium and other actinide nuclides, the same dates as the detonations: indeed, within a fraction of a second immediately following each detonation time.

3.   From the information obtained shortly after each detonation, the average atomic ratios of the "total number of atoms of all alpha emitting actinide nuclides" to (a) "atoms of the specific nuclide 241 AM" (b) "atoms of the specific nuclide 241 PU" were respectively:

    (a)   30,000 to 1;

    (b)   1200 to 1.

The specific nuclide 239 PU constituted on average 97% by atoms of the total number of atoms of all plutonium and other actinide nuclides. These data are for times of detonations.

4.   Turning to the Vixen Bravo shots; the "birth dates" for the plutonium and other actinides should be taken to be 180 days prior to each of the 12 detonations viz 3 in Vixen Bravo 1, 5 in Vixen Bravo 2 and 4 in Vixen Bravo 3. Our contemporary information led to the following later (November 1984) alpha activity ratios for the "activity of specific nuclide 239 PU (Bq)" to "activity of 241 AM (Bq)":
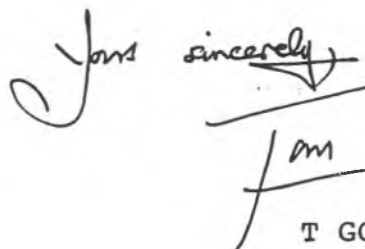
    Vixen Bravo 1 average 14 to 1 (values are 19/1, 11.2/1 and 12.3/1).

    Vixen Bravo 2 average 5.4 to 1 (range 5.2/1 to 5.7/1).

    Vixen Bravo 3 average 6.6 to 1 (range 6.5/1 to 6.6/1).

The overall average is 6.6 to 1. Note that the overall average of activity ratios for "total alpha activity (Bq)" to "activity of 241 AM (Bq)" is 8 to 1. All these activity ratios are as calculated for the month of November 1984. The overall average Vixen Bravo content of the specific nuclide 239 PU was 96% by mass. It can be seen that the ARL ratio of 7.4 is consistent with our information. It would be helpful however to learn what you mean by "PU 239 (Bq)": Is it (P) activity of the specific nuclide or (Q) total alpha activity using "239 PU" as an abbreviation for convenience?

5.   All the above ratios and percentages, without amplification, are UK UNCLASSIFIED and may be quoted in ARL Unclassified documents and statements dealing with Maralinga and/or the UK Nuclear Weapons Tests and Experimental Programmes in Australia, 1952-1957.

Yours sincerely,

Tom Goff

T GOFF
EXECUTIVE ASSISTANT

DR G. WILLIAMS ARL

As *pin-raised*

Nuike Chelelle

6/6/95

available in ORE if required.

D/Sc(Nuc)2/5/6/10

28 March 1985

MINOR TRIALS SCHEDULE

The following unclassified tabulation is extracted from classified material which has been provided for the use of Australian officials who may be granted access to UK information at the classification level which it carries. The three classified documents are referenced MTS(60)VB, MTS(61)VB and MTS(63)VB all dated 15 March 1985 and originate from Science(Nuclear)2.

Extract from MTS(60)VB

Date	Round No	Site	Quantity	Met Info	Composition
		Taranaki			
29 Aug	Calibration	Pad B	)	)	)
			)	)	)
8 Sep	VB AH	Pad D	) Pu, U^{235}, U^{238}	) See AWRE	)
			) and Beryllium	) Report	) See Below
29 Sep	VB DH	Pad C	) See Below	) No T4/61	)
			)	)	)
3 Oct	VB EH	Pad E	)	)	)

Extract from MTS(61)VB

Date	Round No	Site	Quantity	Met Info	Composition
		Taranaki			
-	Calibration	Pad L	)		)
			)		)
13 Apr	C	Pad F	)	15kn 170°	)
			)		)
23 Apr	D	Pad J	) Pu, U^{235}, U^{238}	8kn 165°	)
			) and Beryllium		) See Below
8 May	B	Pad G	) See Below	9kn 190°	)
			)		)
18 May	E	Pad H	)	10kn 190°	)
			) -		)
25 May	G	Pad A	)		)

└ ----- *Not as per Intermediate TAG or Cornish 1987*

Extract from MTS(63)VB

Date	Round No	Site	Quantity	Met Info	Composition
		Taranaki			
19 Mar	5301/1	Pad K	)		)
			)		)
26 Mar	5301/2	Pad PD	)	15kn 170°	)
			) Pu, U^{235}, U^{238}		)
2 Apr	5301/3	Pad PE	) and Beryllium	10kn 190°	) See Below
			) See Below		)
9 Apr	5301/4	Pad PC	)	8kn 165°	)
			)		)
14 Apr	5301/5	Pad M	)	10kn 190°*	)

*Records conflict 190°
is best estimate

Quantity of Material

Total Plutonium (including 1% Gallium alloying agent)   22.2 kg

Total U^{235} (all of composition close to data below)   22.4 kg

Total U^{238} (assume natural uranium)   24.9 kg approx

Total Beryllium   17.6 kg approx

Composition of Materials

Plutonium	–	Bulk* of material	Pu^{239}	~95%	)	
			Pu^{240}	~5%	)	of Pu
			Pu^{241}	~0.5%	)	

*The Pu^{240} content varied from 1 to 5%

			Pu	~99%	)	
			Ga	1%	)	of alloy
			Am	0.1%	)	

U^{235}	–	Typical figures	U^{235}	~93%	)	
			U^{234}	1%	)	
			U^{236}	0.3%	)	of Uranium
			U^{238}	~6%	)	

Science(Nuclear)2
Ministry of Defence
Main Building
Whitehall
London SW1A 2HB